

STATUS OF THESIS

Title of thesis SIZING OPTIMIZATION OF STANDALONE PHOTOVOLTAIC SYSTEM FOR RESIDENTIAL LIGHTING

I, DIMAS FIRMANDA AL RIZA

hereby allow my thesis to be placed at the Information Resource Centre (IRC) of Universiti Teknologi PETRONAS (UTP) with the following conditions:

1. The thesis becomes the property of UTP
2. The IRC of UTP may make copies of the thesis for academic purposes only.
3. This thesis is classified as


Confidential

Non-confidential

If this thesis is confidential, please state the reason:

The contents of the thesis will remain confidential for _____ years.

Remarks on disclosure:




Signature of Author

Permanent address:
Jl. Bengawan Solo No. 163
Lumajang, Jawa Timur
67314, Indonesia

Date: 16 - 08 - 2011

Endorsed by



Signature of Supervisor

Name of Supervisor
Syed Ihtsham ul Haq Gilani

Date: 16th August, 2011

DR SYED IHTSHAM-UL-HAQ GILANI
Senior Lecturer
Mechanical Engineering Programme
UNIVERSITI TEKNOLOGI PETRONAS
Serri Iskandar, 31750 Tronoh
Perak Darul Ridzuan, Malaysia.

UNIVERSITI TEKNOLOGI PETRONAS


SIZING OPTIMIZATION OF STANDALONE PHOTOVOLTAIC SYSTEM FOR
RESIDENTIAL LIGHTING

by

DIMAS FIRMANDA AL RIZA

The undersigned certify that they have read, and recommend to the Postgraduate Studies Programme for acceptance this thesis for the fulfilment of the requirements for the degree stated.

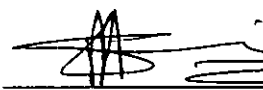
Signature:



Main Supervisor:

Dr. Syed Ihtsham ul Haq Gilani

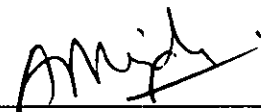
Signature:



Co-Supervisor:

Ir. Dr. Mohd. Shiraz B. Aris

Signature:



Head of Department:

Assoc. Prof. Dr. Ahmad Majdi B. Abdul Rani

Date:

Dr Ahmad Majdi Abdul Rani
Head of Department/Senior Lecturer
Mechanical Engineering Department
Universiti Teknologi PETRONAS
Bandar Seri Iskandar 31750 Tronoh,
Perak Darul Ridzuan, Malaysia
1/8/11

SIZING OPTIMIZATION OF STANDALONE PHOTOVOLTAIC SYSTEM FOR
RESIDENTIAL LIGHTING

by

DIMAS FIRMANDA AL RIZA

A Thesis

Submitted to the Postgraduate Studies Programme

as a Requirement for the Degree of

MASTER OF SCIENCE

MECHANICAL ENGINEERING DEPARTMENT

UNIVERSITI TEKNOLOGI PETRONAS

BANDAR SERI ISKANDAR,

PERAK

AUGUST 2011

DECLARATION OF THESIS

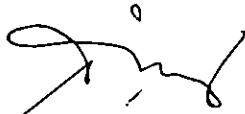
Title of thesis

SIZING OPTIMIZATION OF STANDALONE
PHOTOVOLTAIC SYSTEM FOR RESIDENTIAL LIGHTING

I, DIMAS FIRMANDA AL RIZA

hereby declare that the thesis is based on my original work except for quotations and citations which have been duly acknowledged. I also declare that it has not been previously or concurrently submitted for any other degree at UTP or other institutions.

Witnessed by



Signature of Author

Jl. Bengawan Solo No. 163
Lumajang, Jawa Timur
67314, Indonesia

Date: 16 - 08 - 2011



Signature of Supervisor

Dr. Syed Idris bin Haq Gilani

DR. SYED IDRIS BIN HAQ GILANI
Senior Lecturer
Mechanical Engineering Programme
UNIVERSITI TEKNOLOGI PETRONAS
Bandar Seri Iskandar, 31750 Tronoh
Perak Darul Ridzuan, Malaysia.

Date: 16th August, 2011

ACKNOWLEDGEMENT

Bismillaahirrohmaanirrohiim

Alhamdulillah, thank to Allah for giving me strength, health, patience and knowledge to complete this study.

The acknowledgement is due to the Universiti Teknologi PETRONAS for the support given to this research through its excellent facilities and for granting me the opportunity to pursue my graduate studies with financial support under Graduate Assistantship (GA) schemes and Short Term Internal Research Funding (STIRF).

I acknowledge, with deep gratitude and appreciation, the inspiration, encouragement, valuable time and guidance given to me by Dr. Syed Ihtsham ul Haq Gilani as my supervisor. Thereafter, I am deeply indebted and grateful to Dr. Mohd. Shiraz Aris as my co-supervisor. Finally, I would also like to thank everyone who has directly or indirectly contributed towards this research work, especially my parents, my beloved wife, family, friends, colleagues, Postgraduate Study Programme staff members, Mechanical Engineering Department staff members, and others.

ABSTRACT

This study presents a sizing methodology to optimize photovoltaic array and battery storage in a standalone photovoltaic (PV) system with lighting load. Sizing using the deterministic method was carried out for initial design. Stochastic method by mean of Loss of Power Supply Probability (LPSP) calculation was developed using daily weather data input. The weather data consists of ambient temperature, relative humidity and solar radiation. An estimation method of hourly solar radiation data is also developed in this study to complete any missing solar radiation data in the dataset. Then, complete time-series dataset can be used for LPSP calculation and system simulation. Size optimization was carried out using a graphical method. System size was optimized based on desired system performance (indicated by LPSP value) and minimum cost that consist of Capital Cost and Life-cycle cost. In addition, Excess energy value is used as over-design indicator. A comparison of sizing optimization methods was carried out, and it was found that the design space approach giving flexibility in the selection of PV panel and battery capacity compared to other methods. The sizing result of this method is a configuration of 500Wp PV array and 400Ah battery. Economic analyses, including cost of the energy and payback period for selected configuration are studied. A simulation model was developed using TRNSYS 16 to test the sizing results. Experimental data was used to validate the simulation results. Simulation validation shows that result accuracy has improved. The results indicated that Root Mean Square Error (RMSE) between simulated and measured battery voltage has decreased by 50% compared to previous work. The validated simulation model then was used to test and analyse the selected PV system configuration.

ABSTRAK

Kajian ini membentangkan satu kaedah pensaihan bagi mengoptimumkan kapasiti photovoltaik array dan bateri dalam sistem photovoltaik (PV) sendiri dengan beban lampu. Pensaihan untuk reka bentuk awal telah dilakukan menggunakan kaedah penentuan. Kaedah stokastik dengan pengiraan min Kebarangkalian Lesapan Bekalan Kuasa (KLBK) telah dihasilkan dengan menggunakan input data cuaca harian. Data cuaca terdiri daripada suhu sekeliling/ambien, kelembapan dan sinaran suria. Satu kaedah anggaran data radiasi solar secara jam juga dihasilkan dalam kajian ini untuk melengkapkan mana-mana kehilangan data radiasi solar di dalam set data itu, seterusnya, set data siri -masa yang lengkap itu boleh digunakan untuk pengiraan KLBK dan simulasi sistem. Pengoptimuman saiz telah dijalankan menggunakan kaedah grafik. Sistem saiz dioptimumkan berdasarkan prestasi sistem, yang ditunjukkan oleh nilai KLBK, dan minimum kos yang terdiri daripada Kos Modal dan Kos Kitaran Hayat. Nilai tenaga lebihan digunakan sebagai penunjuk reka bentuk lampau. Perbandingan kaedah-kaedah pengoptimuman saiz telah dijalankan pada sistem PV yang dicadangkan dan telah didapati bahawa pendekatan reka bentuk ruang memberikan fleksibiliti pemilihan kapasiti PV panel dan bateri dibandingkan dengan kaedah-kaedah yang lain. Keputusan yang menggunakan kaedah ini adalah konfigurasi tatasusunan PV 500Wp dan kapasiti bateri 400Ah. Analisis ekonomi termasuk kos tenaga dan tempoh bayar balik untuk konfigurasi yang terpilih dikaji. Satu model simulasi dibangunkan menggunakan TRNSYS 16 untuk menguji keputusan pensaihan. Data eksperimen digunakan untuk mengesahkan hasil simulasi. Pengesahan simulasi menunjukkan bahawa ketepatan hasil telah bertambah baik. Hasil pengesahan menunjukkan Ralat Punca Mean Kuasa Dua antara voltan bateri yang disimulasikan dan diukur telah menurun sebanyak 50% berbanding dengan kerja sebelumnya. Model simulasi yang disahkan kemudiannya digunakan untuk menguji dan menganalisis konfigurasi sistem PV yang terpilih.

In compliance with the terms of the Copyright Act 1987 and the IP Policy of the university, the copyright of this thesis has been reassigned by the author to the legal entity of the university,

Institute of Technology PETRONAS Sdn Bhd.

Due acknowledgement shall always be made of the use of any material contained in, or derived from, this thesis.

© Dimas Firmanda Al Riza, 2011
Institute of Technology PETRONAS Sdn Bhd
All rights reserved.

TABLE OF CONTENTS

STATUS OF THESIS.....	i
APPROVAL PAGE.....	ii
TITLE PAGE.....	iii
DECLARATION OF THESIS	iv
ACKNOWLEDGEMENT	v
ABSTRACT.....	vi
ABSTRAK.....	vii
COPYRIGHT PAGE	ix
TABLE OF CONTENTS.....	xi
LIST OF FIGURES	xiv
LIST OF TABLES.....	xviii
LIST OF ABBREVIATIONS.....	xx
NOMENCLATURES	xxi
CHAPTER 1 INTRODUCTION	1
1.1 Research overview	1
1.2 Problem statements.....	5
1.3 Research objectives	7
1.4 Scope of study	7
1.5 Thesis outline	8
CHAPTER 2 LITERATURE REVIEW	9
2.1 Solar radiation model	9
2.1.1 Extraterrestrial radiation and solar radiation geometry	9
2.1.2 Terrestrial solar radiation.....	12
2.1.3 Parametric and meteorological model for solar radiation estimation.....	13
2.1.4 Decomposition model of solar radiation on horizontal surface	16
2.1.5 Solar radiation on the tilted surface	19
2.2 Peak Sun Hour (PSH) concept	21
2.3 PV system sizing and optimization	22
2.3.1 Deterministic method.....	22
2.3.2 Stochastic method	24

2.3.3	PV system sizing optimization.....	26
2.4	Available modeling software.....	29
2.4.1	Solar radiation model.....	29
2.4.2	PV array model	29
2.4.3	Charge controller model	30
2.4.4	Battery and load model	31
2.5	Summary	32
CHAPTER 3 METHODOLOGY		35
3.1	Initial design using deterministic method	35
3.1.1	Solar radiation availability	35
3.1.2	Malaysian typical terraced house load profile	37
3.1.3	Calculation procedure	38
3.2	Data Preparation for LPSP calculation.....	40
3.2.1	Missing data estimation	43
3.2.2	Atmospheric transmittance determination procedure: Method 1.....	45
3.2.3	Atmospheric transmittance determination procedure: Method 2.....	46
3.2.4	Statistical techniques to validate the model	47
3.2.5	Data required for LPSP calculation	48
3.3	Daily data based LPSP calculation procedure.....	50
3.3.1	Global solar irradiance received on the tilted surface data generation.....	51
3.3.2	PV panel power output calculation procedure	52
3.3.3	Estimation of daily battery condition.....	54
3.3.4	Daily analysis of PV system behavior	56
3.4	Sizing optimization of the PV system	60
3.5	PV panel Characterization in actual condition	63
3.6	PV system for residential lighting	64
3.6.1	System Installation.....	64
3.6.2	Load used in the experiment	66
3.7	Measurement System Set-up	67
3.7.1	Data logger.....	68
3.7.2	Sensor.....	68
3.7.3	Power source.....	70
3.7.4	Ambient Temperature and Relative Humidity Sensor Circuit.....	71
3.7.5	Low-cost naturally aspirated radiation shields design.....	71
3.8	PV panel efficiency calculation from measured data	73
3.9	Modeling and simulation.....	73
3.9.1	Component selection.....	75
3.9.2	Simulation setting	75
3.10	Summary	76
CHAPTER 4 RESULTS AND DISCUSSIONS.....		77
4.1	Initial design results.....	77
4.1.1	Solar radiation availability data	77
4.1.2	Calculation results.....	79
4.2	Missing data estimation results	81
4.2.1	Calculation results and statistical analysis.....	81
4.2.2	Selected results (Method 1)	83

4.2.3	Final estimation results and discussion.....	85
4.3	Solar radiation on the tilted surface calculation results.....	86
4.4	Sizing and optimization results	89
4.4.1	Calculation results.....	90
4.4.2	Sizing curve and optimization	92
4.4.3	Analysis for selected configuration	96
4.4.4	Economic evaluations	98
4.5	Experimental results	99
4.5.1	PV panel's I-V curve	100
4.5.2	Charge controller performance	101
4.5.3	PV panel efficiency.....	102
4.5.4	Weather parameter, energy input and output of the system.....	104
4.5.5	PV panel and Battery voltage monitoring.....	105
4.6	Simulation results.....	107
4.6.1	Simulation validation results.....	107
4.6.2	Simulation for selected configuration.....	113
4.7	Summary	117
CHAPTER 5 CONCLUSIONS AND RECOMMENDATIONS		119
5.1	Conclusions	119
5.2	Directions for future works	120
5.4	Publications	120
REFERENCES		122
APPENDICES		
A. Residential House Load Profile Details		
B. Daily-data based LPSP calculation algorithm		
C. Electricity Tariff for Domestic Costumer		
D. PV System Specification		
E. Simulation Setting		
F. Experimental Results		

LIST OF FIGURES

Fig. 1.1: Oil and gas production profiles 2008 base case	1
Fig. 1.2: Oil production and consumption of Malaysia	2
Fig. 1.3: Malaysia energy demand by sources in 2008.....	3
Fig. 1.4: Malaysia energy mix	3
Fig. 1.5: Malaysia electrical energy sales by sector in 2008	4
Fig. 2.1: The hour angle (ω) is defined as the angle between the meridian parallel to sun rays and the meridian containing the observer	10
Fig. 2.2: Zenith angle, slope, surface azimuth angle, solar azimuth angle for tilted surface, plan view showing solar azimuth angle.....	11
Fig. 2.3: Section of earth showing angle for south facing surface.....	11
Fig. 2.4: Solar Irradiance component.....	12
Fig. 2.5: Diffuse ratio/fraction vs. clearness index	16
Fig. 2.6: PSH (Peak Sun Hour).....	21
Fig. 2.7: Global Solar Power Map	22
Fig. 2.8: Contour plot for different size combinations of solar array and battery at different LPSP values	26
Fig. 2.9: Optimum solution configuration by mean of minimum capital cost.....	27
Fig. 2.10: Sizing curve by design space approach	28
Fig. 2.11: Equivalent circuit model for PV arrays	31
Fig. 2.12: Battery model (Voltage-SOC relation).....	33
Fig. 3.1: Global Solar Power Map for South East Asia	36
Fig. 3.2: PSH obtained from measured data in Bandar Sri Iskandar (5 May 2010).....	36
Fig. 3.3: Load Profile of typical Malaysian Residential House.....	38

Fig. 3.4: Life Cycle vs <i>DoD</i> of deep cycle battery	39
Fig. 3.5: One year hourly solar radiation data with 23 days missing data	41
Fig. 3.6: Complete hourly data of RH and ambient temperature.....	42
Fig. 3.7: Measured solar radiation data from UTP solar laboratory (5 July 2010).....	42
Fig. 3.8: Flow chart to estimate Solar Irradiation from limited meteorological data	45
Fig. 3.9: Scatter plot of Relative humidity and Clearness Index of the data obtained from local meteorological office	46
Fig. 3.10: Linear, quadratic and cubic regression results of Beam transmittance vs RH with limitation	47
Fig. 3.11: Energy balance description in PV system	50
Fig. 3.12: Procedure to calculate solar radiation on the tilted surface	52
Fig. 3.13: Graphical comparison of $\overline{T_{cell}}$ estimation in the month of June 2010.....	53
Fig. 3.14: Self discharge characteristic curve of lead acid battery	55
Fig. 3.15: Discharge characteristic curve of lead acid battery	55
Fig. 3.16: Daily cycle of PV system description	57
Fig. 3.17: Daily variation of battery condition description.....	58
Fig. 3.18: Simplified flow chart to calculate LPSP	59
Fig. 3.19: Solar Panel testing configuration	63
Fig. 3.20: PV panel I-V curve at STC.....	65
Fig. 3.21: Solar Power System installed	65
Fig. 3.22: Solar Power System scheme.....	66
Fig. 3.23: Measurement system configuration.....	67
Fig. 3.24: Picolog 1216 input module.....	68
Fig. 3.25: Kipp & Zonen Pyranometer SPLite series	68

Fig. 3.26: RH sensor and typical application circuit.....	69
Fig. 3.27: LM 35 Temperature sensor and typical application circuit.....	69
Fig. 3.28: HTFS 200 current transducer and typical application scheme.....	70
Fig. 3.29: USB cable.....	70
Fig. 3.30: RH measurement circuit configuration	71
Fig. 3.31: Hand-made radiation shields.....	72
Fig. 3.32: Sensor placement inside the radiation shield	72
Fig. 3.33: Standalone PV system components.....	73
Fig. 3.34: Solar Power System modeling in TRNSYS 16.....	75
Fig. 4.1: Measured PSH from Ipoh weather station on 2003	77
Fig. 4.2: Measured PSH in Bandar Seri Iskandar from May to December 2010	78
Fig. 4.3: Monthly averaged PSH value comparison between Ipoh data and Bandar Seri Iskandar on-site measurement	79
Fig. 4.4: PV panel sizing curve based on deterministic method.....	79
Fig. 4.5: Battery sizing curve for DoD = 50% and $V_{rated} = 12V$	80
Fig. 4.6: Scatter plot of measured and predicted solar radiation	82
Fig. 4.7: Graphical comparison of predicted (all radiation components) and measured solar radiation on random dates using Method 1	83
Fig. 4.8: Graphical comparison measured and predicted (Method 1)	85
Fig. 4.9: Estimation results of missing measured data on 25 March – 13 April (Method 1).....	85
Fig. 4.10: Complete one year hourly solar radiation data set	86
Fig. 4.11: TRNSYS simulation results for total solar radiation received on the tilted surface for one year using Reindl and Perez model.....	87
Fig. 4.12: Monthly total radiation on the tilted surface	88
Fig. 4.13: PSH on the tilted surface	89

Fig. 4.14: LPSP surface graphic	90
Fig. 4.15: Excess energy surface graphic	91
Fig. 4.16: Capital cost surface graphic	91
Fig. 4.17: LCC surface graphic.....	92
Fig. 4.18: Sizing curve based on minimum Capital cost and LCC on desired LPSP.....	93
Fig. 4.19: Design space approach results.....	94
Fig. 4.20: Design space (zoom) option 1 and 2	94
Fig. 4.21: Daily excess and losses energy for configuration obtained using deterministic method	96
Fig. 4.22: Daily excess and losses energy for design space option 1 configuration	96
Fig. 4.23: Daily SOC of the battery for deterministic method results	97
Fig. 4.24: Daily SOC of the battery for design space approach (option 1) results	97
Fig. 4.25: Schematic Diagram of Standalone PV system.....	99
Fig. 4.26: I-V curve characteristics of PV panel for different solar radiation level	100
Fig. 4.27: Power curve characteristics of PV panel for different solar radiation level	101
Fig. 4.28: Solar Charge Controller output compared with power curve	102
Fig. 4.29: Effect of Solar radiation and cell temperature on PV panel Efficiency (30 June 2010).....	103
Fig. 4.30: Monitored solar radiation on the site 1-5 July 2010 (5 min. time step)	104
Fig. 4.31: Ambient Temperature and Relative Humidity on the site 1-5 July 2010 (5 min. time step).....	104
Fig. 4.32: Power in and out of the battery 1-5 July 2010 (5 min. time step).....	105
Fig. 4.33: PV panel and battery voltage 1-5 July 2010 (5 min. time step).....	106

Fig. 4.34: Battery voltage 1-5 July 2010 (5 min. time step).....	106
Fig. 4.35: Weather data used as the input for simulation	108
Fig. 4.36: Measured Power in and out to/from battery to validate the simulation	108
Fig. 4.37: Measured battery voltage to validate the simulation.....	108
Fig. 4.38: Parameter setting in TRNSYS 16 simulation studio	109
Fig. 4.39: Running simulation in TRNSYS simulation studio	109
Fig. 4.40: Comparison between measured and simulated panel output.....	110
Fig. 4.41: Scatter plot of measured and simulated panel output.....	110
Fig. 4.42: Comparison between measured and simulated battery voltage.....	111
Fig. 4.43: Scatter plot of measured and simulated battery voltage.....	111
Fig. 4.44: Simulation results of FSOC (A-E points refer to Fig. 4.33).....	112
Fig. 4.45: Print screens of TRNSYS 16 simulation studios.....	113
Fig. 4.46: Simulation results: PV panel output power (Full simulation).....	114
Fig. 4.47: Simulation results: PV panel output power	114
Fig. 4.48: Load setting in the simulation	115
Fig. 4.49: Simulation results: Power input and Output (Full simulation).....	115
Fig. 4.50: Simulation results: Power input and Output.....	116
Fig. 4.51: Simulation results: Battery voltage monitoring.....	116
Fig. 4.52: Simulation results: Battery voltage monitoring (Full Simulation).....	117
Fig. 4.53: Simulation results: Battery SOC	117
Fig. 4.54: Simulation results: Battery SOC (Full simulation)	118

LIST OF TABLES

Table 1.1: Distribution of lighting and air-conditioning energy consumption in Malaysian Buildings (%).....	4
Table 2.1: List of several existing meteorological model	14
Table 2.2: List of several models to calculate r_d	20
Table 2.3: PV software classification 1	29
Table 2.4: PV software classification 2	30
Table 3.1: Residential House Energy Consumption (adapted from	37
Table 3.2: Determination criteria of beam transmittance by mean of RH	44
Table 3.3: System parameter value used for calculation	49
Table 3.4: Component costs and parameters used in <i>LCC</i> analysis	61
Table 3.5: <i>LCC</i> calculation example (400Wp PV panel- 864Ah battery).....	62
Table 3.6: Experimental load list.....	66
Table 3.7: Load treatment list.....	67
Table 3.8: Measurement system component list	67
Table 4.1: PV panel size calculation	80
Table 4.2: Battery Size Calculation.....	81
Table 4.3: Statistical analysis results comparison	82
Table 4.4: Monthly total irradiation on the tilted surfaces (simulation results) using Reindl model.....	88
Table 4.5: Comparison of sizing optimization results.....	95
Table 4.6: Economic analysis results	99

LIST OF ABBREVIATIONS

AC	Alternating current
ACC	Annualized Capital Cost
AES	Annual Energy Services
Ah	Ampere hour
ALCC	Annual Life Cycle Cost
AM	Air Mass
AMC	Annualized Maintenance and operation cost
BIPV	Building Integrated Photovoltaic
CC	Capital Cost
COE	Cost of Energy
CRF	Capital Recovery Factor
DC	Direct current
DoD	Depth of discharge
FSOC	Fractional State of Charge
GA	Genetic Algorithm
GDP	Gross Domestic Product
GST/VAT	Goods and Services Tax/Value added Tax
IC	Integrated Circuit
LCC	Life cycle cost
LLP/LOLP	Loss of Power Probability
LOLE	Loss of Energy Probability
LPS	Loss of Power Supply
LPSP	Loss of Power Supply Probability
LVD	Low Voltage Disconnect
MPPT	Maximum Power Point Tracking
NRMSE	Normalized Root Mean Square Error
PC	Personal Computer
PP	Payback Period
PSH	Peak Sun Hour
PV	Photovoltaic
PWM	Pulse Width Modulation
RH	Relative Humidity
RM	Ringgit Malaysia
RMSE	Root Mean Square Error
SAPV	Standalone Photovoltaic
SOC	State of charge
STC	Standard Test Condition
TRNSYS	Transient System Simulation program
USB	Universal Serial Bus
UTP	Universiti Teknologi PETRONAS

NOMENCLATURES

Symbol	Meaning
α	Solar altitude angle
α_{PV}	Price per PV panel
β	Surface slope
β_{batt}	Price of Battery
γ	Surface azimuth angle
γ_s	Solar azimuth angle
γ_t	Negative temperature coefficient
ΔT	Ambient temperature difference
δ	Declination
η_{actual}	Calculated PV panel efficiency
η_{batt}	Charging efficiency
η_c	Connection losses and dust factor
η_{inv}	Inverter efficiency
η_{STC}	PV panel efficiency at STC
η_{self}	Self discharge coefficient
θ	Angle of incidence
θ_z	Zenith angle
ρ_{gr}	Ground reflectivity coefficient
$\sigma(T)$	Temperature dependent correction factor
τ	Beam transmittance
ϕ	Latitude
ω	Hour angle
A	Sum of money for uniform present value
AES	Annual energy service
ALCC	Annualized life cycle cost
A_{PV}	PV panel area (datasheet)
A_{total}	Total area of the panel
a	Elevation of the site
C_0	Other Cost
C_{bat}	Battery capacity
CC	Capital Cost
COE	Cost of energy
CRF	Capital recovery factor
DoD	Depth of Discharge
d	Index of agreement
E	Factor accounting for the eccentricity of the earth's orbit
$E_{B(n)}$	Battery energy on the day n
$E_{B(n-1)}$	Battery energy on the day $n-1$
$E_{Bhalf(n)}$	Battery energy on the half of day n
E_{Bmax}	Battery maximum energy
E_{Bmin}	Battery minimum energy
$E_{L(n)}$	Load energy on the day n

Symbol	Meaning
$E_{PV(n)}$	PV panel energy output
F	Sum of money for single present value
\bar{G}	Daily averaged solar radiation
G_{0h}	Extraterrestrial solar radiation on horizontal surface
G_{actual}	Measured solar radiation
G_{Bh}	Solar beam radiation on horizontal surface
G_{Bp}	Solar beam radiation on perpendicular surface
G_{Dh}	Solar diffuse radiation on horizontal surface
G_{Rh}	Solar reflected radiation on horizontal surface
G_{STC}	Solar radiation at STC
G_{sc}	Solar Constant
G_{Th}	Total solar radiation on horizontal surface
G_{Tt}	Total solar radiation on the tilted surface
h_c	Current hour
I	Current
I_d	Discount rate
k_d	Diffuse fraction
k_T	Clearness Index
LCC	Life cycle cost
LPSP	Loss of Power Supply Probability
LPS(n)	Loss of Power Supply on the day n
M	Maintenance Cost
m	Optical mass number
N_a	Number of autonomy days
N_{batt}	Number of battery
N_{cd}	Maximum number of charge–discharge cycles at 25°C and X DoD
N_d	Number of the day in the year
N_{PV}	Number of PV panel
NRMSE	Normalized root mean square error
n	Number of data
n_{cd}	Number of charge–discharge cycles per year
P	Power
PB	Payback period
PSH	Peak Sun Hour
PSH_t	Peak Sun Hour on the tilted surface
P_{PV}	Nominal peak power of PV panel
P_a	Atmospheric pressure
P_{actual}	Measured PV panel output
P_{load}	Load power
P_s	Single present value
P_u	Uniform present value
R	Resistance
R^2	Coefficient of determination
RR	Repair and Replacement Cost
RH	Relative humidity

Symbol	Meaning
RMSE	Root mean square error
r	Pearson correlation coefficient
r_b	Ratio of beam radiation on the tilted surface to horizontal surface
r_d	Ratio of diffuse radiation on the tilted surface to horizontal surface
r_r	Ratio of ground reflected radiation incident on the tilted surface
r_s	Solar radius vector
S	Salvage value
SOC	State of Charge
$\overline{T_{cell}}$	PV cell daily averaged temperature
$\overline{T_{amb}}$	Daily averaged ambient temperature
t_3	Battery life time
V	Voltage
V_{rated}	Rated voltage
x_i	Predicted variable
\bar{x}_i	Averaged predicted variable
y_i	Measured variable
\bar{y}_i	Averaged measured variable
Y_c	Predicted variable
Y_0	Measured variable
Y_{max}	Maximum measured data
Y_{min}	Minimum measured data

CHAPTER 1

INTRODUCTION

1.1 Research overview

Life on Earth is driven by energy. It is a fact that human activities and most sustainability issues are closely related to energy use. Energy is one of the basic needs of human life. Fossil fuels are the main energy source used by humans to achieve rapid technological developments to date. Since the industrial revolution in the mid-18th century, agriculture, manufacturing, mining, transportation and technology have been growing rapidly [1]. This development is inseparable from the use of fossil fuels that was heavily mined either in the form of coal, oil, or gas. Fossil fuels are non-renewable-energy sources. It is predicted that fossil energy sources would peak in about 2011 and will decrease thereafter as presented in Fig. 1.1 [2]. Furthermore, the use of fossil fuel pollutes the environment and contributes to global warming.

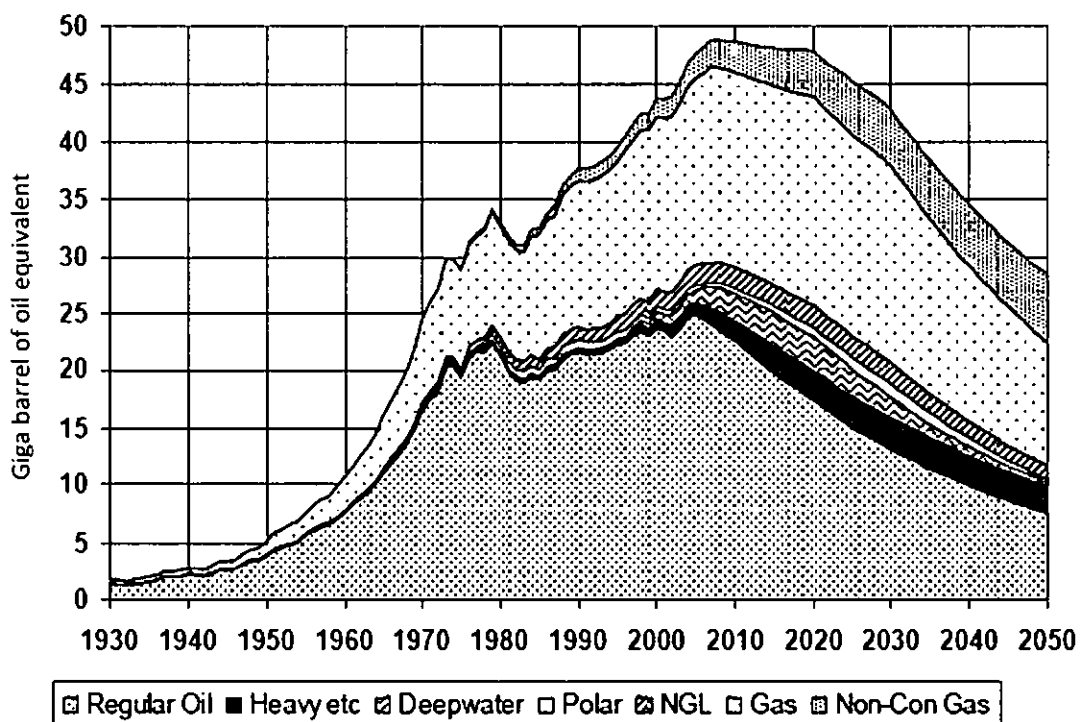


Figure 1.1: Oil and gas production profiles 2008 base case [3]

Meanwhile, the human population continues to increase, which would certainly lead to an increase of energy demand. Therefore, alternative and clean energy source is needed to ensure sustainable development.

Follow the trends happening in the world, Malaysia, as one of the oil-producing countries will be greatly affected by shortages of fossil fuels. In the near future, Malaysia is expected to be a net importer of oil, and the nation will have to live up to issues related to the security of supply and their economic consequences [4]. It is also anticipated that the energy demand for the country would increase with the increase in population and Gross Domestic Product (GDP). Based on the current economic growth rates, Pusat Tenaga Malaysia has projected that Malaysia would become a net importer of energy between 2010 and 2015 [5].

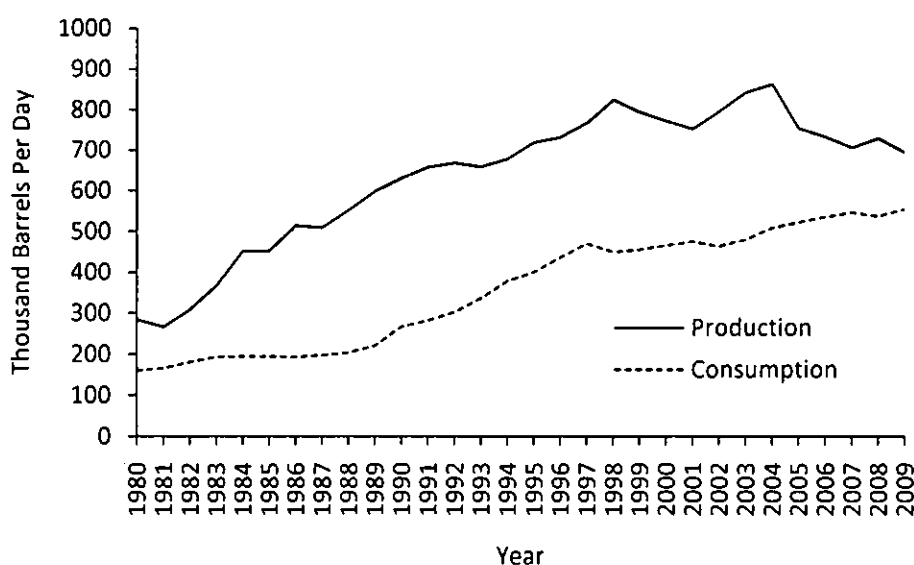


Figure 1.2: Oil production and consumption of Malaysia (adapted from [6])

It is seen in Fig. 1.2, the gap between oil production and consumption of Malaysia are narrowing and if this condition is continuing, the breakeven point will occur soon. Therefore, further emphasis that is given into the diversification of energy resources becomes important to overcome the situation. One method is the exploitation of renewable energy, which can also minimize the effects of global warming. Although technology and design play an important role, individual energy consumption patterns also have a great impact on reducing the national energy demand. Consequently, energy-saving initiatives need to be practiced within the society.

One of the major uses of fossil fuels is for electricity power generation. In terms of source, petroleum products constituted about 54% of energy demand in 2008 followed by natural gas (24%), electricity (18%) and coal and coke (4%), as shown in Fig. 1.3 [7]. Electrical energy sources in Malaysia are dominated by fossil fuels as seen in Fig. 1.4. The contribution of renewable energy is still insignificant.

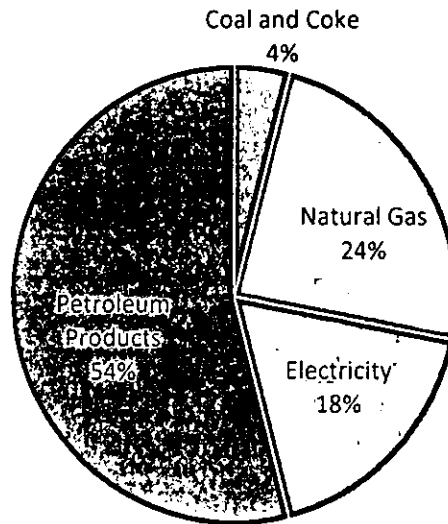


Figure 1.3: Malaysia energy demand by sources in 2008 (adapted from [7])

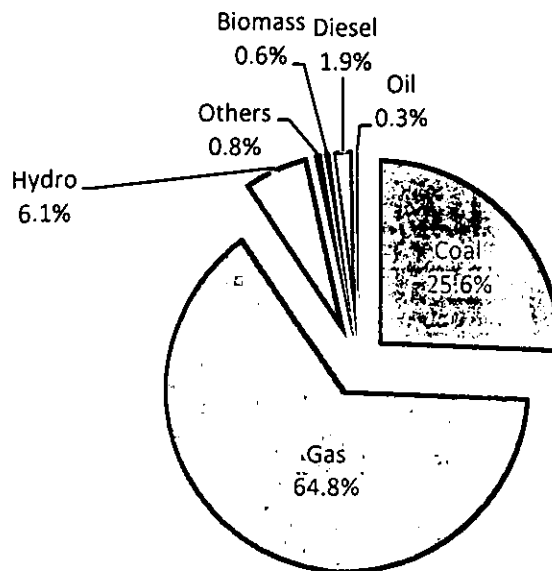


Figure 1.4: Malaysia energy mix (adapted from [8])

Fig. 1.5 shows electrical energy sales by sector in Malaysia, which is dominated by industrial sector, follow by commercial sector and residential sector. As one of the

three main energy consumers, application of renewable energy and energy efficiency initiatives will significantly affect country energy demand.

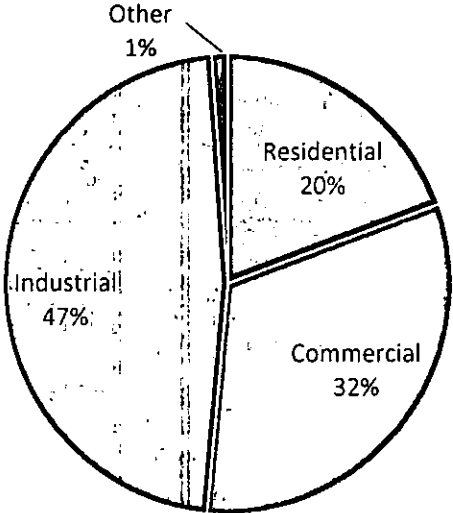


Figure 1.5: Malaysia electrical energy sales by sector in 2008 (adapted from [9])

Table 1.1 shows the distribution of energy consumption in Malaysian buildings [10], which shows in residential building the average lighting energy consumption could be higher than air-conditioning energy consumption since air-conditioning systems are not widely used as lighting in residential building in Malaysia. The energy consumption for lighting in Malaysia is about 25 - 35% of the total energy supplied to buildings [11].

Table 1.1: Distribution of lighting and air-conditioning energy consumption in Malaysian Buildings (%) [10]

	Residential	Hotels	Shopping Complexes	Offices
Lighting	25.3	18	51.9	42.5
Air-Conditioning	8.3	38.5	44.9	51.8
Total	33.6	56.5	96.8	94.3

There is an opportunity to implement energy-efficiency initiatives and renewable-energy application for the residential lighting case. Solar energy may become the most potential renewable-energy resources for this case since it is abundant everywhere in Malaysia.

Photovoltaic (PV) systems, especially standalone PV systems, are becoming a popular renewable-energy system for rural applications in Malaysia. More than 90% of installed PV systems in Malaysia are standalone applications. Standalone applications are mainly for rural electrification and non-building structures [12]. Current developments in PV technology, however, have improved the commercial viability and point towards higher demand in future residential applications. Hence, investigation and improvement of this kind of system for application are necessary.

An appropriate supply and demand matching exercise is required to convince potential investors. Here, the sizing and analysis tools are important features, which can strengthen the reliability of PV system. Sizing is an essential part of solar PV system design to ensure reliability of the system. Sizing considers reliability of energy supply by ensuring the number of solar modules used to capture solar energy and the capacity of the batteries for energy storage is sufficient.

Among the current approaches used for modeling and sizing PV system, include the use of the deterministic, stochastic, empirical, and statistical model. Deterministic methods are sometimes chosen because of its simplicity, but it will be only suitable for an initial design or quick estimate. Due to the stochastic nature of solar radiation as the resource of the system, results that are more sophisticated will be obtained by using the statistical method. The Loss of Power Supply Probability (LPSP) calculation is one of the statistical approaches used in PV system sizing. In this study, sizing algorithm of daily-data-based LPSP calculation was developed. Optimization was carried out using LPSP, Capital Cost (CC), Life-cycle Cost (LCC) and Excess energy value as design criteria. Transient system modeling was carried out to test the sizing result and investigate the transient behavior of standalone PV system. This study is focusing on a standalone PV system application for residential lighting in Malaysia.

1.2 Problem statement

With increasing of population, the number of houses will be increasing as well as energy demand for the residential sector. This shows the potential of PV system application in the residential sector will also increase. Various appliances are used in

the house. Lighting is one of the primary appliances used in the house. Lighting energy demand also have unique characteristic, that it operational hours are only during the night when solar radiation is not available. That is why residential lighting is interesting to take as a study case in this research for PV system application.

Sizing optimization of PV panel and battery is an essential task for standalone photovoltaic system application. Sizing using the deterministic method can be used for location where solar radiation data is unavailable. On the other hand, stochastic method is used for more accurate and satisfying results. However, time-series data is required to apply this method. Loss of Power Supply Probability (LPSP) calculation is one example of the stochastic method. At least one-year hourly or daily time step data is required to perform the LPSP calculation. Simulation method using hourly data in LPSP calculations may be able to provide detail information of the system, but the availability and amount of the data can sometimes add constraints in its implementation. Daily data can be used for LPSP calculation, but sometimes it does not provide sufficient information as hourly data. Therefore, there is an opportunity to improve LPSP calculation method using daily data to provide more information required for sizing optimization. By using the algorithm that is developed in the present study, it is expected to obtain more information from LPSP calculation using daily data for better sizing optimization results.

Although numerous research works have been dedicated to the enhancement of PV system sizing strategies, issues related to availability of data still pose a challenge to the researchers. A complete time series solar radiation data is significant for performance prediction. However, solar radiation data sometimes unavailable for the location, even there is a nearby weather station, not all people can access the data. Furthermore, the data recording may be missing some data due to unavoidable circumstances. Therefore, missing data estimation is required in order to utilize the data set for various purposes. A method to estimate missing solar radiation data in a weather data set was presented in this study.

Transient modeling is required to test the performance of sizing results and further simulate PV system in various hypothetical conditions. There are some software that can be used to model, simulate and estimate photovoltaic system performance. In this

study, modeling of standalone PV system was carried out using TRNSYS 16 and validated using experimental data.

1.3 Research objectives

The main objectives of the research are to develop a sizing optimization methodology of standalone PV system for residential lighting and to verify the method using transient model simulation that is validated using experimental data. These main objectives are achieved by following methods:

- i. Prepare complete weather data as input for LPSP calculation algorithm and simulation model by develop solar radiation estimation method, using available meteorological data to fill missing data in hourly solar radiation data set.
- ii. Develop a daily data based LPSP calculation algorithms for standalone PV system (SAPV) for residential lighting load.
- iii. Carry out sizing optimization of SAPV system using LPSP value as performance indicator and system cost.
- iv. Carry out performance and economic analysis of selected configuration.
- v. Develop simulation model of SAPV system in TRNSYS 16.
- vi. Establish experimental set-up to monitor the performance of SAPV system in actual condition for simulation model validation.
- vii. Validate simulation model using experimental data.
- viii. Test and analyze sizing optimization results using simulation model.

1.4 Scopes of study

The scopes of the research are described as follow:

- a. Data estimation is carried out for hourly solar radiation based on data from Ipoh weather station and data from Universiti Teknologi PETRONAS weather station.
- b. The system investigated in this study is standalone PV system with battery storage.

- c. Load for the PV system is typical Malaysian residential lighting load, the load assumed to be constant over the year.
- d. Experimental load used in the research is DC load.
- e. LPSP calculation is carried out using daily weather data.
- f. Optimization performed based on LPSP, excess energy, capital cost and LCC value, using design space approach.

1.5 Thesis outline

The thesis is arranged as follows:

Chapter 1 provides the research overview, problem statement, objectives, general methodology, scopes of the study, and thesis outline.

Chapter 2 details the literature review, consist of literature review of PV system sizing and optimization, solar radiation modeling and estimation, PV system modeling and some theory used in this study

Chapter 3 gives details methodology of data preparation, solar radiation estimation procedure, LPSP calculation algorithm formulation, optimization procedure, economic analysis procedure, simulation model in TRNSYS 16 and establishing experimental set-up.

Chapter 4 presents data estimation results, calculation results, optimization results experimental results, simulation results and analysis.

Chapter 5 concludes the research, provides a summary of key findings, and gives suggestions for future research.

CHAPTER 2

LITERATURE REVIEW

This chapter presents a review of previous works related to this research. The literature reviews here consists of models of solar radiation, sizing optimization methods and PV system modeling. The chapter will begin with solar radiation model reviews include basic of solar radiation, parametric model, meteorological model, decomposition model and solar radiation on the tilted surface model. In sizing optimization part, deterministic and stochastic sizing methods were reviewed. The PV system modeling reviews here consist of the available modeling software and specific components model in TRNSYS 16 that were used for standalone PV system model.

2.1 Solar radiation model

The solar radiation models have been discussed in numerous literatures [13-14]. However, this sub-chapter only discusses and reviews material that is related to this research. The review was written sequentially in accordance with methodology steps that carried out by the author.

Generally, solar radiation model can be classified into two categories, parametric model, and decomposition model [15]. Parametric models require detail information of atmospheric conditions. Some parametric models use meteorological data as predictors. Decomposition models only use global solar radiation data to predict the beam and sky components [15]. Both models require information of extraterrestrial radiation and solar radiation geometry. Therefore, the following reviews will explain first about extraterrestrial radiation and solar radiation geometry, and then discuss both of solar radiation models.

2.1.1 Extraterrestrial radiation and solar radiation geometry

Extraterrestrial radiation is the radiation received on the atmosphere of the earth. Extraterrestrial radiation value is changed due to earth-sun motion. The variation of extraterrestrial radiation due to the motion of the earth described in Eq. 2-1 as follows [16]:

$$G_{0h} = G_{sc} \cdot r_s \cdot \sin(\alpha) \quad (2-1)$$

G_{0h} is the total radiation falling on the atmosphere on horizontal surface (extraterrestrial radiation), G_{sc} is the solar constant equal to 1367 (W/m^2), r_s is the solar radius vector (to be assumed 1) [17]. α is the solar elevation or altitude angle, the solar altitude angle is calculated from following equation [14]:

$$\sin(\alpha) = \sin(\phi)\sin(\delta) + \cos(\phi)\cos(\delta)\cos(\omega) \quad (2-2)$$

ϕ is the latitude of the location, δ is the sun's declination angle, and ω is the solar hour angle, δ and ω are calculated from Eq. 2-3 and 2-4 as follow [3, 17 and 18]:

$$\sin(\delta) = 0.39795 \cos[0.98563(N_d - 1)] \quad (2-3)$$

$$\omega = 15(h_c - 12) \quad (2-4)$$

N_d is the day of the year and h_c is the current hour. Fig. 2.1 shows the description of hour's angle and Fig. 2.2 and 2.3 shows the description of the angles on tilted surface.

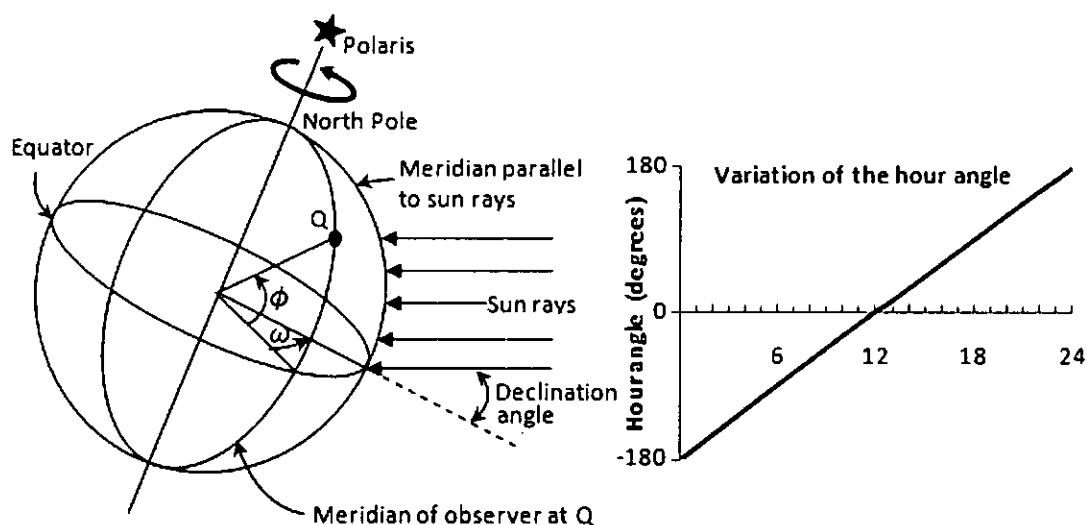


Figure 2.1: The hour angle (ω) is defined as the angle between the meridian parallel to sunrays and the meridian containing the observer [18]

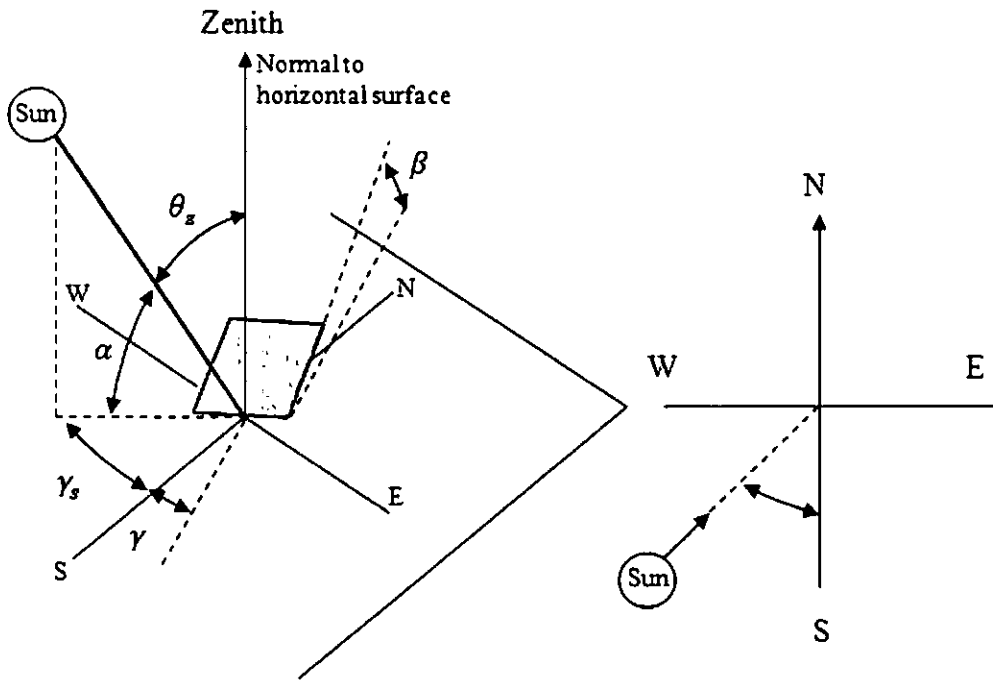


Figure 2.2: Zenith angle, slope, surface azimuth angle, solar azimuth angle for tilted surface, plan view showing solar azimuth angle [14]

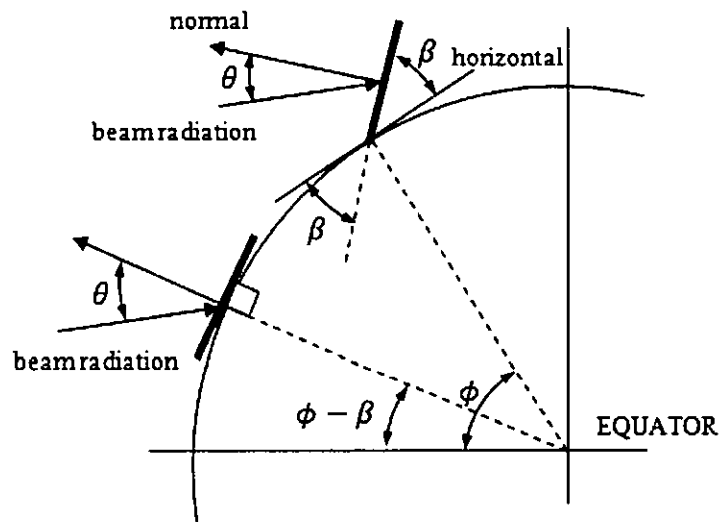


Figure 2.3: Section of earth showing angle for south facing surface [14]

The total extraterrestrial radiation between hour angles ω' and ω'' is calculated from Eq. 2-5 as follows [19]:

$$G_{0h_{\omega'}} = \int_{\omega'}^{\omega''} G_{sc} E (\sin(\phi) \sin(\delta) + \cos(\phi) \cos(\delta) \cos(\omega)) d\omega \quad (2-5)$$

2.1.2 Terrestrial solar radiation

Terrestrial radiation is the solar radiation that reaches the earth surface. Generally, it is measured in horizontal surface and called global horizontal solar radiation. Global horizontal solar radiation that is received on the earth surface consists of three components namely direct/beam radiation, diffuse radiation and reflected radiation. Beam solar radiation is that which radiate in a straight line from the sun to the earth's surface. After the solar radiation enters the earth's atmosphere, it is partially scattered and partially absorbed. The scattered radiation is called diffuse radiation. Radiation that is reflected by ground or other surfaces on the earth is called reflected radiation [16, 18, and 20]. Total solar radiation that is received on a horizontal surface on the earth is described in Fig. 2.4 and Eq. 2-6 as follows:

$$G_{Th} = G_{Bh} + G_{Dh} + G_{Rh} \quad (2-6)$$

G_{Th} is the total solar radiation on horizontal surfaces, G_{Bh} is the beam radiation on horizontal surfaces, G_{Dh} is the diffuse radiation on horizontal surfaces and G_{Rh} is the ground reflected horizontal surfaces. Since G_{Rh} magnitude is small for horizontal surface, sometimes it can be neglected. Most of the weather stations only provide total/global radiation on horizontal surfaces, while less of them also measures direct and diffuse radiation [6]. Hence, solar radiation models are required.

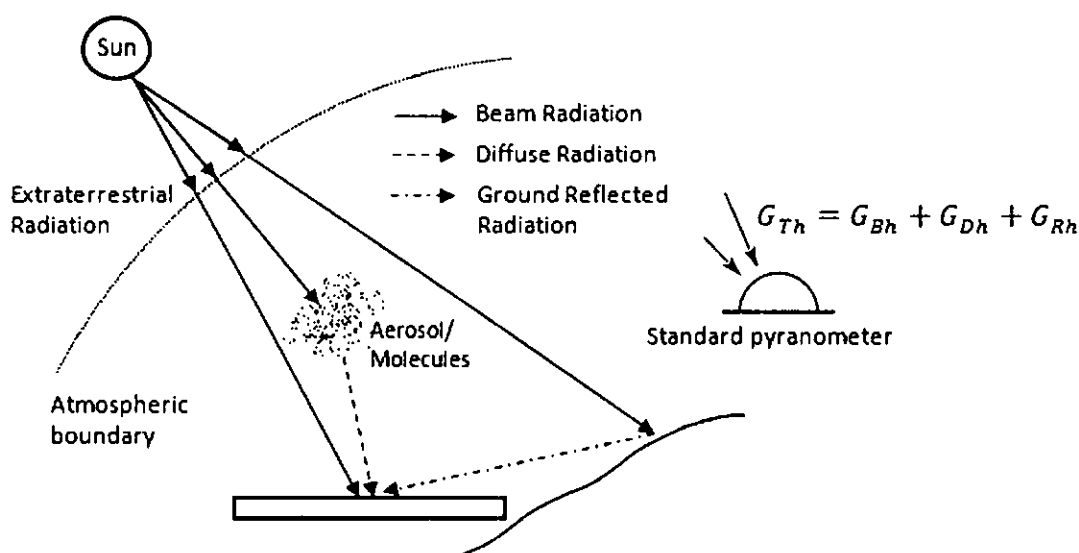


Fig 2.4: Solar Irradiance component (adapted from [20])

2.1.3 Parametric and meteorological model for solar radiation estimation

Parametric or atmospheric transmittance model requires details atmospheric characteristic information [15]. This model gives high-accuracy for clear sky/cloudless conditions, which is leading some author to use this model to evaluate the performance of an empirical model under cloudless conditions [21]. There are numerous authors proposed this kind of model as mentioned in [22]. However, pure parametric model was not used in this study, since there is no detail atmospheric condition data for the site.

The measurements of detail atmospheric parameters require an advance measurement. Therefore, meteorological parameters are frequently used as predictors of atmospheric parameters. Sunshine duration, cloud cover, ambient temperature, relative humidity, and precipitation have been used to estimate the atmospheric transmittance coefficient in parametric model equation [23-32]. This kind of model is called meteorological model. Some authors also proposed to estimate directly total global radiation using meteorological parameter [23-26], and then the calculation of the beam and diffuse solar radiation are carried out using the decomposition model.

Global solar radiation estimation from the sunshine duration was initiated by Angström [23] and then other researchers developed similar model based on sunshine duration such as those which mentioned by M. Yorukoglu and A.N. Celik [24]. Bristow and Campbell [25] and Hargreaves and Samani [26] proposed solar radiation estimation using the differences between maximum and minimum ambient temperature. Some studies also add measured precipitation to the temperature based hourly solar radiation prediction, and the methods are claimed to perform well [27, 28]. Mehreen et al. [29] used and compared meteorological radiation models to cloud cover models. K. Yang and Toshio K. proposed estimation method of solar radiation using upper-air humidity [30]. Kamal Skeiker proposed correlation between the solar radiation and common meteorological parameters in Syria [31]. G. Wu et al. [32] evaluate the existing models; develop a model to estimate missing global solar radiation and proposed strategy to choose a model based on available meteorological data. Table 2.1 shows several existing formulae to estimate solar radiation.

Table 2.1: List of several existing meteorological model

No	Model	Formula/Note	Data needed	Ref.
1	Angstrom	$\frac{H}{H_{cl}} = a + (1 - a) \frac{S}{S_0}$	Sunshine duration (S), a is numerical parameter which are specific for certain area	[23]
2	Bristow and Campbell	$R_s = R_a \cdot A [1 - \exp(B(\Delta T)^c)]$	Daily maximum and minimum ambient temperature, R_a is extraterrestrial radiation	[25]
3	Hargreaves and Samani	$R_s = R_a(k_R) \sqrt{T_{max} - T_{min}}$	Daily maximum and minimum ambient temperature, k_R is adjustment coefficient	[26]
4	Hunt et al.	$S = a_0 S_0 \sqrt{T_{max} - T_{min}} + a_1 T_{max} + a_2 P + a_3 P^2 + a_4$	Daily precipitation (P), maximum and minimum ambient temperature	[27]
5	Kurt and Spokas	Combine analytical atmospheric transmittance model of [23] and built decision matrix (use precipitation data for beam atmospheric transmittance determination) and add following formula for $\Delta T < 10^\circ\text{C}$: $\tau' = \frac{\tau}{11 - \Delta T}$	Daily precipitation, maximum and minimum ambient temperature	[28]
5	Mehreen S.G et al. MRM model	Combine analytical atmospheric transmittance model, with numerical correlation using meteorological data. $DBR = 0.285 \cdot k_b^{-1.00648}$ $G_b = (SF) G_0 \cdot \tau_r \cdot \tau_a \cdot \tau_g \cdot \tau_o \cdot \tau_w$ $G_d = DBR \cdot G_b$ $G_t = G_d + G_b$ (for detailed formula please refer to the reference)	Dry and wet bulb temperature, sunshine fraction	[29]
6	Mehreen S.G et al. CRM model	$G_{t,o} = (A \cdot \sin \gamma - B)$ $\frac{G_t}{G_{t,o}} = 1 - C \left(\frac{N}{8}\right)^D$	Cloud cover/amount (N) in octa.	[29]
7	K. Yang and T. Koike	For clear sky: $G_0 = I_0 (0.909 \bar{\tau}_b + 0.628 \bar{\tau}_d)$ Cloud effect was parameterized through upper air RH, by dividing atmosphere into 3 layers. $\frac{G_t}{G_0} = \frac{f(SCI)}{1 - \tau_s \tau_a}$ (for detailed formula please refer to the reference)	Upper air relative humidity	[30]

Table 2.1 continued

No	Model	Formula/Note	Data needed	Ref.
8	Hargreaves, Samani and Annandale	$R_s = R_a \cdot k_R \cdot (1 + 2.7 \cdot 10^{-5} \cdot Z) \sqrt{T_{max} - T_{min}}$	Daily maximum and minimum ambient temperature, site elevation in m (Z)	[31]
9	Kamal Skeiker	Develop correlation of solar radiation and meteorological parameters (sunshine duration, mean daily RH, mean daily maximum air temperature, mean daily maximum dew point temperature, mean daily atmospheric pressure) $y = a + bx_1 + cx_2 + dx_3 + ex_4 + \dots$	Sunshine duration, mean daily RH, mean daily maximum air temperature, mean daily maximum dew point temperature, mean daily atmospheric pressure	[32]
10	Guofeng Wu et al.	Calibrated existing model using local data set from Nanchang station, China, and proposed 2 new model as follows: $R_G = R_E(a_0 + a_1 \ln \sqrt{\Delta T})$ $R_G = R_E(a_0 + a_1 \ln \sqrt{\Delta T}) + a_2 \frac{H^{a_3}}{H_0}$	Daily maximum and minimum ambient temperature, R_a is extraterrestrial radiation	[33]
11	S.M Robaa	$G = k(n)^{1.24} \cdot (h)^{-0.19} + 10.550(\sinh)^{2.1} + 300(\sinh)^3$	k is regional parameter empirical value, n is day length/measured sunshine duration	[35]

Note: In this table, the equation are directly cited from the references without changing the nomenclature, please refer to the references.

Some authors evaluated and compared the performance of existing meteorological models, and some of them extend their work by developed their own model. S.M. Robaa compared 10 existing model and developed a new model, he claimed that his model was better than other models for Egypt's area [35]. The estimation results of Kurt and Spokas draw attention to this study due to the simplicity of the model and its satisfactory results. Furthermore, the model does not need an empirical coefficient [28]. Other methods that develop a correlation between solar radiation components were studied and become a motivation in this study to develop a correlation for specific site, in this case Bandar Sri Iskandar, Malaysia [32, 36].

2.1.4 Decomposition model of solar radiation on horizontal surface

Decomposition model usually uses global radiation on horizontal data to obtain beam and diffuse components of solar radiation [15]. This model is important for solar engineering applications since most of the weather stations only provide global radiation data. Commonly, the correlation is developed by correlating Diffuse Fraction (k_d) and Clearness Index (k_T). k_d is the ratio of diffuse radiation on a horizontal surface to the global horizontal radiation while k_T is the ratio of global horizontal to extraterrestrial horizontal radiation described as follows [37]:

$$k_d = \frac{G_{Dh}}{G_{Th}} \quad (2-7)$$

$$k_T = \frac{G_{Th}}{G_{0h}} \quad (2-8)$$

Fig. 2.5 shows the explanation of plot area in diffuse ratio (k_d) vs. clearness index (k_T) correlation graphic. Diffuse ratio equal to one means the sky is in overcast condition. Clearness index never reach one due to the presence of atmosphere.

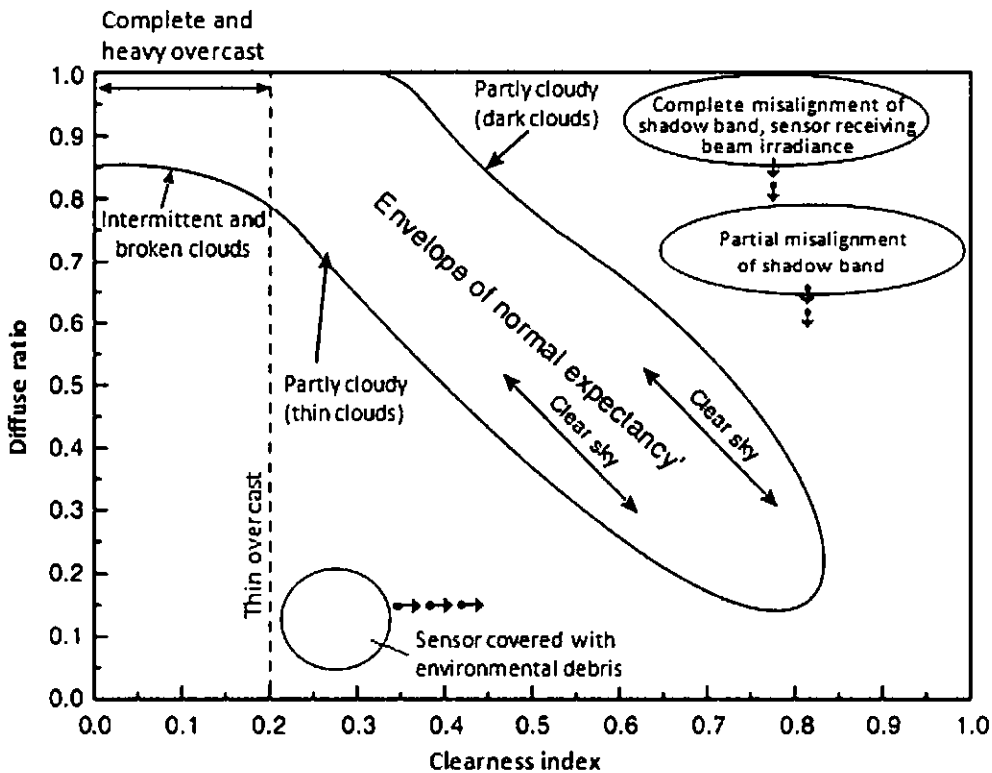


Fig 2.5: Diffuse ratio/fraction vs. clearness index [16]

The sky cover can be categorized by three conditions: cloudy (overcast), partially cloudy and clear sky [38]. Cloudy (overcast sky) is the condition with high diffuse ratio (near 1) and low clearness index (near 0). Clear sky is the condition when diffuse ratio low and clearness index high. Partially cloudy condition is between clear sky and overcast sky. Each of this condition described in Fig. 2.5. This classification is important. Envelope of normal expectancy in Fig 2.5 is the normal area for k_d vs. k_T correlation. Some authors use three-stage piecewise regressions based on this classification for linear correlation model such as Reindl et al. [39] and A. Skartveit and J.A. Olseth [40].

J.L. Torres et al. [41] compared seven teen models and suggested Dirint [42] and BLR [36] model as the best model to estimate hourly diffuse solar irradiance. R. Posadillo and R. L. Luque [43] recommend Reindl et al. [39] model for its simplicity and good results after comparing three different models. J.D. Mondol et al. [44] found in their study that model developed from correlation of local data perform better than direct use of existing models. G. Notton et al. [38] conclude in their study that there is no model largely better than other models. In the TRNSYS 16, radiation processor component only provides Reindl model [39] to decompose global solar radiation. Mode 1 using Reindl model reduced correlation is used if only global horizontal solar radiation data available. Mode 2 using Reindl full correlation is used if global horizontal solar radiation, ambient temperature and relative humidity data are available [19]. Reindl reduced, and full correlations are described in Eq. 2-9 to 2-15 as follows [39, 19]:

Reindl reduced correlation

Interval: $0 \leq k_T \leq 0.3$; Constraint: $0.98 \leq \frac{G_{Dh}}{G_{Th}} \leq 1$

$$\frac{G_{Dh}}{G_{Th}} = 1.020 - 0.254 k_T + 0.0123 \sin(\alpha) \quad (2-9)$$

Interval: $0.3 \leq k_T \leq 0.78$; Constraint: $0.1 \leq \frac{G_{Dh}}{G_{Th}} \leq 0.97$

$$\frac{G_{Dh}}{G_{Th}} = 1.4 - 1.749 k_T + 0.177 \sin(\alpha) \quad (2-10)$$

Interval: $0.78 \leq k_T$; Constraint: $\frac{G_{Dh}}{G_{Th}} \leq 0.1$

$$\frac{G_{Dh}}{G_{Th}} = 0.486 k_T - 0.182 \sin(\alpha) \quad (2-11)$$

Reindl full correlation

Interval: $0 \leq k_T \leq 0.3$; Constraint: $0.98 \leq \frac{G_{Dh}}{G_{Th}} \leq 1$

$$\frac{G_{Dh}}{G_{Th}} = 1 - 0.232 k_T + 0.0239 \sin(\alpha) + 0.000682 T_{amb} + 0.0195 \left(\frac{RH}{100}\right) \quad (2-12)$$

Interval: $0.3 \leq k_T \leq 0.78$; Constraint: $0.1 \leq \frac{G_{Dh}}{G_{Th}} \leq 0.97$

$$\frac{G_{Dh}}{G_{Th}} = 1.329 - 1.716 k_T + 0.267 \sin(\alpha) + 0.00375 T_{amb} + 0.106 \left(\frac{RH}{100}\right) \quad (2-13)$$

Interval: $0.78 \leq k_T$; Constraint: $\frac{G_{Dh}}{G_{Th}} \leq 0.1$

$$\frac{G_{Dh}}{G_{Th}} = 0.426 k_T - 0.256 \sin(\alpha) + 0.00349 T_{amb} + 0.0734 \left(\frac{RH}{100}\right) \quad (2-14)$$

Then if $\frac{G_{Dh}}{G_{Th}} = k_d$ has already found, G_{Dh} and G_{Bh} can be calculated as follows:

$$G_{Dh} = G_{Th} \cdot k_d \quad (2-15)$$

By assuming ground reflected solar radiation is very small and neglected, following equation were obtained from Eq. 2-6:

$$G_{Th} = G_{Bh} + G_{Dh} \quad (2-16)$$

$$G_{Bh} = G_{Th} - G_{Dh} \quad (2-17)$$

$$G_{Bh} = G_{Th} - G_{Th} \cdot k_d \quad (2-18)$$

In this study, the simulation only uses the available components in TRNSYS 16. Since most of weather stations only provide global horizontal solar radiation data, the decomposition model is required and will be used in this study.

2.1.5 Solar radiation on the tilted surface

Information of beam and diffuse solar radiation components are required to calculate solar radiation on the tilted surface. That is why beam and diffuse solar radiation on the horizontal surface were calculated first using the decomposition model if global horizontal solar radiation data available [38].

There are various kinds of models to calculate the solar radiation on the tilted surface developed by researchers. Some researchers evaluated and compared the performance of these existing models. G. Notton et al. were carried out several studies to evaluate existing decomposition model and then use the results to predict hourly solar radiation on inclined surfaces [38, 45 and 46]. Efim G. E. and Avraham I. K. [47] carried out an assessment of eleven models to predict the global solar radiation on a surface tilted to the south. A. M. Noorian et al. [48] evaluated twelve models of diffuse irradiation estimation on inclined surfaces. They suggest Skartveit and Olseth [49], Hay [50], Reindl et al. [51] and Perez et al. [52] models. Available models in TRNSYS 16 are isotropic model [53], Hay and Davies model [54], Reindl [51] model, and Perez model [52]. P.G. Loutzenhiser et al. [55] carried out an empirical validation of seven models using several software of building energy simulation and found that Perez model [52] model performed best in TRNSYS simulation.

Total solar radiation on the tilted surface is calculated by using beam, diffuse and reflected solar radiation components. The calculations are described in Eq. 2-19 and 2-20 as follows:

$$G_{Tt} = G_{Bt} + G_{Dt} + G_{Rt} \quad (2-19)$$

$$G_{Tt} = G_{Bh} \cdot r_b + G_{Dh} \cdot r_d + G_{Th} r_r \quad (2-20)$$

r_b can be calculated using geometrical parameter as described in Eq. 2-21 to 2-24.

$$r_b = \frac{\cos(\theta)}{\cos(\theta_z)} \quad (2-21)$$

where,

$$\cos(\theta) = \cos(\theta_z)\cos(\beta) + \sin(\theta_z)\cos(\gamma_s - \gamma)\sin(\beta) \quad (2-22)$$

$$\cos(\theta_z) = \sin(\phi)\sin(\delta) + \cos(\phi)\cos(\delta)\cos(\omega) \quad (2-23)$$

r_r can be calculated as follow:

$$r_r = \frac{\rho_{gr} \cdot [1 - \cos(\beta)]}{2} \quad (2-24)$$

where ρ_{gr} is ground reflectivity coefficient.

r_d calculation is more complex than r_b and r_r calculations. Table 2.2 shows several models to predict r_d .

Table 2.2: List of available models to calculate r_d in TRNSYS 16

No	Model	Formula of r_d	Note	Ref.
1	Isotropic model (Liu and Jordan) 1962	$r_d = 0.5(1 + \cos\beta)$	Isotropic	[53]
2	Reindl et al. 1990	$r_d = 0.5(1 - A_l)(1 + \cos\beta) \left(1 + (f)\sin^3\frac{\beta}{2}\right) + (A_l r_b)$	Anisotropic	[51]
3	Perez et al. 1988	$r_d = 0.5(1 - F'_l)(1 + \cos\beta) + F'_l \frac{a}{c} + F'_2 \sin\beta$	Anisotropic	[52]
4	Hay and davies 1980	$r_d = 0.5(1 - A_l)(1 + \cos\beta) + (A_l r_b)$	Anisotropic	[54]

Finally, the expression of global irradiation on the tilted surface (Eq. 2-20) can be written as follows:

$$G_{Tt} = G_{Bh} \cdot \frac{\cos(\theta)}{\cos(\theta_z)} + r_d G_{Dh} + \frac{G_{Th} \cdot \rho \cdot [1 - \cos(S)]}{2} \quad (2-25)$$

For r_d calculation, TRNSYS 16 weather data processor provide Isotropic (Liu and Jordan), Anisotropic (Hay and Davies), Reindl and Perez model. Reindl and Perez model were used in this study as explained in section 3.3.1.

2.2 Peak Sun Hour (PSH) concept

Solar energy availability can be presented by mean of Peak Sun Hour (PSH). PSH is defined as the equivalent number of hours per day when solar irradiance averages 1,000 W/m². For example, six peak sun hours means that the energy received during total daylight hours equals the energy that would have been received had the irradiance for six hours been 1,000 W/m² [13]. Fig. 2.6 describes the way to obtain PSH from solar insolation during the day. By using this concept, PV array energy output can be calculated using the Wp (watt peak) value of PV panel, which is obtained from STC. The advantage of using PSH concept in PV systems sizing is that there is no need for detailed data of PV panel characteristics.

The total radiation in Wh/m² is an integral of solar flux radiation $G(t) dt$ as described in Eq. 2-26 to 2-29.

$$G_{Th}(\text{daily}) = \int_{\text{sunrise time}}^{\text{sunset time}} G_{Th}(t) dt \quad (2-26)$$

$$PSH = \frac{G_{Th}(\text{daily})}{1000} \quad (2-27)$$

PSH on the tilted surface is calculated as follows:

$$G_{Tt}(\text{daily}) = \int_{\text{sunrise time}}^{\text{sunset time}} G_{Tt}(t) dt \quad (2-28)$$

$$PSH_t = \frac{G_{Tt}(\text{daily})}{1000} \quad (2-29)$$

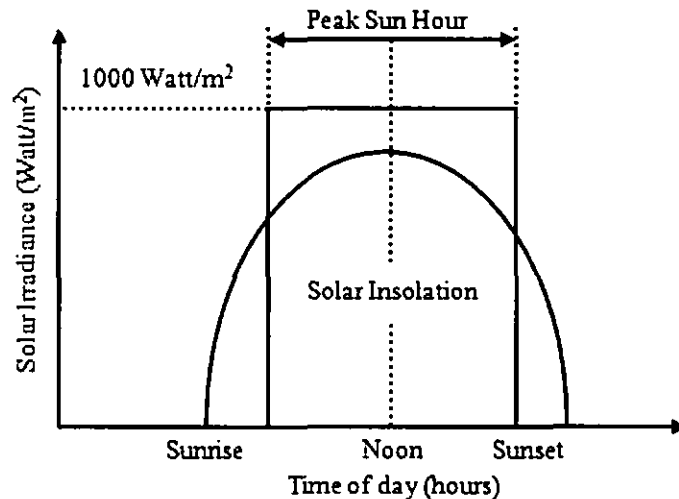


Figure 2.6: PSH (Peak Sun Hour) [1]

2.3 PV systems sizing and optimization

In general, PV systems sizing can be carried out using deterministic and stochastic methods. Both methods have advantages and disadvantages. In this chapter, PV systems sizing method reviewed by discussed both of the methods. Size optimization methods that incorporate economic parameters also presented here.

2.3.1 Deterministic method

A deterministic method refers to the assumption that the load profiles and energy resources are constant, neglecting the statistical phenomenon of each component of the system. Although this method will be less accurate than the statistical approach, it can be used to provide initial size design of PV panel and storage systems. A simple deterministic method using the Peak Sun Hour (PSH) concept can be used to obtain a quick sizing estimate of the PV system [13]. This method is suitable for the locations where daily solar radiation data is not available, so the PSH value from Global Solar Map can be used. System size is calculated based on the energy balance concept by means energy produced by PV system and stored in the battery can fully supply the load energy demand [13].

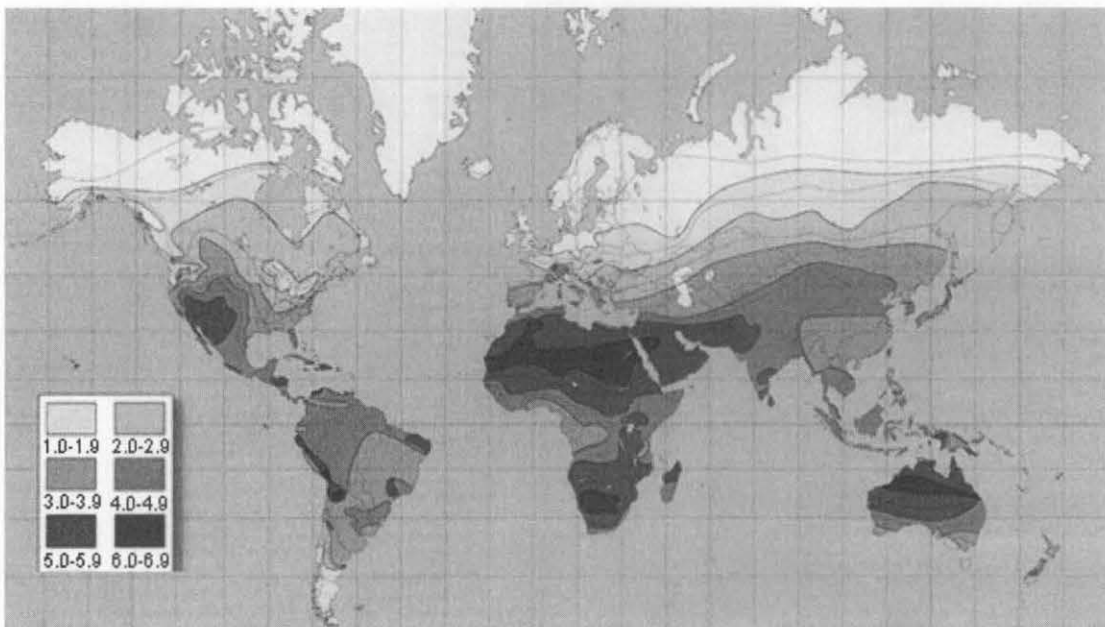


Figure 2.7: Global Solar Power Map [57]

In general, average PSH value on the earth can be observed from Global Solar Power Map (Fig. 2.7). The map was developed by Solarex using solar radiation data measured at various locations on the globe [56]. The map shows the average amount of solar energy, received on horizontal surfaces at different geo-locations.

Alberto E.P. [58] explained simple sizing method by prioritizing PV system performance on the worst month, which demanded energy greater than solar energy available. This method performed by calculating energy balance of total energy input and output in the worst month, and the reliability of the systems is represented by the number of autonomy day. Arvind Chel et al. [59] investigated sizing and cost estimation using deterministic method and data from the global solar map. A. Benatiallah et al. [60] compared simplified (deterministic) and statistical methods of sizing PV installation. They found only insignificant differences between the two methods and suggest the simplified method may be suitable in the area where data are not available to perform method that is more sophisticated.

Deterministic method has been proposed by M.M.H. Bhuiyand and M.A. Asgar [61] to carry out stand-alone PV system sizing for lighting load at Dhaka, although it is a deterministic method, they also consider monthly seasonal variation of solar radiation. Following data are required to carry out the method [61]: (i) The daily or hourly load requirement during a typical year. (ii) Typical current and voltage characteristics of the selected type of module at various irradiances and temperatures. (iii) The mean daily irradiation on the plane of the array for every month of a typical year. (iv) The tilt factors for different tilt and azimuth angles. (v) The maximum number of consecutive sunless days likely to be experienced. (vi) The mean daily ambient temperature for every month of a typical year. (vii) The estimated cell temperature rise above ambient of the modules in the array. (viii) The required security of supply. (ix) The selected DC bus voltage. (x) The estimated percentage of energy losses in the battery, power conditioning equipment and control system. (xi) The estimated losses in the array due to module mismatch, cable, dust and shading and voltage drop across blocking diodes. In the deterministic method performance of the system is defined by number of autonomy day, number of the days that the system still can supply the load whether solar radiation is low.

The first step to carry out this method is by calculating required PV array. Average PSH value of the location, daily load and system efficiency should be known. Then required battery storage is calculated to supply the load during the autonomy days. Number of autonomy days, battery's Depth of Discharge (DoD) and rated voltage are determined by considering load capacity, load type and lifetime of the battery.

2.3.2 Stochastic method

In the deterministic method, storage system capacity is determined by autonomy day to ensure reliability of the system, but this concept does not employ direct relationships between reliability itself and component capacity of PV systems [62]. Stochastic method considers the stochastic nature of solar radiation as the most important data input for PV systems sizing.

Usually stochastic method is carried out by calculating the Loss of Power Supply Probability (LPSP) as the design parameter representing the reliability of the system [63]. Some author used a different term such as Loss of Power Probability (LPP) [64, 65], Loss of Load Probability (LOLP/LLP) [13, 66 and 67] and Loss of Energy Probability (LOLE) [68].

The stochastic method largely used and developed for PV system sizing. W.X. Shen [70] carried out solar array and battery sizing for stand-alone PV system in Malaysia using a daily PSH data and energy balance concept to calculate LPSP. R. Posadillo and R.L. Luque [71, 72] develop sizing method for stand-alone PV system using LLP concept and proposed the annual number of system failures and standard deviation of the annual number of failures as new sizing parameters. T. Markvart et al. [73] proposed sizing method based on LLP concept using a graphical method of solution. The sizing curve was obtained by combining climatic cycle line. A. Fragaki and T. Markvart [74] presented the results of new sizing approach and recommended a combination of a large array and smaller storage size to reduce loss of load. Some authors also implement simulation method using hourly data to calculate LLP [75-76]. A.N. Celik [75] investigated the effect of different load profiles on LLP of the PV

system. A. Balouktsis et al. [77] used stochastic time series's model as the data input for PV system sizing for locations where no actual data exist.

In the stochastic method, sizing curve can be plotted by mean of solar array and battery capacity or by mean of dimensionless variable, C_{A1} (ratio of array capacity to load) and C_{S1} (ratio of storage capacity to load) [74]. Other authors were plotting the sizing curve by mean of SLR (solar to load ratio) and BLR (battery to load ratio) [75]. Fig. 2.8 shows an example of sizing curve obtained from LLP calculation, which plotted by mean of C_{A1} and C_{S1} [71]. LLP value described the performance of the system. Lower LPSP shows better system's performance.

Loss of Power Supply Probability (LPSP) is the probability that loss of power supply occurs, meaning the total time of the power supply is not able to supply the load [62]. Different definition of LPSP is the ratio between the estimated energy deficit and the energy demand over the total operation time of the installation [13]. From these two definitions, the LPSP calculation can be carried out using service time of the system or using the energy balance concept. In this study, LPSP is calculated using Eq. 2-30 as follows [69]:

$$LPSP = \frac{\sum_{n=1}^N LPS(n)}{\sum_{n=1}^N E_{L(n)}} \quad (2-30)$$

where LPS is total loss of power supply on the day n and $E_{L(n)}$ is total load/demand energy on the day n. The LPS is calculated by following step:

1. First step: Calculation of daily PV panel power output

Time series solar radiation data is compulsory for this calculation. PV panel efficiency, system efficiency, panel tilt angle effect and cell temperature effect on the power production is considered in the calculation.

2. Second step: Calculation of daily battery energy states

Daily battery energy states are estimated by system's energy balance calculation. Daily PV panel power input and daily load power data is required to carry out the calculation. Inverter efficiency and charging efficiency are also incorporated in the calculation.

3. Third step: Calculation of *LPS* and Excess energy

Daily *LPS* can be obtained from system's energy balance calculation. *LPS* is occurred when the battery energy state reaches the minimum value and cannot supply energy to the load. The amount of load energy that is not supplied by the system is the *LPS*. Detail's calculation procedures are explained in chapter 3.

The calculation of *LPSP* requires time series solar radiation data in hourly or daily time-step. The data that is used for calculation can be measured data or synthetic data. K. G. Rueb used Markov method to generate synthetic data of solar radiation for *LPSP* calculation [68]. However, results that are more accurate would be obtained using measured data since it is indeed represented the characteristic of weather at the location. Time-series simulation can be carried out to calculate daily energy balance of the system if the time-series data is available. From this calculation, daily energy losses (*LPS*) and excess energy are obtained. At least, one-year data that contain seasonal variation information is required to perform this calculation. The calculation result is used to plot *LPSP* contour plot such as shown in Fig. 2.8 [70], then one value of *LPSP* is selected to plot a sizing curve. Lower *LPSP* value shows better system's performance and vice versa. Maximum *LLP* value of 0.001 is commonly used for performance limitation in size selection [71].

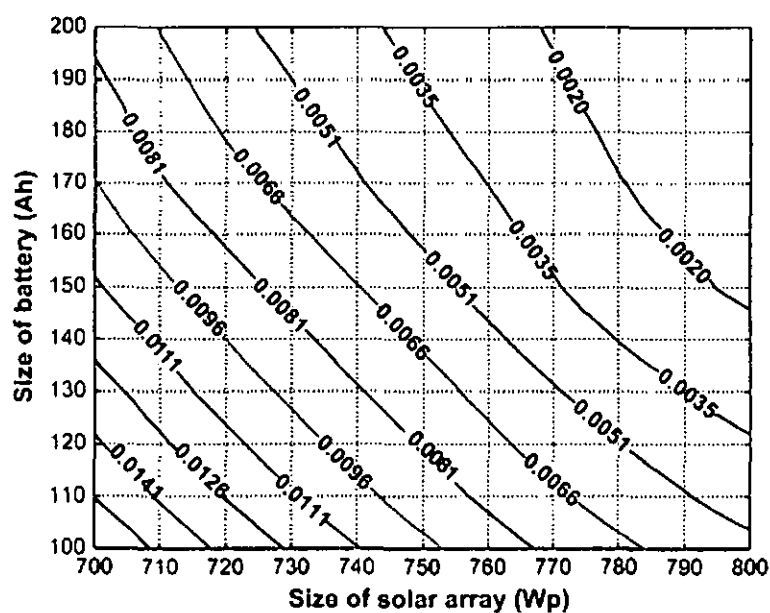


Figure 2.8: Contour plot for different size combinations of solar array and battery at different *LPSP* values [70]

2.3.3 PV systems sizing optimization

Some researchers were suggested to carry out the sizing optimization based on system cost [69, 70, 78 and 79]. Optimum size of PV array and battery can be obtained based on minimum cost of the system. Z.M. Salameh and B.S. Borowy [69] used total cost of battery and PV arrays to find optimum configuration in desired LPSP value, function of the system can be defined as follows [69]:

$$CC = \alpha_{PV} \cdot N_{PV} + \beta_{batt} \cdot N_{batt} + C_0 \quad (2-31)$$

where CC is the capital cost, α_{PV} is the cost of the PV panel, β_{batt} is cost of the battery, C_0 is the other cost. N_{PV} and N_{batt} are the number of PV panel and battery. Optimum solution obtained by following condition:

$$\frac{\partial N_{PV}}{\partial N_{batt}} = -\frac{\beta_{batt}}{\alpha_{PV}} \quad (2-32)$$

Fig. 2.9 illustrated optimum solution from the above condition.

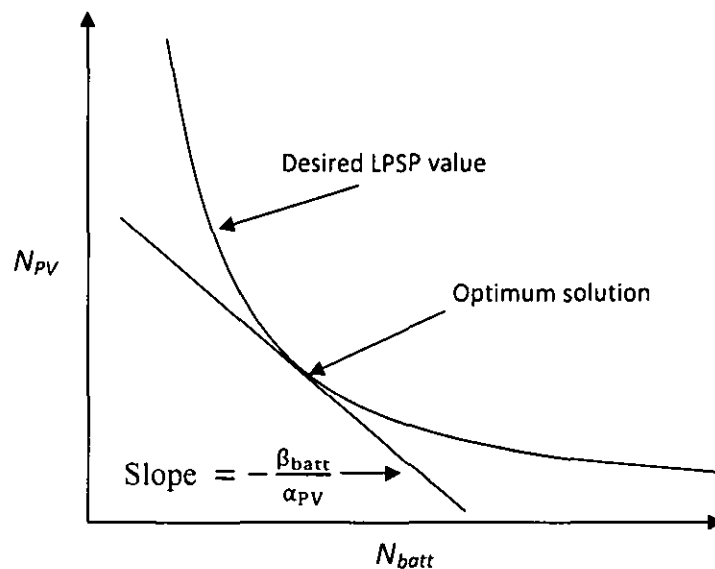


Figure 2.9: Optimum solution configuration by mean of minimum capital cost [69]

Some researchers also used different economic parameters such as Life Cycle Cost (LCC) and payback period. A.N. Celik et al. [78] used LCC concept to find optimal size of PV system configuration. J.K. Kaldellis et al. [79] carried out optimization based on analysis of energy payback. While P. Arun et al. [80] used Cost

of Energy (COE) and Annualized Life Cycle Cost (ALCC) in their study. LCC analysis is presented by the following equation:

$$LCC = CC + M + R - S \quad (3-33)$$

CC is the capital cost. M is operation and maintenance cost. R is repair and replacement cost, and S is the salvage value.

P. Arun et al. [80] proposed design space approach for choosing optimum PV-battery system configuration. The design space approach was originally proposed for sizing of the system with deterministic resource and demand. In their report, chance constrained programming approach has been utilized for incorporating the resource uncertainty in the system sizing, and the concept of design space is extended to incorporate resource uncertainty [80]. The set of all feasible design configurations is represented by a sizing curve. The sizing curve for a given confidence level, connects the combinations of the photovoltaic array ratings and the corresponding minimum battery capacities capable of meeting the specified load, plotted on an array rating vs. battery capacity diagram. Fig. 2.10 describes design space approach in PV-battery systems sizing.

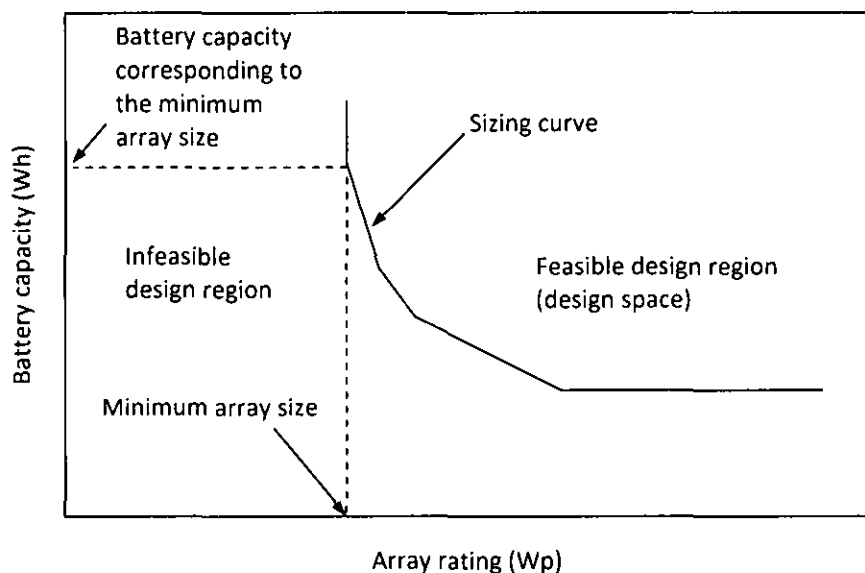


Figure 2.10: Sizing curve by design space approach [80]

Some authors also proposed Artificial Intelligent method to generate sizing curve of a standalone photovoltaic system [81, 82 and 83]. J. Lagorse et al. [81] used

genetic algorithm (GA) and simplex algorithm find optimal size of hybrid PV system for street lighting. A. Mellit [82, 83] proposed artificial neural network (ANN)-based genetic algorithm for photovoltaic systems sizing. However, application of an artificial intelligent is computationally burdensome, and it will take relatively longer time of a simulation and iteration process.

2.4 Available modeling software

Transient simulation can be carried out to predict/test the performance of PV system configuration since an experimental investigation would be costly and unviable for large-scale systems. Many authors developed mathematical and computer model for PV system components or complete PV systems over the past three decades. These models were developed using various kinds of software. H.L Tsai [84] implemented insolation-oriented PV model under Matlab/Simulink. R. Perez et al. [85] developed web-based simplified PV simulation engine using PVFORM. F. Shao [86] reviewed some PV modeling software and preferred TRNSYS to simulate standalone PV system. L.K. Nkhonjera [87] also used TRNSYS to develop battery-based standalone PV systems model.

D. Turcotte [88] classified PV system adapted software tools based on the form and purpose as described in Table 2.3. The categories consist of pre-feasibility, sizing, simulation and open architecture.

Table 2.3: PV software classification 1 [88, 86]

<i>No</i>	<i>Category</i>	<i>Software tools available</i>
1	Pre-feasibility tools	RETScreen
2	Sizing tools	HOMER, PVSYST
3	Simulation tools	Hybrid2, INSEL, PV-DesignPro, PVSYST
4	Open architecture research tools	MATLAB, PSPICE, TRNSYS and general purpose programming languages such as C, Pascal, Visual Basic, FORTRAN

Other classifications was given by Bales [89] whose classified the computer based solar heating system software tools and multifunctional simulation programs into

simple computer tools and detailed simulation programs with varying degrees of detail and complexity as presented in Table 2.4.

Table 2.4: PV software classification 2 [89, 86]

<i>No</i>	<i>Category</i>	<i>Software tools available</i>
1	Simplest tools	F.Chart, PSDMI
2	System-based	Polysun, T-Sol
3	Component-based	TRNSYS, INSEL
4	Equation-based	Colsim, Smile, IDA, MATLAB,

TRNSYS is one of the most complete and extensible simulation environments for the transient simulation of solar energy systems, which is developed in the University of Wisconsin. The modular structures of TRNSYS give the software tremendous flexibility and facilitate an addition of new models into the program [86]. Following sections will explain solar power system components model in TRNSYS 16.

2.4.1 Solar radiation model

There are several types of weather data reader and processor in TRNSYS 16. The weather data component is chosen based on the type of data file that would be used as input. TRNSYS supported various standard formats of the weather data file such as TMY, TMY2, TM2, IWEC, etc. If the user wants to insert non-standard data type 109 can be used. This component serves to read weather data at regular time intervals from a data file, converting them into a desired system of units that generates direct and diffuse radiation outputs, for an arbitrary number of surfaces, with arbitrary orientation and inclination [19].

The solar radiation model needs at least two components of solar radiation in-order to calculate the radiation on a tilted surface. It can use different combinations of following parameters: G_b - G_d , G - G_d , G - G_{bn} , G - T_{amb} -RH (The diffuse radiation is estimated using Reindl's full correlation) and G only. The diffuse radiation is estimated using Reindl's reduced correlation. Commonly, most of the weather stations provide G , T_{amb} and RH data, while only few weather stations can provide G_b and G_d data.

2.4.2 PV array model

In the TRNSYS's components library, there are several types of the PV panel model. Type 194 can be used to determine the performance of PV array [19]. Type 194 contains two kinds of models: four parameter model and five-parameter model. Five-parameter model is preferred due to the accuracy in predicting PV array output for various types of the module.

The four-parameter equivalent circuit model was developed largely by Townsend [90] and detailed by Duffie and Beckman [14]. The model was first incorporated into a TRNSYS component by Eckstein [91]. W. De Soto et al. [92] have improved and validated five parameter model for PV array performance, which developed from King et al. works [93, 94]. The model accurately predicts energy production with simple model and use parameters that normally available from the manufacturers. A.N. Celik [95] modeled and carried out experimental verification of mono-crystalline PV model operating current using four and five parameter model and found that five parameter model better than four-parameter model. Parameters required for five-parameter models are a_{ref} , $I_{o,ref}$, $I_{L,ref}$, $R_{s,ref}$ and $R_{sh,ref}$. Fig. 2.11 shows the equivalent circuit for five-parameter model. For the detail procedure and equation, please refer to the reference [90-95]. Temperature and incidence angle also incorporated in the model mostly based on the works of Duffie and Beckman [14].

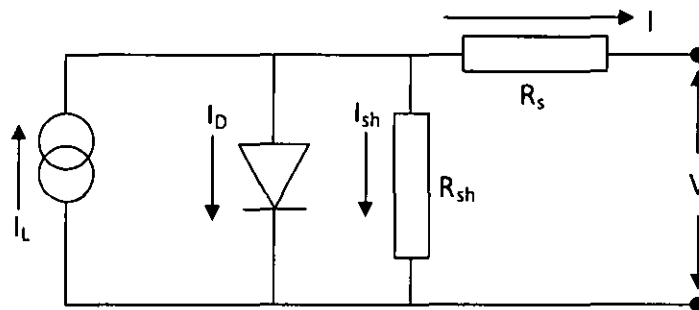


Figure 2.11: Equivalent circuit model for PV arrays

2.4.3 Charge controller model

There are two power-conditioning devices required in standalone PV system, charge controller, and inverter. Charge controller will control the energy input and output to the battery. Since PV and battery work in DC electricity, inverter is needed if the load type is AC load. In TRNSYS 16, type 48 is used as the controller model. In type 48, both the regulator and inverter can operate in one of four modes. Modes 0 and 3 are based upon the "no battery/feedback system" and "direct charge system," respectively. Modes 1 and 2 are modifications of the "parallel maximum power tracker system" in the same reference [19].

There are two types of the charge controller: Maximum Power Point Tracking (MPPT) type and Pulse Width Modulation (PWM) type (without MPPT). A PWM charge controller does not operate to optimize power transfer to the batteries. It is optimized to extend the life of the batteries by controlling current flow to/from the battery. The MPPT charge controller unit is designed to regulate the voltage from PV panel to the optimum voltage for maximum transfer of power to the battery [96]. Charge controller which supports MPPT is more expensive than PWM type without MPPT. For small to a medium scale system, PWM type controller would be more suitable.

To achieve long battery lifetime and better energy supply, P. Diaz and M.A. Egido [97] suggested that for on/off charge controllers, end of charge voltage at 25°C should be limited between 13.8 to 14.4 V and the load connection point should be between 0.9 and 1.2 V higher than low voltage disconnect (LVD).

2.4.4 Battery and load model

The battery models in the TRNSYS 16 only support Lead-Acid battery type. The models consist of chemical-kinetics model and Shepherd equation based model. Since the chemical-kinetic's model depends heavily on datasheet and experimental data, Shepherd equation based model is used. Shepherd battery model is the first battery model that estimates the State of Charge (SOC) based on the voltage. The Shepherd

model is modified by Hyman by adding an expression to the Shepherd formula, which providing a more realistic model at very low currents [98-99]. For the details of the formula, please refer to the TRNSYS 16 Manual [19].

Type 47c (Shepherd modified Hyman's battery model) is used as the battery model. This model of a lead-acid storage battery operates in conjunction with solar cell array and power conditioning components. Fig. 2.12 specifies how the battery state of charge varies over time, at a given rate of charge or discharges. V is battery voltage and F is Fractional State of Charge (FSOC).

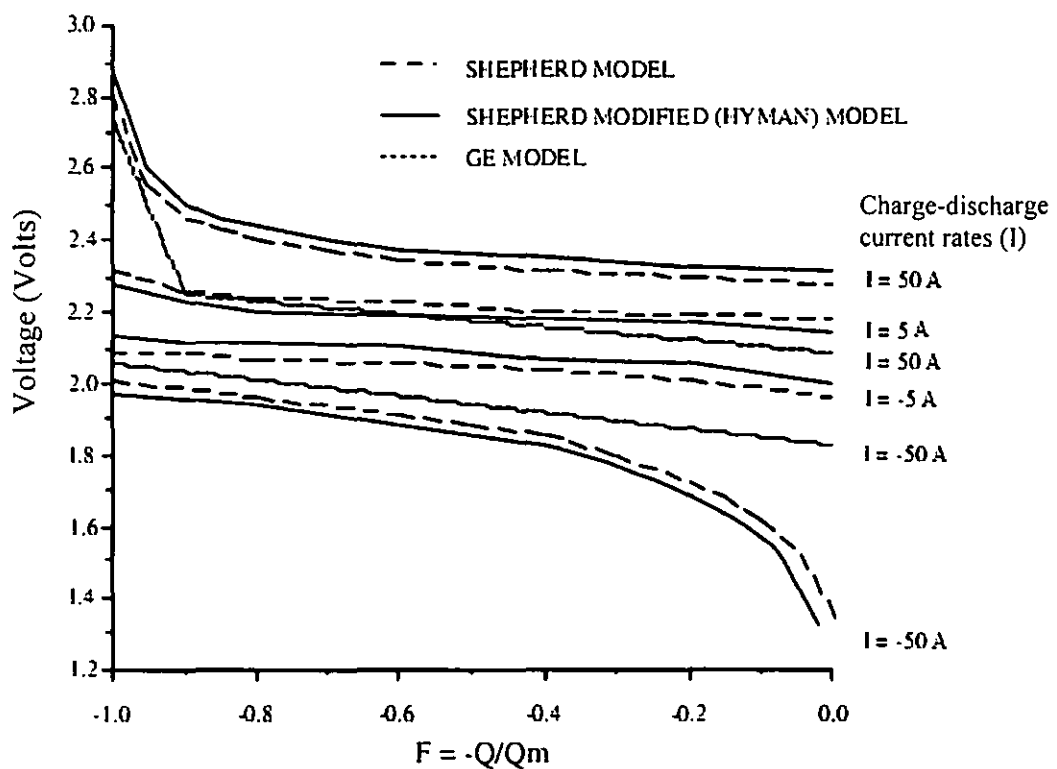


Figure 2.12: Battery model (Voltage-SOC relation) [19]

There are no specific models for the electric load. TRNSYS component Type 9 (Generic data files) is used to input the hourly load profile data [19]. The charge and discharge efficiency is configured in the charge controller component. For DC load, the inverter efficiency is configured to be one, means that there are no conversion from DC to AC electricity.

2.5 Summary

Literature reviews have been presented in this chapter. The literature reviews include solar radiation model, PV system sizing and optimization and PV system modelling. Solar radiation model literature reviews consist of solar system geometry, decomposition model, parametric model and solar radiation calculation on the tilted surface methods. These reviews are important for the calculation step presented in the next chapter. PV system sizing and optimization reviews include the deterministic and stochastic methods. PV system modelling has been reviewed by focusing on modelling using TRNSYS 16 software.

CHAPTER 3

METHODOLOGY

Methodology in this study consists of three main parts. First part is initial design using the deterministic method. Second part is the formulation of sizing optimization procedure using the stochastic method by mean of LPSP calculation with economic analysis. This part also includes weather data preparation, which consist of solar radiation missing data estimation to obtain complete time-series data, incorporation of tilt angle effect in LPSP calculation, and system parameters data preparation. Third part of methodology is modeling and simulation of standalone PV system with lighting load using TRNSYS 16. Experimental setup for model validation and system investigation are also included in this part.

3.1 Initial design using deterministic method

Deterministic method was used to perform initial design. Daily average solar energy availability and daily average demand energy must be known to calculate solar arrays and battery capacity required. This section presents the required data and calculation procedure of deterministic method.

3.1.1 Solar radiation availability

The solar energy availability data can be obtained from global solar power maps for any area on the earth. The Peak Sun Hour (PSH) presented in the global solar power maps represent the worst-case seasonal PSH (hours) values that used for calculating year-round application. It can be seen in Fig. 3.1, that Malaysia has an average PSH value of 4-5 hours. A.W. Azhari et al. in their study conclude that Malaysia receives average solar radiation between 4.21 to 5.56 kWh/m² [100].

PSH value that is more satisfactory at specific locations is obtained from measured data on the site. PSH value is obtained from measured solar radiation data by integrating solar radiation during the day and dividing it by 1000 (Eq. 2-28). Fig. 3.2 shows the example of PSH value, which is obtained from measured data for Bandar Sri Iskandar. The data was taken on 14 May 2010, on a sunny day from morning until afternoon and for the cloudy sky in the afternoon. The total radiation for the day is 4510 Wh/m^2 , which is equal to PSH value of about 4.5. PSH monitoring results in Bandar Sri Iskandar for the longer periods is presented in the next chapter.

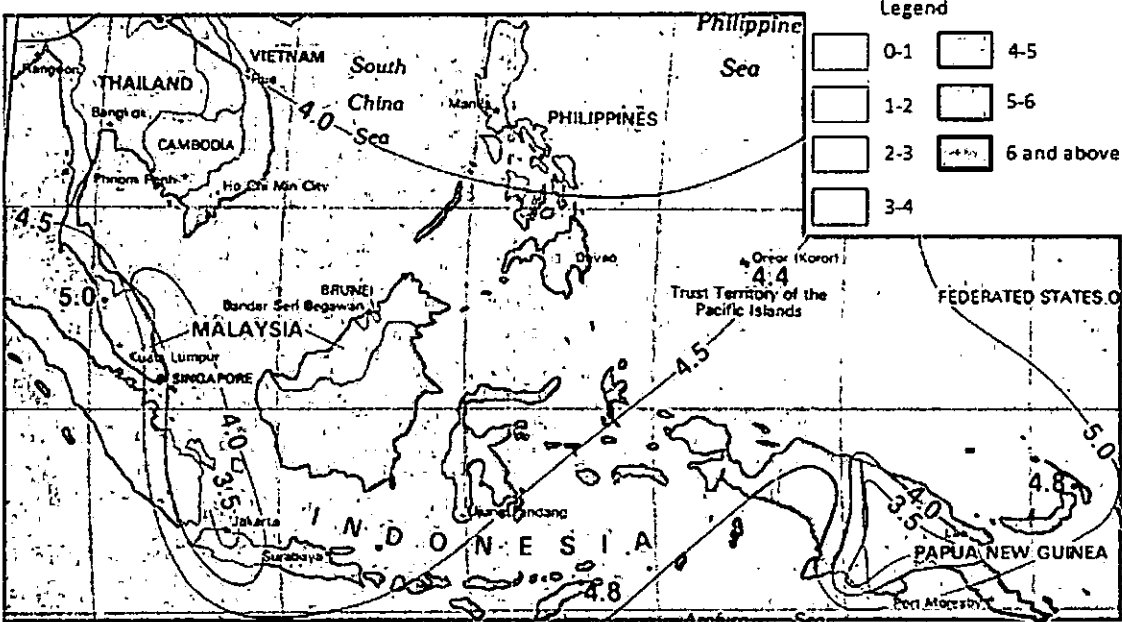


Figure 3.1: Global Solar Power Map for South East Asia [18]

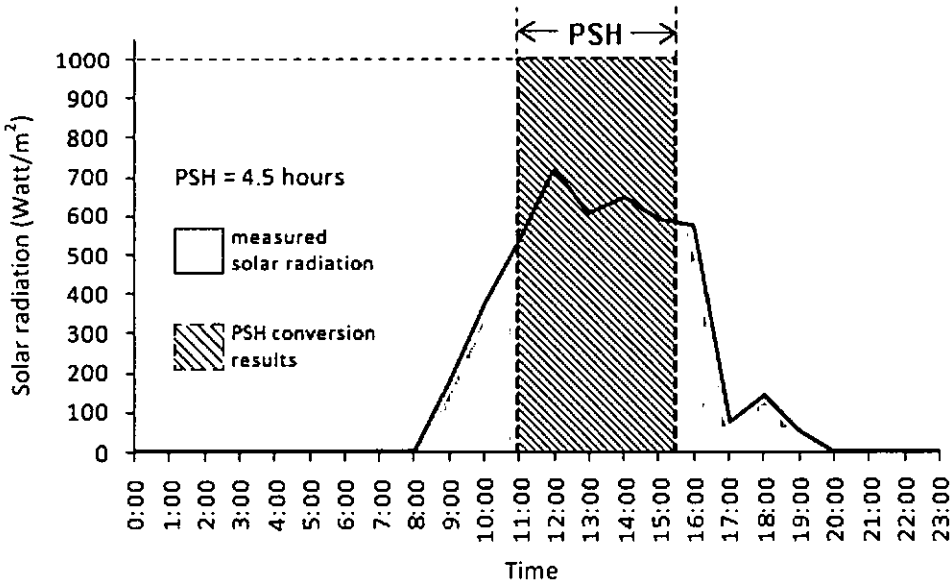


Figure 3.2: PSH obtained from measured data in Bandar Sri Iskandar (5 May 2010)

3.1.2 Malaysian typical terraced house load profile

Based on the available data, the average household electricity consumption was calculated to be approximately 2200 kWh/yr per house in Malaysia. Refrigerator consumes the highest energy compared to other electrical appliances. The average energy consumption of a domestic refrigerator for households in Malaysia is about 2.03 kWh/day [101]. It is also reported that average lighting load for residential building in Malaysia is about 25% of total load of the building [102]. Table 3.1 shows one case of residential house energy consumption where the electricity devices may vary, but their average total value, as reported from previous studies is about 6 kWh/day. The operation hours of household appliances are varying due to the occupants' behavior.

Table 3.1: Residential House Energy Consumption (adapted from [101-103])

No	Item	Power (Watt)	Qty	Operation Hrs	Wh/ day	%
1	Lamp 1	18	3	12	648	} 23
2	Lamp 2	18	3	6	324	
3	Lamp 3	18	2	2	72	
4	Lamp 4	40	2	4	320	
5	Ceiling Fan	80	2	6	960	16
6	Refrigerator	85*	1	24	2040	34
7	Television	100	1	6	600	10
8	Misc.	-	-	-	1000	17
TOTAL					5964	

Note: *Average power

For above case the electrical energy demand for house lighting is 1364 Wh or 23% of the total house energy consumption. A different lamp selection and operation hours may be varied, but the total energy demand for lighting load is about 25% of total energy demand of the house [102]. If the PV Systems are used to supply residential electricity, it is more efficient to use DC lamps for lighting since DC lamps do not need inverters so power dissipation in inverter can be avoided. However, it is an option for occupants to use DC or AC lamps since each kind of lamps has its own advantages. Refrigerator power in Table 3.1 is an average power. Refrigerator's energy demand is varied during the day dependent on ambient temperature and cooling load. Refrigerator would consume more energy during the day since ambient temperature is higher than during the night.

Fig. 3.3 show hourly load profile of a residential house in a day. The lighting load is only operates during the night when solar radiation are unavailable, assuming the house has good passive lighting design during the day. The energy to supply the lighting load is obtained from the battery. In this case, hourly load variation is less important for calculation and total load energy during the night that is mainly considered in the calculation. The detail of load energy profile for Fig. 3.3 is explained in Appendix A.

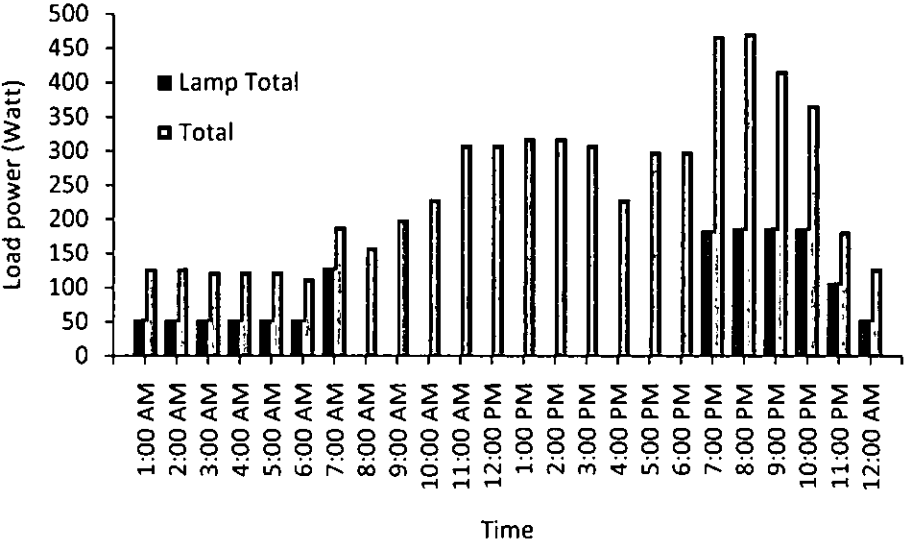


Figure 3.3: Load Profile of typical Malaysian Residential House

3.1.3 Calculation procedure

To calculate the size of the PV panel by using the simple deterministic method, first, the electricity demand per day and solar energy availability for the sites with respect to PSH have to be determined. PSH value that is used in this calculation is obtained from Global Solar Power Map or on-site measurement as explained in section 3.1.1. Load energy for typical Malaysian terraced house is explained in section 3.1.2. Eq. 3-1 is used to calculate the PV array capacity.

$$P_{PV} = \frac{P_{load}}{PSH \cdot \eta_{system}} \tag{3-1}$$

P_{PV} is PV panel nominal peak power. P_{load} is total energy demand for a day, PSH is Peak Sun Hour and η_{system} is overall system efficiency.

After total P_{PV} of PV panel is determined, the battery capacity can be calculated using Eq. 3-2 as follows:

$$C_{bat} = \frac{P_{load} \cdot N_a}{DoD \cdot V_{rated} \cdot \eta_{system}} \quad (3-2)$$

C_{bat} is the battery capacity in Ampere hour (Ah) and N_a is the number of autonomy days (day with minimum solar irradiation) required consecutively. DoD is the depth of discharge and V_{rated} is the voltage of the system in Volts.

The lifetime of the batteries depends on the DoD design. If the DoD design is small, the battery lifetime will be longer, and if the DoD design is larger, then the battery lifetime will become shorter. The lifetime of the batteries is described by the life cycle number. A life cycle of the battery is one cycle of charge and discharge process. Battery life cycle decreases as DoD increases, as shown in Fig. 3.4. This graph assuming the charge and discharge process is occurred at constant DoD value.

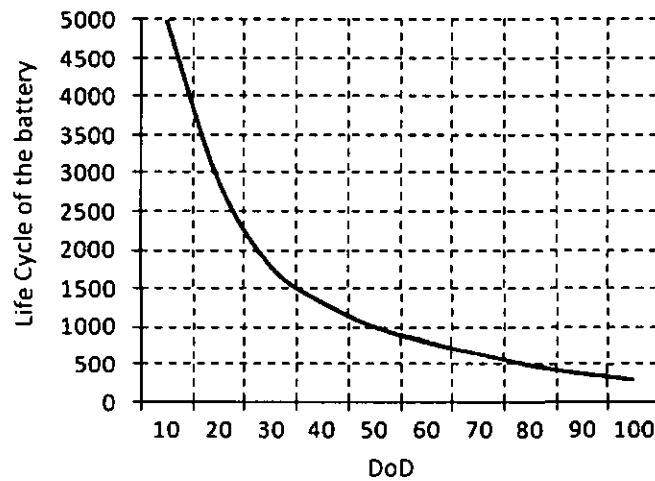


Figure 3.4: Life Cycle vs DoD of deep cycle battery [adapted from 104]

A DoD greater than 80% should be avoided. The "sweet spot" (optimum DoD for the greatest amount of power produced over the service life) is generally somewhere between 20% and 60% on the average [104].

For critical systems such as telecommunication equipment, a reasonable number of autonomy days (N_a) are five (5) and for low cost client equipment, it can be reduced to a N_a of three (3) or two (2). House lighting is considered as low-cost client load, so N_a value of 3 or 2 can be used. 12 Volts system voltage is commonly used for small system under 1-kWp.

To calculate battery lifetime, following equation was used [105]:

$$t_3 = \frac{N_{cd}}{n_{cd}} \times \sigma(T) \quad (3-3)$$

N_{cd} is the maximum number of charge–discharge cycles at 25°C and at a specified DoD (depth of discharge) and n_{cd} is the number of charge–discharge cycles yearly. The service life is dependent on the temperature T (°C) and $\sigma(T)$ is a temperature dependent correction factor.

Nevertheless, it is complex to predict battery life, because daily energy balance of PV system is a stochastic process. Charge-discharge cycles would be occurred in different DoD level every day. For example, battery with maximum DoD design 70% and with N_a number 2 will reach the maximum DoD level only if there are two consecutive day which solar radiation is low. On the other day which solar radiation high, the charge-discharge processes might be occurred in 35% DoD. Increasing battery capacity or PV panel capacity will increase the battery lifetime.

3.2 Data Preparation for LPSP calculation

Daily variation of solar radiation is the main factor that affects PV system performance since it is the only energy source for the system. Hence, complete time series solar radiation data is significant for performance prediction of PV system. Sometimes the solar radiation data is not available for the test site. The data access often limited, even though there is a weather station near the locations. Furthermore, the data may contain missing data for several days in the absence of measurement. This might happen due to sensor error or damage. This missing data may only occur for some parameter in meteorological data set, while other parameters are complete

data. Therefore, missing data estimation is required in order to utilize the data set for various purposes.

In the LPSP calculation, time-series data is required (at least hourly or daily solar radiation data must be available for 1 year). In this study, hourly weather data for the year of 2003 from Ipoh meteorological station was used to calculate LPSP. There are 23 days missing solar radiation data in the data set as shown in Fig. 3.5.

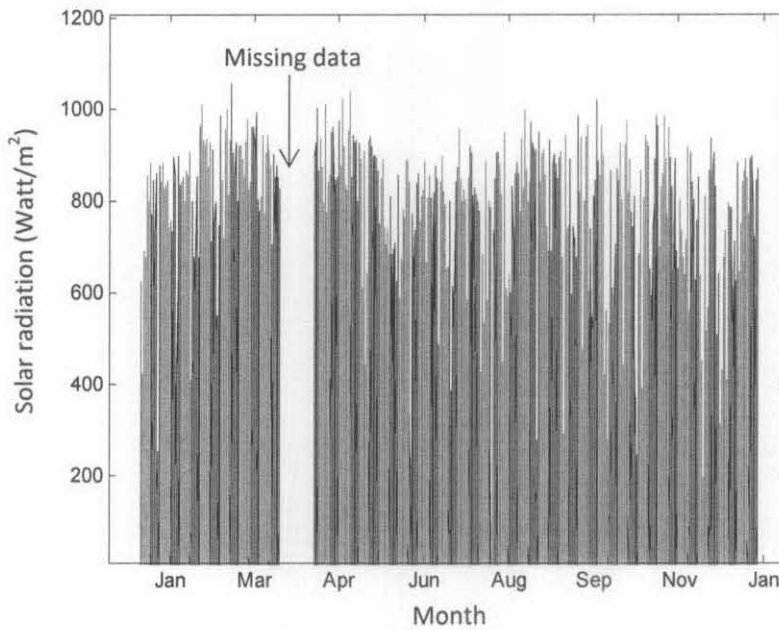


Figure 3.5: One-year hourly solar radiation data with 23 days missing data

There are various ways to estimate solar radiation on certain locations on the earth. In this study, the available data are hourly Relative Humidity and Air Temperature data from Ipoh meteorological station (one-year data) and 5-minutes time-step Beam, Diffuse, Global Horizontal Solar radiation data from UTP Solar laboratory (one-month data). Hence, two methods are proposed in this study based on the available data. The first method use beam atmospheric transmission determination using measured RH and ambient temperature data. The second method use RH-beam transmittance correlation through the clearness index-beam transmittance correlation. Fig. 3.6 shows complete data set of ambient temperature and relative humidity, and Fig. 3.7 shows one-day sample data from UTP solar laboratory.

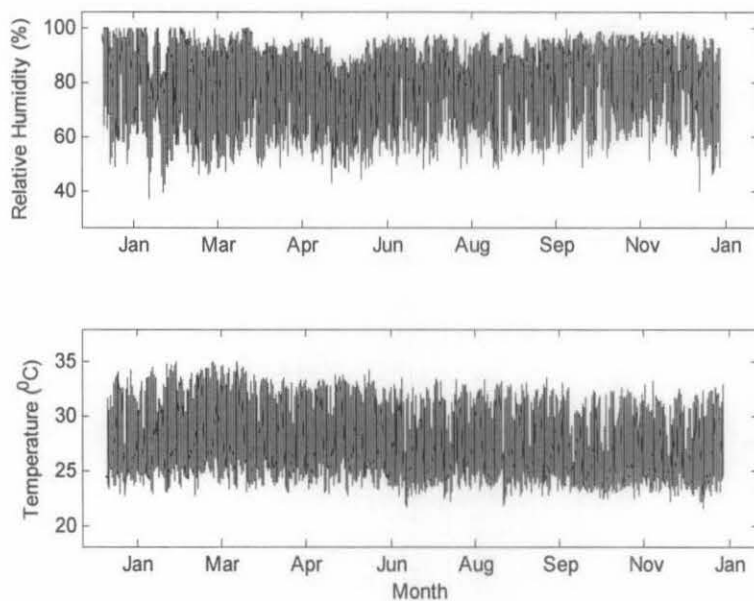


Figure 3.6: Complete hourly data of RH and ambient temperature

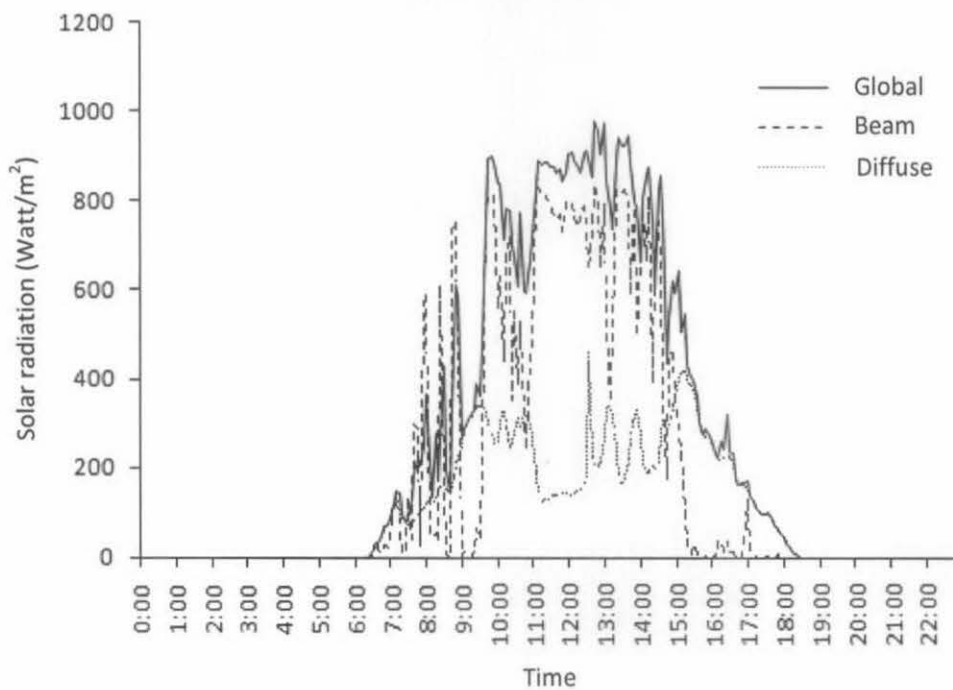


Figure 3.7: Measured solar radiation data from UTP solar laboratory (5 July 2010)

Statistical parameters comparison between proposed methods and some existing methods were used to validate the estimation results. After the results have been validated, it can be used to fill missing data in the data set. Then complete hourly time series solar radiation data set would be available for LPSP calculations.

3.2.1 Missing data estimation

Missing data estimation in this study is based on solar radiation decomposition model and atmospheric transmittance determination using meteorological data. In the decomposition model, total radiation on horizontal surfaces (G_{Th}) is decomposed into two basic components: direct beam radiation (G_{Bh}) and diffuse solar radiation (G_{Dh}) as stated in Eq. 2-17.

The local intensity of solar beam radiation is determined by the angle between the direction of the sun's rays and the earth's surface. The location of the sun is given by the angle between the sun location and the normal to the surface, referred as the zenith angle (θ_z). Zenith angle is dependent on geo-location and time. It is a function of the latitude, time of the day, and time of the year as shown in Eq. 2-2.

To calculate beam radiation on horizontal surface Eq. 3-4 was used as follows:

$$G_{Bh} = G_{Bp} \times \cos(\theta_z) \quad (3-4)$$

(G_{Bp}) is beam radiation on the surface perpendicular to the beam. The model chosen to calculate G_{Bp} is from Liu and Jordan [106], described in Eq. 3-5 as follows:

$$G_{Bp} = G_{sc} \tau^m \quad (3-5)$$

where G_{sc} is the solar constant ($1,367 \text{ W/m}^2$), τ is the atmospheric transmittance, and m is the optical air mass number. The optical mass number (m) is found from the following relationship [34]:

$$m = \frac{P_a}{101.3 \cos \theta_z} \quad (3-6)$$

with P_a being the atmospheric pressure (kPa) at the site, and the zenith angle from Equation 3.40. Average barometric pressure was estimated from the relationship [33]:

$$P_a = 101.3 \times e^{-(a/8200)} \quad (3-7)$$

where a is the elevation of the site in meters (m).

However, not all of the beam radiation reach the earth's surface. Radiation is reflected or absorbed by atmospheric gases, clouds, and dust particles. Some of this

radiation is scattered toward earth and is referred to as diffuse radiation (G_{Dh}). Campbell and Norman [34] devised an empirical relationship based on work of Liu and Jordan [106] for an estimation of diffuse radiation. This relationship is given by:

$$G_{Dh} = 0.30(1 - \tau^m) \times G_{0h} \times \cos \theta_z \quad (3-8)$$

The key for the accuracy of above method is in the determination of atmospheric transmittance (τ). Atmospheric transmittance is the percentage of the beam (direct) radiation that will penetrate the atmosphere without being scattered.

3.2.2 Atmospheric transmittance determination procedure: Method 1

Spokas and Forcella [28] used precipitation data to build a decision matrix of atmospheric transmittance. However, in this research precipitation data was not available. Some literature stated that there is a negative correlation between atmospheric transmittance and RH [107]. Therefore, the decision matrix for atmospheric transmittance can be built using RH and ambient temperature data. In method 1, the decision matrix is built with the concept that water vapor (by mean of RH) reduce the incoming radiation. Figure 3.8 shows flow chart for the decision of τ value. The τ value in the flow chart was locally determined using the training of data set to get a minimum error. Table 3.2 shows determination criteria of beam transmittance by mean of relative humidity (RH).

Table 3.2: Determination criteria of beam transmittance by mean of RH

<i>No</i>	<i>RH condition (%)</i>	<i>τ value</i>
1	$RH \leq 40$	0.69
2	$40 < RH \leq 45$	0.67
3	$45 < RH \leq 55$	0.57
4	$55 < RH \leq 65$	0.47
5	$65 < RH \leq 75$	0.41
6	$75 < RH \leq 80$	0.3
7	$RH > 80$	0.2

In the Spokas and Forcella method [28], if $\Delta T < 10^\circ C$, the value of τ is modified using the following relationship (assumed that the site was not near the poles) as described by Eq. 3-9 as follows [21]:

$$\tau' = \tau / (11 - \Delta T) \quad (3-9)$$

In the Method 1, limitation of ΔT was adjusted for tropical area. The above equation was used for $\Delta T < 8^\circ\text{C}$. Table 3.2 shows criteria for the decision of τ value. τ value of 0.6-0.7 are commonly used for clear sky atmospheric transmittance coefficient value. In this study τ value of 0.69 was used for clear sky, assumed that the clear sky condition occurred when $\text{RH} < 40\%$ and ambient temperature more than 8°C . Calculation algorithm was built based on decision matrix and the τ values was locally determined using the training of data set to get a minimum error. Fig. 3.8 shows the complete systematic procedure to determine beam transmittance.

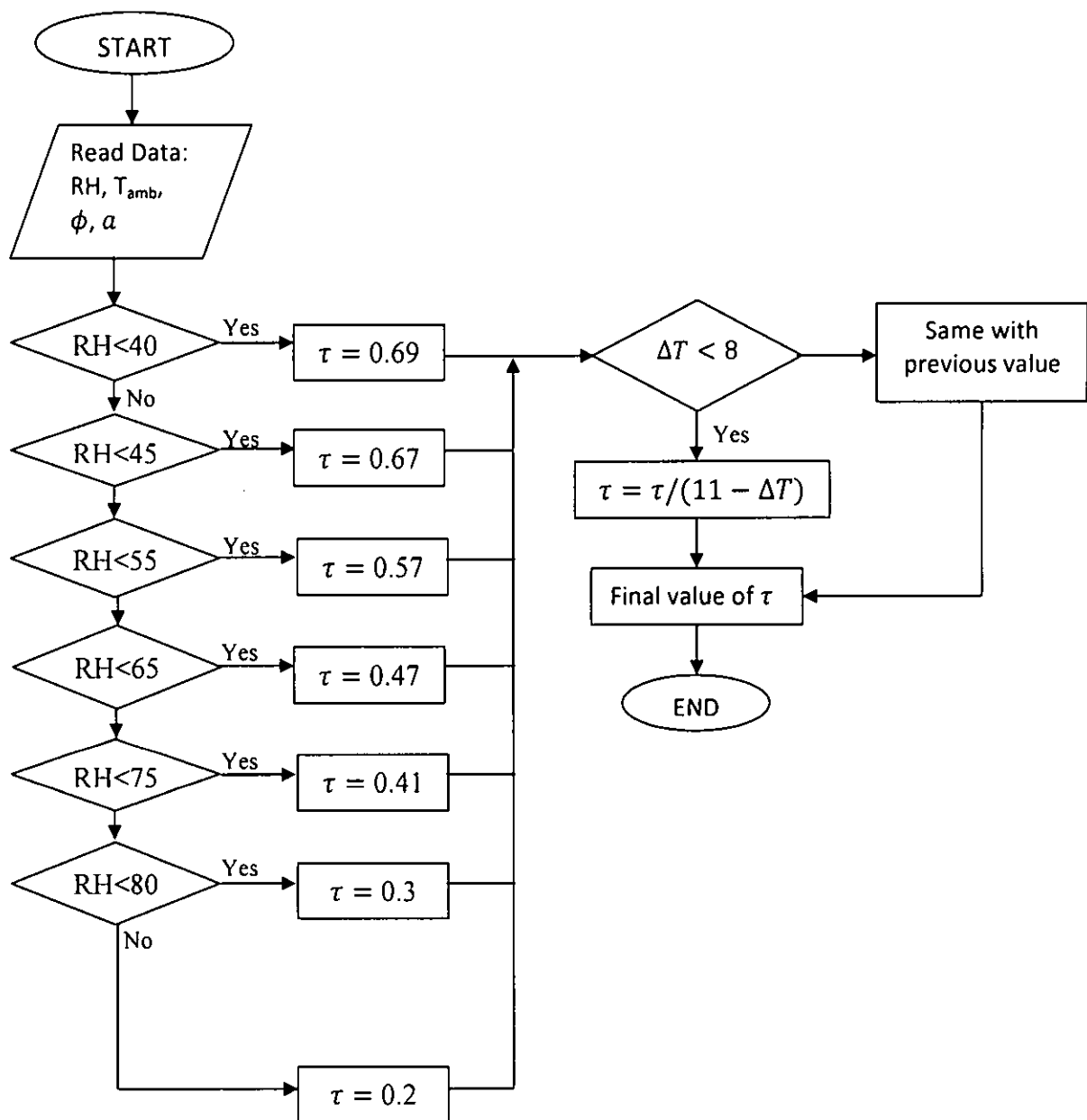


Figure 3.8: Flow chart to estimate Solar Irradiation from limited meteorological data

3.2.3 Atmospheric transmittance determination procedure: Method 2

The second method used in this study is by developing a correlation of RH, clearness index and beam transmittance. The data to find the correlation between beam transmittance and clearness index is measured data from UTP solar laboratory. Five minutes time step data of global, beam and diffuse radiation from June to July 2010 was used. Before finding the correlation of beam transmittance and clearness index at the test site, RH-clearness index correlation was obtained from Ipoh city available data as presented in Fig. 3.9.

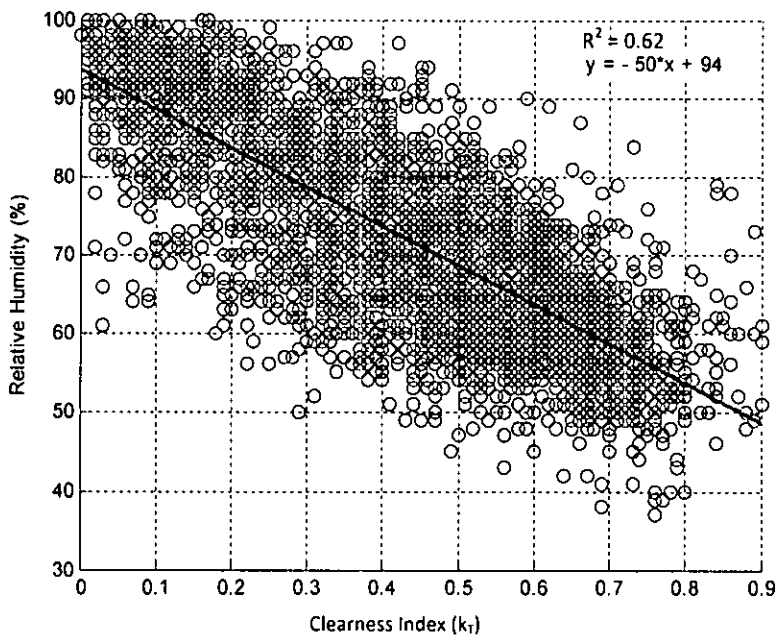


Figure 3.9: Scatter plot of Relative humidity and Clearness Index of the data obtained from local meteorological office

Beam transmittance-clearness index correlation was obtained from UTP solar laboratory data. Some erroneous data were rejected. Following constraint were used as data rejection criteria:

- Reject data if solar radiation less than 100 W/m^2
- Reject data if clearness index >1
- Reject data if beam transmittance >1

Then, RH-Clearness Index data is correlated with Beam transmittance-Clearness Index data to get RH-Beam transmittance correlation. Correlation between RH and

beam transmittance was obtained using linear, quadratic, and cubical regression as plotted in Fig. 3.10. Regression equations were obtained as follows:

$$\text{Linear} \quad : \tau = -0.019 \text{ RH} + 1.576 \quad (3-10)$$

$$\text{Quadratic} \quad : \tau = 0.00075 \text{ RH}^2 - 0.12676 \text{ RH} + 5.36 \quad (3-11)$$

$$\text{Cubical} \quad : \tau = 0.0000072 \text{ RH}^3 - 0.0008 \text{ RH}^2 - 0.0161 \text{ RH} + 2.779 \quad (3-12)$$

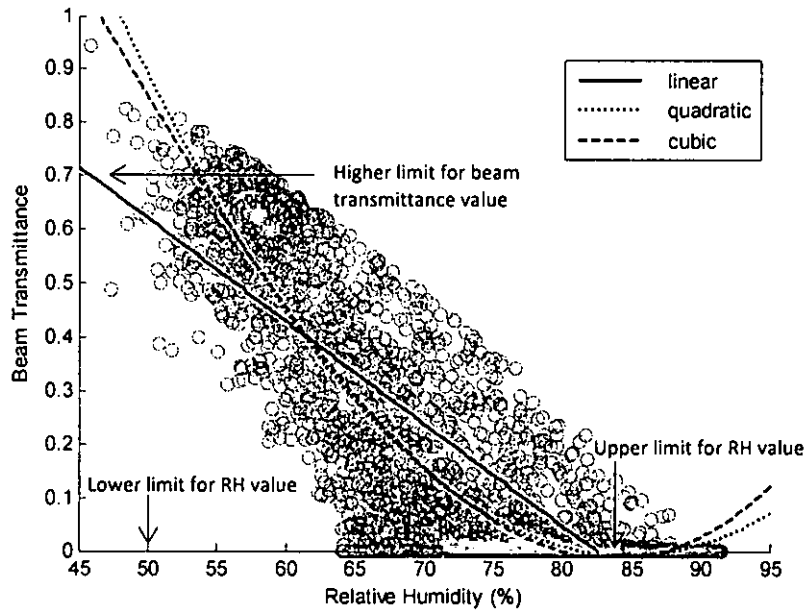


Figure 3.10: Linear, quadratic, and cubic regression results of Beam transmittance vs RH

In fitting a polynomial to a set of data pairs, it is possible to determine the necessary degree of the polynomial by study of the scatter diagram and get the higher correlation coefficient with the higher polynomial degree. S.M. Ross [107] emphasize that one should always use the lowest possible degree that appears to adequately describe the data. Thus, for instance, whereas it is usually possible to find a polynomial degree n that passes through all the n pairs (x_i, y_i) , $i=1, \dots, n$, it would be hard to ascribe much confidence to such a fit. That is why in this study, the regressions were limited to the cubical or third degree.

3.2.4 Statistical techniques to validate the model

Estimation results were validated using statistical techniques. Pearson correlation coefficient (Eq. 3-13) was calculated as a routine correlation indicator [108].

$$r = \frac{\sum_{i=1}^n (x_i - \bar{x}_i) + (y_i - \bar{y}_i)}{\sqrt{\sum_{i=1}^n (x_i - \bar{x}_i)^2 \sum_{i=1}^n (y_i - \bar{y}_i)^2}} \quad (3-13)$$

Residual error was calculated using Root Mean Square Error (RMSE) and presented in Normalized Root Mean Square Error (NRMSE) as follows:

$$RMSE = \sqrt{\frac{\sum \{Y_c - Y_o\}^2}{n}} \quad (3-14)$$

$$NRMSE = \frac{RMSE}{Y_{max} - Y_{min}} \quad (3-15)$$

where Y_c is predicted variable Y_o is measured variable, n is number of data, Y_{max} is maximum measured data Y_{min} is measured minimum data.

Good correlation coefficients do not automatically indicate a good model. Therefore, index of agreement can be used to assess model performance. Index of agreement was calculated using Eq. 3-16 as described below:

$$d = 1 - \sqrt{\frac{\sum \{Y_c - Y_o\}^2}{[\sum (|x_i - \bar{x}_i| + |y_i - \bar{y}_i|)]}} \quad (3-16)$$

where x_i is predicted variable y_i is measured variable, \bar{x}_i is averaged value of predicted variable and \bar{y}_i is averaged value of measured variable.

3.2.5 Data required for LPSP calculation

Aside from solar radiation data, the data required for LPSP calculation are daily averaged ambient temperature (T_{amb}), daily averaged incident solar radiation (H), daily energy demand (total lighting load during the night, E_L) and system parameters. The daily averaged ambient temperature data and daily averaged incident solar radiation were obtained from hourly ambient temperature and solar radiation data. These data were required to estimate PV panel temperature using Eq. 3-24. System parameters required are system voltage (V_{rated}), minimum state of charge of the battery design (E_{Bmin}) design, maximum state of charge of the battery design (E_{Bmax}), negative temperature coefficient of PV panel (γ_t), daily self-discharge coefficient (η_{self}), system efficiency (η_{system}), charging efficiency (η_{batt}) and inverter efficiency (η_{inv}). Two more parameters to be considered after calculation are the

number of autonomy day and or useful battery energy. Table 3.3 shows the initial value of the parameters used in the calculation.

Table 3.3: System parameter value used for calculation

No.	Parameter	Value	Unit
	<i>Fixed parameters:</i>		
1	Minimum SOC design (E_{Bmin})	30	% of E_{Bmax}
2	Maximum SOC design (E_{Bmax})	100	% of E_{Bmax}
3	System voltage (V_{rated})	12	Volt
4	Negative temperature coefficient (γ_t)	-0.005	$^{\circ}\text{C}^{-1}$
5	Connection losses, dust factor (η_c)	90	%
6	Daily self discharge rate (η_{self})	1	%
7	Inverter Efficiency (η_{inv})	90	%
8	Charging Efficiency (η_{batt})	99	%
9	Nominal load value (constant during the night)	140	Watt
10	Daily load operation hour	10	hour
11	Daily load (nominal load x operation hour)	1400	Wh
	<i>Parameters to be considered after calculation:</i>		
12	Desired N_a	2-5	Days

Minimum and maximum State-of-Charge (SOC) designs are determined based on reference [86]. Sometimes the term Depth-of-Discharge (DoD = 1-SOC) is used. Deep discharges may reduce the cycle life of the battery dependent on battery characteristics. For lead-acid battery, DoD design should not exceed 80%. In this study, minimum SOC is the minimum battery SOC during one-year system operation. The daily cycle would be varied. The common system voltage for small-scale PV system is 12V as mentioned by some literature [13, 14]. Negative temperature coefficient was obtained from PV panel datasheet. System efficiency, daily self-discharge coefficient, inverter efficiency, and charging efficiency are assumed based on references [13, 71, 99, and 115]. The nominal load value and operation hours are assumed as constant lighting load for Malaysian typical terraced house. N_a is the number of Autonomy day. As explained in previous chapter the reasonable value for N_a is about three days for a low-cost client. In LPSP calculation, the number of autonomy day and ideal useful battery energy were not determined before calculation but can be considered after calculation.

3.3 Daily data based LPSP calculation procedure

Proper sizing of PV panel and Battery in SAPV system is important to satisfy the total load demand. Deterministic method as described in section 3.1 is unable to provide satisfactory solutions. Statistical method such as Loss of Power Supply Probability (LPSP) calculation would give the better approach and provide a solution that is more satisfactory [63-76]. This section will explain LPSP calculation procedure that is developed in this study.

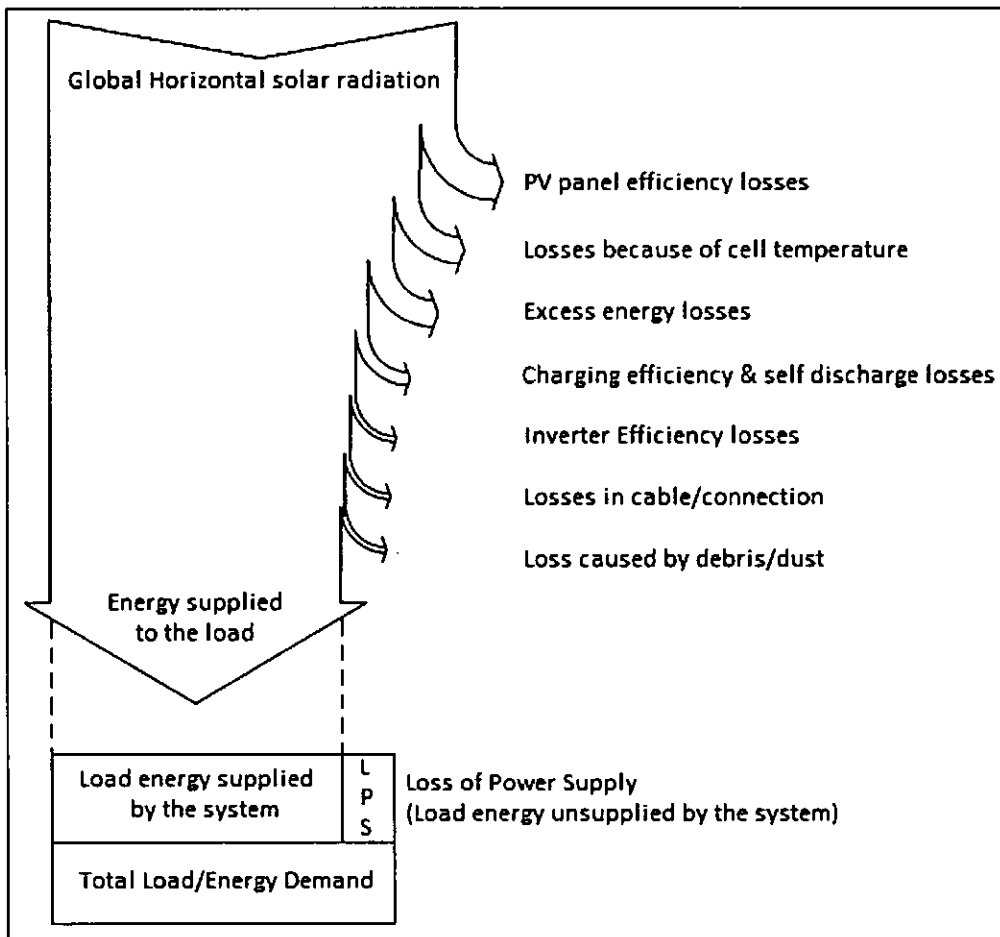


Figure 3.11: Energy balance description in PV system

PV system performance is affected by various parameters. Fig. 3.11 shows energy balance description in PV system. In this study, the parameters being considered to determine PV panel performance are solar irradiance received on tilted surface, PV panel temperature, daily energy load and daily battery condition. Energy losses

because of connections, charge controller efficiency, and other various losses will be considered by using the efficiency factor in the calculation.

3.3.1 Global solar irradiance received on the tilted surface data generation

Commonly only global horizontal solar irradiance data is available from the weather station or global solar map, whereas the PV panel installation is at various tilted angles. In Building Integrated Photovoltaic (BIPV), rooftop PV panel installation is commonly used. PV panel sometimes is not installed in optimal tilted angle for the site due to various building roof orientations, tilted angle and some difficulties in installation. Hence, global solar irradiance received on the tilted surface prediction is important to predict PV system performance. First, decomposition model was used to calculate solar radiation component and then solar radiation on the tilted surface can be calculated using existing model.

In the decomposition model, if Relative Humidity (RH), Ambient temperature (T_{amb}) and global horizontal solar radiation (G_{Th}) are known, Reindl full correlation is used (Eq. 2-12 – Eq. 2-14). If the only parameter known is G_{Th} , then G_{Dh} estimation is given by Reindl reduced correlation (Eq. 2-9 – Eq. 2-11).

The calculation of accurate global solar irradiance received on the tilted surface prediction is not an easy task. Various models have been developed and compared by researchers to predict the amount of global solar irradiance incidents on inclined surfaces [46-56]. From existing models, Perez's model was suggested as one of the best models to calculate hourly mean solar irradiation on the tilted surface [49], while other researchers said that it is difficult to compare well-known existing models [47]. In TRNSYS 16 there are four models available to calculate irradiation component received on the tilted surface [45]. The models are Isotropic model [53], Hay and Davies model [55], Reindl model [52] and Perez model [53]. From literature review, Reindl model and Perez model are better than two other models. Reindl model is preferred due to simplicity and accuracy while Perez's model preferred for better accuracy.

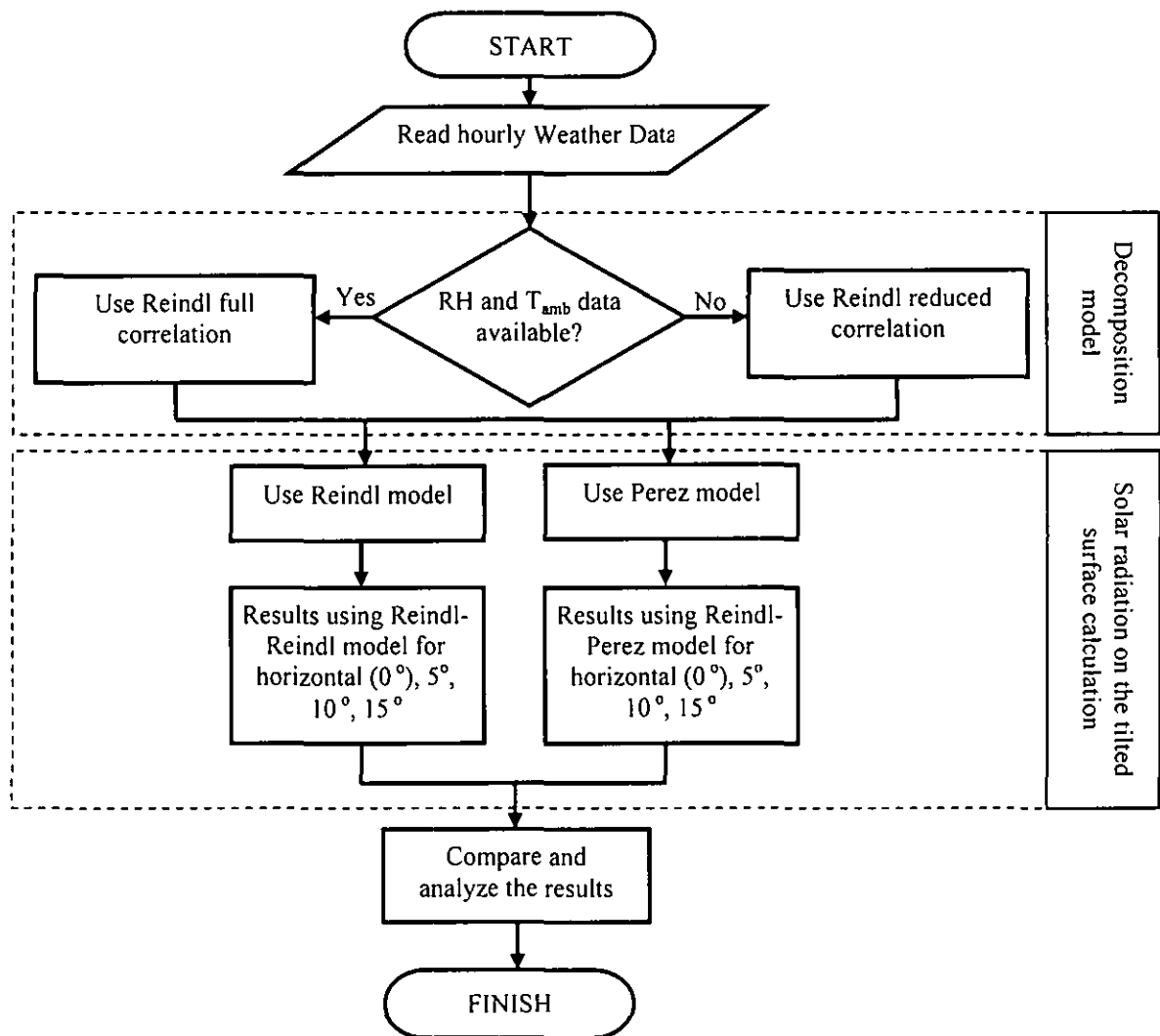


Figure 3.12: Procedure to calculate solar radiation on the tilted surface

The step to calculate radiation on the tilted surface was explained in section 2.1.5. Diffuse radiation ratio (τ_d) can be calculated using Reindl model or Perez model on TRNSYS 16. After radiation on the tilted surface (G_{Tt}) is found, then it is used to calculate PSH_t which is used to calculate $E_{PV(n)}$. Fig. 3.12 shows the systematic procedure to obtain solar radiation on the tilted surface.

3.3.2 PV panel power output calculation procedure

After solar radiation on the tilted surface are obtained, PV panel power output ($E_{PV(n)}$) can be calculated. Cell temperature affects the efficiency of the PV panel, whereas PV panel temperature is not always monitored. Hence, PV panel

temperature prediction is necessary. PV panel temperature can be approximately estimated by using ambient temperature and solar radiation as described in Eq. 3-17 as follows [71]:

$$\overline{T_{cell}} = \overline{T_{amb}}(1 + 1.25\overline{G}) \quad (3-17)$$

where $\overline{T_{amb}}$ are daily average of ambient temperature ($^{\circ}\text{C}$) and \overline{G} are daily average solar radiation (Watt/m^2). PV panel temperature (T_{cell}) measurement was carried out in this research, measured and calculated $\overline{T_{cell}}$ have been compared. Fig. 3.12 shows the graphical comparison of $\overline{T_{cell}}$ estimation. An RMSE value of comparison results in the month of June 2010 is 2.43°C . Fig. 3.13 shows a good compromise between measured and predicted $\overline{T_{cell}}$, with RMSE and NRMSE value of 2.4°C and 5%.

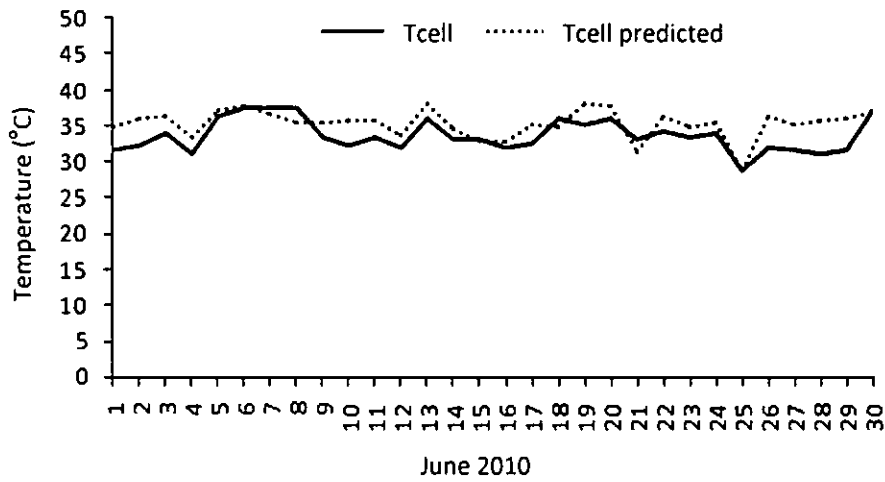


Figure 3.13: Graphical comparison of $\overline{T_{cell}}$ estimation in the month of June 2010

PV panel output calculated using following equation [71]:

$$E_{PV(n)} = P_{PV} \left(1 + \gamma_t (\overline{T_{cell(n)}} - 25^{\circ}\text{C}) \right) PSH_{t(n)} \cdot \eta_{system} \quad (3-18)$$

P_{PV} is nominal peak power of PV panel. γ_t is the negative temperature coefficient of power with respect to solar cell temperature. PSH_t is Peak sun hour on the tilted surface. $PSH_{t(n)}$ is calculated using Eq. 2-8 and 2-9. η_{system} is overall system efficiency ($\eta_c \cdot \eta_{batt}$ when used to charge the battery or η_c when directly used for load). Since in this study there is no day load, so $\eta_{system} = \eta_c \cdot \eta_{batt}$.

3.3.3 Estimation of daily battery condition

The operating condition of PV system is influenced by the weather condition on the site that is a stochastic phenomenon. That is why the PV system performance prediction rather complicated. The output power of PV panels, which is used to charge the battery, varies with solar radiation and temperature. The estimation of the battery state of charge (SOC) is complicated under such uncontrolled charge/discharge cycles. The energy stored in the battery on the day n ($E_{B(n)}$) is calculated using Eq. 3-19 and 3-20 as follows:

$$E_{Bhalf(n)} = E_{B(n-1)} + E_{PV(n)} \quad (3-19)$$

$$E_{B(n)} = E_{Bhalf(n)}(1 - \eta_{self}) - \frac{E_{load(n)'}}{\eta_{inv}} \quad (3-20)$$

η_{self} is a daily self-discharge factor, which is occurred during discharge period. $E_{load(n)'}$ is nominal load energy of the day and η_{inv} is inverter efficiency. The self-discharge rate is a measure of how quickly a cell will lose its energy while sitting on the shelf due to unwanted chemical actions within the cell. The rate depends on the cell chemistry and the temperature of the battery bank. Typical self-discharge rates for common rechargeable cells are as follows [109]:

- Lead Acid 4% to 6% per month
- Nickel Cadmium 15% to 20% per month
- Nickel Metal Hydride 30% per month
- Lithium 2% to 3% per month

Fig. 3.14 shows self-discharge characteristic of common lead acid battery, while Fig. 3.15 shows discharge's characteristic curve of common lead acid battery from the references [110-111]. However, in this research daily self-discharge factor (η_{self}) is assumed to be 1%. This value was obtained by assuming battery bank temperature about 30 °C and weekly self-discharge rate about 7%. On any day (n), the energy stored in the battery is subject to the following constraints:

$$E_{Bmin} \leq E_{B(n)} \leq E_{Bmax} \quad (3-21)$$

$$E_{Bmin} = (1 - DoD) \times E_{Bmax} \quad (3-22)$$

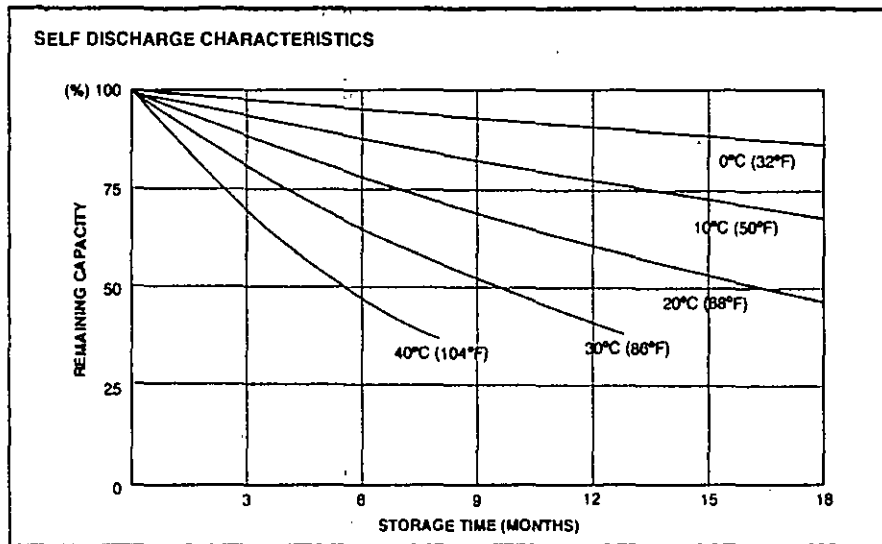


Figure 3.14: Self-discharge characteristic of lead acid battery [110]

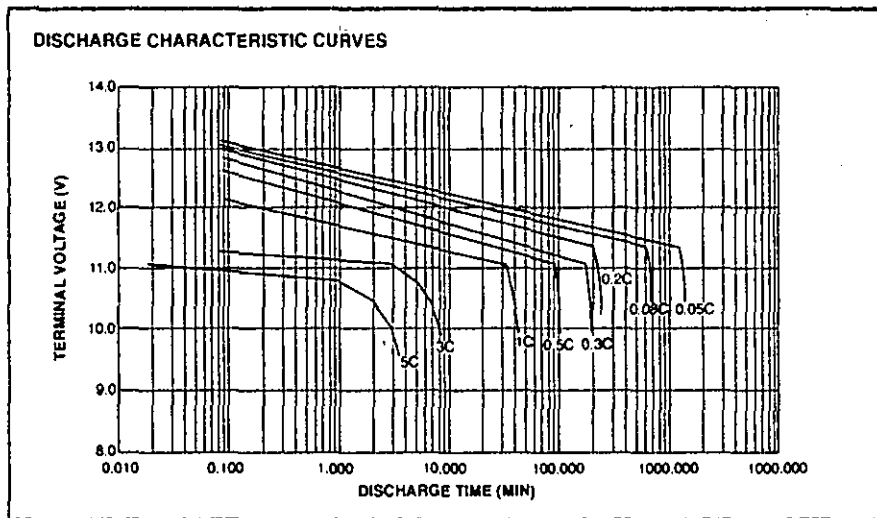


Figure 3.15: Discharge characteristic curve of lead acid battery [111]

E_{Bmin} and E_{Bmax} are the minimum energy stored in the battery and the maximum energy stored in the battery respectively. The selection of the maximum allowable DoD is actually a compromise between system life and cost. Thus, the calculation of the battery SOC is:

$$SOC_{(n)} = \frac{E_{B(n)}}{C_{bat} \cdot V_{rated}} \quad (3-23)$$

3.3.4 Daily analysis of PV system behavior

When the value of SOC of the battery is 1 (fully charged), the system controller will stop charging and prevent the battery from overcharging. Otherwise, if the SOC of battery reach minimum allowable value of SOC, the controllers will cut-off the load. In terms of the allowable minimum battery SOC, the LPSP can be mathematically defined as described in Eq. 3-24 and 3-25 [70]:

$$LPSP = P\{E_{B(n)} \leq E_{Bmin}; n \leq N\} \quad (3-24)$$

$$LPSP = \frac{\sum_{n=1}^N LPS_{(n)}}{\sum_{n=1}^N E_{load(n)}} \quad (3-25)$$

where $E_{B(n)}$ is battery energy level on the day n , E_{Bmin} is minimum energy level of the battery, N is number of days, $LPS_{(n)}$ is Loss of Power Supply for day n and $E_{load(n)}$ is load energy for day n .

Hourly data is preferred in Loss of Power Supply Probability (LPSP) calculations, but the management of a large database can sometimes add constraints in its implementation. On the other hand, daily data can be used, but sometimes it does not provide sufficient information as hourly data. In this study, daily data by mean of daily Peak Sun Hour (PSH) value was used for LPSP calculation. A new algorithm is proposed to improve daily data based LPSP calculation. In the method that is described by WX. Shen there is no constrain declared for LPS value [70], so the value of LPS can be positive, zero or negative. Negative value is illogical, but it means there is excess or wasted energy. The lowest logic value for LPS should be zero and excess energy during the day (E_{excess}) can be calculated using the procedure that is described in this section.

In the daily cycle of PV-system, time of the day can be differentiated into two conditions. First, the daytime when solar radiation are available: during this period, battery charging is possible as long as load energy during the daytime is less than input energy. Second, the nighttime (no solar radiation): when only battery discharges conditions is possible. Fig. 3.16 describes the example of PV system daily cycle. In the first day, only night load existed, while in second day, the day, and night load

existed. Since this study focused on lighting load, it was assumed that the lighting load only occurs during the night for the LPSP calculation. However, if the system is designed to contain the day loads, the day load value needs to be added to the calculation algorithm.

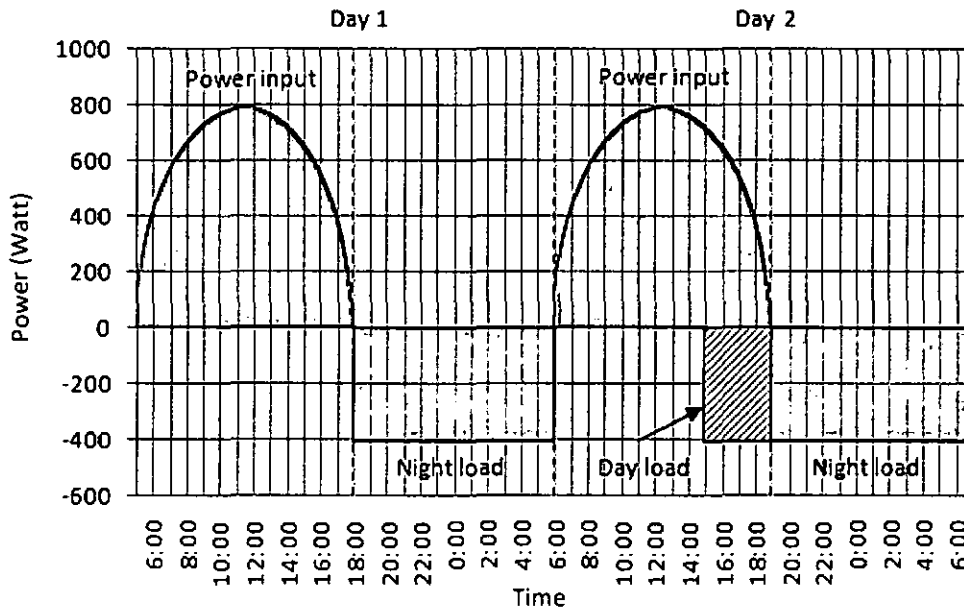


Figure 3.16: Daily cycle of PV system description

In tropical countries like Malaysia, duration of daytime and nighttime is almost the same throughout the year. Therefore, the term “half day” was used in this study to describe this condition. Condition in half day is a condition at sunset, and full day is at sunrise. During charging period, at half of the day, there are two possibilities of the battery conditions. The first possible condition is $E_{Bhalf(n)} = E_{Bmax}$, which is occurred when $E_{PV} + E_{B(n-1)} > E_{Bmax}$ (in this condition excess energy is existed) or when $E_{PV} + E_{B(n-1)} = E_{Bmax}$ (in this condition excess energy is 0). Second possible condition is $E_{Bhalf(n)} < E_{Bmax}$ which is occurred when $E_{PV} + E_{B(n-1)} < E_{Bmax}$. The battery condition will never reach over E_{Bmax} because it is maximum battery capacity and the controller controls input energy to avoid overcharge.

Fig. 3.17 shows the example of the battery condition during the daily cycle of PV system. The figure describes a general event that can be occurred during the PV system operation. It can be seen in Fig. 3.17 full charge condition occurs at day 1, 2, 4, and 5 while battery condition below E_{Bmax} occurs at day 3 when energy input is low. The battery energy is always between E_{Bmax} and E_{Bmin} .

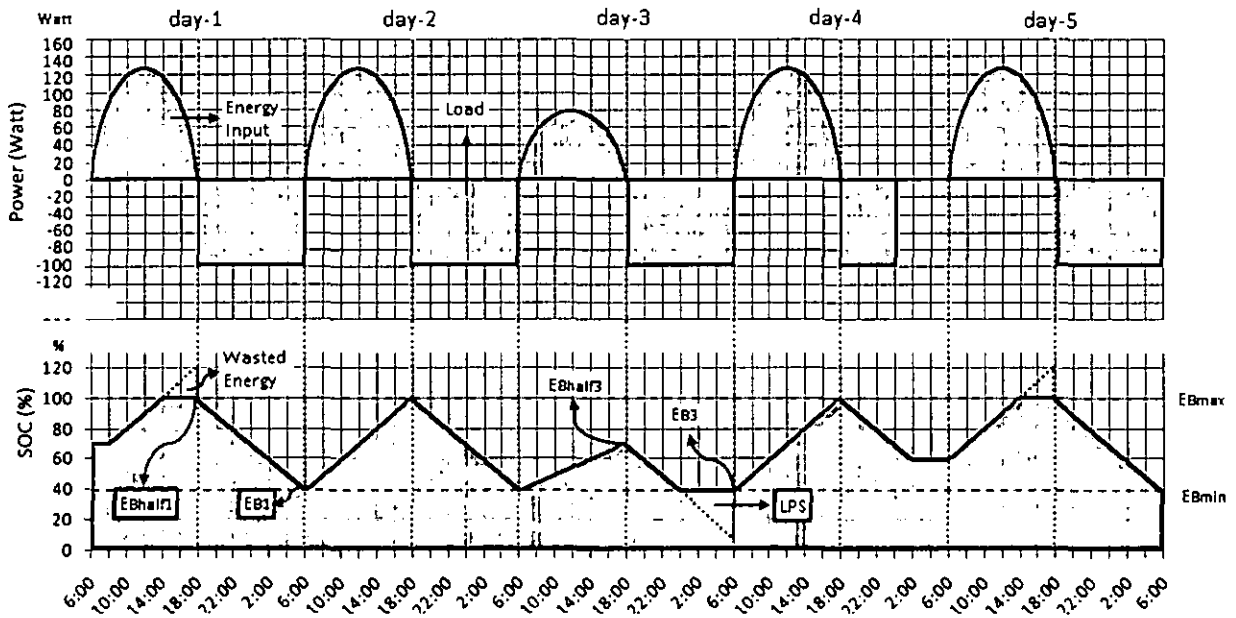


Figure 3.17: Daily variation of battery condition description

During the discharge period, there are two possibilities of the battery conditions at the end of a day, first $E_{B(n)} = E_{Bmin}$, which is occurred when $E_{Bhalf(n)} - E_{load} < E_{Bmin}$ (in this condition LPS is existed) or when $E_{Bhalf(n)} - E_{load} = E_{Bmin}$ (in this condition LPS is 0). Second possible condition is $E_{B(n)} > E_{Bmax}$ which is occurred when $E_{Bhalf(n)} - E_{load} > E_{Bmin}$. The battery condition would never reach below E_{Bmin} because the controller also controls load energy to avoid over-discharge. It can be seen in Fig 3.17 minimum battery charge condition occurs at day 1, 2, 3, and 5 while battery condition below E_{Bmin} occurs at day 4 when load energy input is low. Using above analysis LPSP calculation algorithm was developed as described in Appendix B. Flow chart to calculate LPSP based on above constraint is described in Fig. 3.18.

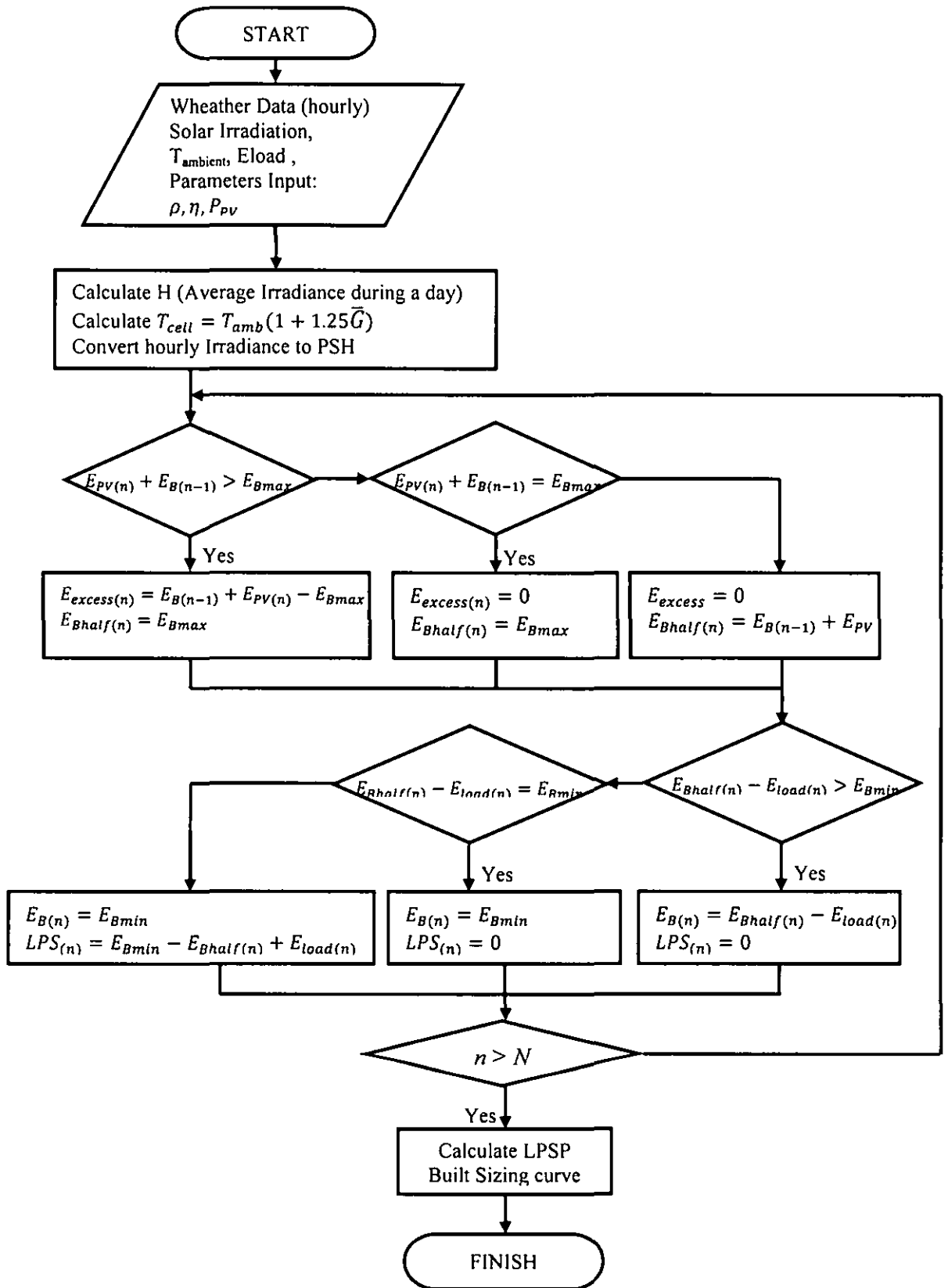


Figure 3.18: Simplified flow chart to calculate LPSP

3.4 Sizing Optimization of the PV System

Optimum configuration the PV system was obtained using minimum LPSP, Excess Energy, Capital Cost and Life Cycle Cost. LPSP and Excess energy calculation procedure was described in previous sections. Cost analysis was carried out using Life Cycle Cost analysis adopted from [112, 113, and 114] as follows:

$$LCC = CC + M + RR - S \quad (3-26)$$

CC is capital cost. M is operation and maintenance cost. RR is repair and replacement cost and S is the salvage value (the estimated value of an asset at the end of its useful life). All costs are converted to present worth value for the single present value and for uniform present value respectively [112]:

$$P_s = \frac{F}{(1+I_d)^N} \quad (3-27)$$

$$P_u = \frac{A[1-(1+I_d)^{-N}]}{I_d} \quad (3-28)$$

P_s is present worth value for single payment and P_u is for uniform. F and A are a sum of money (capital equipment), N is a number of years and I_d is the net discount rate i.e. nominal discount rate minus the rate of inflation. The present worth factor for a single payment is P_s/F and for uniform payment is P_u/A .

Further economic analysis can also be carried out. Annual energy service (AES), Annual Life Cycle Cost ($ALCC$), Cost of Energy (COE) and Payback Period are calculated using following formula:

$$AES = \sum \left(\frac{E_{load}}{\eta_{inv}} \right) - \sum LPS \quad (3-29)$$

$$ALCC = ACC + AMC \quad (3-30)$$

AMC is annual maintenance and operation cost, it was taken 1% of capital cost. ACC is Annualized capital cost as follows:

$$ACC = CC \times CRF \quad (3-31)$$

The capital recovery factor (CRF) is a function of discount rate and lifetime described as following equation:

$$CRF = \frac{i_d(1+i_d)^N}{(1+i_d)^N - 1} \quad (3-32)$$

Then the cost of energy can be calculated using following equation:

$$COE = \frac{ALCC}{AES} \quad (3-33)$$

The Cost of Energy is compared to the national grid electricity tariff, forced by Tenaga Nasional Berhad for domestic costumers [115, see Appendix C]. The component cost used for cost analysis in this study was adapted from [116, 117, and 118]. Table 3.4 shows cost of component and parameter that used in cost analysis.

Table 3.4: Component costs and parameters used in *LCC* analysis [116-120]

Component/Parameter	Price ^{*)}
PV panel	15 RM/Wp
Battery	0.8 RM/Wh
Controller	22 RM/Amp
Array installation cost	2 RM/Wp
PV Array life	20 years ^{a)}
Battery life	5 years ^{b)}
Controller life	20 years
Annual operation and maintenance cost	1% of initial capital cost
Net discount rate	5%
Retail markup	30%

^{*)} 1 USD = RM 3.12 (November 2010)

^{a)} Worst case, average lifetime of PV panel is about 20-30 years [76], [105].

^{b)} From calculation using Equation (3-3), with maximum DoD 80%

Table 3.5 shows calculation example of *CC* and *LCC* for 400Wp PV panel and 864Ah battery capacities. The calculation is based on project lifetime of 20 years. This value is taken from the longest lifetime of component in PV-system, in this case PV panel that have lifetime about 20-30 years. The cost presented in the Table 3.5 include GST/VAT rate (Goods and Services Tax/Value added Tax) 15% [119 and 120]. Retail mark-up factor of 30% was used to calculate *CC*. Maintenance Cost was assumed to be 1% of capital cost per year. For Repair and Replacement, it was

assumed that only batteries need to be replaced every 5 years. Salvage cost is assumed to be 10% of *CC*.

Table 3.5: *LCC* calculation example for 400Wp PV panel and 864Ah battery capacity

Component/Parameter	Single present worth year	Uniform present worth year	Cost (RM)	Present worth factor	Present worth (RM)
<i>Capital Cost (CC)</i>					
PV panel	-	-	7800	1	7800
Battery	-	-	10782.72	1	10782.72
Inverter	-	-	858	1	858
Controller	-	-	858	1	858
Other component (10% of PV panel cost)	-	-	780	1	780
Installation cost	-	-	1040	1	1040
<i>Sub total</i>					22118.72
<i>Operation and Maintenance (M)</i>					
Labor: yearly inspection	-	20	221.18	12.46	2756.48
<i>Repair and Replacement (RR)</i>					
Battery	5	-	10782.72	0.78	8448.54
Battery	10	-	10782.72	0.61	6619.65
Battery	15	-	10782.72	0.48	5186.67
<i>Salvage (S)</i>					
10% of original cost of equipment	20	-	2211.87	0.37	833.63
<i>Total</i>					44296.44

In Table 3.5, the first step to calculate *LCC* is by calculate *CC* of the system, consists of PV panel, battery, inverter, controller, other components (accessories) and installation cost. *CC* is the present value so the present worth factor multiplier is one. Operational and maintenance cost for PV system is very low, it is assumed 1% of *CC*. Uniform present values were calculated by multiply operation and maintenance cost with present worth factor for uniform payment that is calculated using Eq. 3-29. Repair and replacement cost for battery are calculated every five years with present worth factor for single payment calculated from Eq. 3.28. Salvage value's present worth factor is also calculated for single payment.

3.5 PV panel characterization in actual condition

This experiment intends to plot the actual Current-Voltage (I-V) and Power-Voltage (P-V) curve of the PV panel. Fig. 3.19 shows the testing configuration. A configuration of several power resistors with different value were used to plot the I-V curve. The power resistor values need to be calculated first using the I-V curve on the PV panel data sheet to determine required power rating.

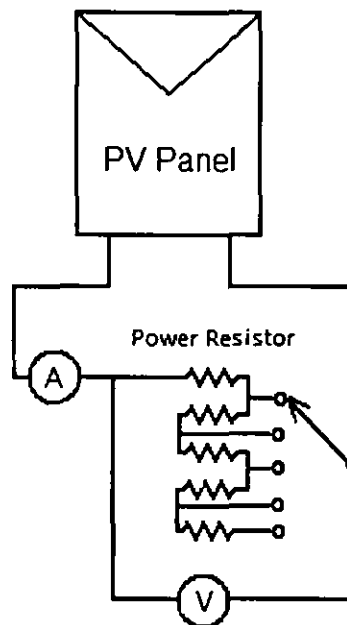


Figure 3.19: PV panel testing configuration

The required resistance value can be calculated and determined from the Standard Test Condition (STC) I-V curve shown in Fig. 3.20. The values of voltage and current from the PV panel I-V curve at STC are then used to determine the resistance value through the following equation:

$$R = V/I \quad (3-34)$$

Total power rating of the resistor configuration needs to be determined. It should not be less than the power of the peak point in the I-V curve. If the power rating of the resistors is lower than the power obtained from I-V curve the resistor will burn out. Eq. 3-35 is used to calculate the minimum required power rating as follows:

$$P = I \times R^2 \quad (3-35)$$

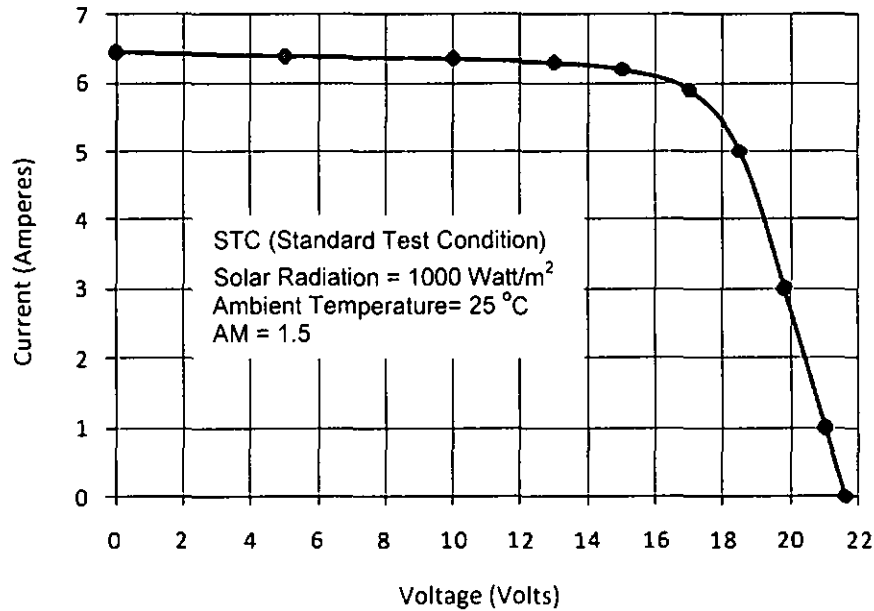


Figure 3.20: PV panel I-V curve at STC (adapted from [121])

Fig. 3.20 shows I-V curve of PV panel obtained from datasheet. The I-V curve presented in Fig. 3.20 is for Standard Test Condition (STC) with solar radiation 1000 Watt/m^2 , ambient temperature of $25 \text{ }^\circ\text{C}$ and AM of 1.5. In this research, ten points were determined to represent STC I-V curve as shown in Fig. 3.20. Then, power resistor value can be calculated and configured for the experiment. The ten points would be represented I-V curve in actual solar radiation.

3.6 PV system for residential lighting

This section presents an experimental set up for PV system application for residential lighting and the measurement system setup.

3.6.1 System Installation

Date : 7 November 2009
 Contractor : A&A Distribution Sdn. Bhd
 Installation Time : 10:00 AM – 06:30 PM
 Installation Site : UTP Weather Station
 Site Coordinate : 4.588° (Latitude), 100.98° (Longitude)

Fig. 3.21 shows the installed PV system. The photovoltaic (PV) array consists of 4 PV panels, each module has 100Wp peak power rate (STC-Standard Test Condition), with total rated peak power 400 Wp. System energy storage or battery has capacity 400Ah at 12V system. The details of PV panel, battery bank and charge controller specifications are available in Appendix D.



Figure 3.21: Solar Power System installed

Solar Power system has already installed in weather station area. PV panel tilt angle is 5° facing south. It is because the site is in the northern hemisphere of the earth, and it is in low latitude (4.588), so PV panel fix mounted tilt angle need to be set at small degree to get optimum energy. Tilt angle determination for optimal energy was explained in previous section.

Fig. 3.22 shows the schematic of an installed standalone PV system, consists of four PV panels, junction box for module connection, battery charge controller, deep cycle battery as energy storage and the DC load for this case is lamps. An Inverter is needed to convert the DC electricity to AC electricity. Whereas, the load in this research is DC load, no inverter was installed.

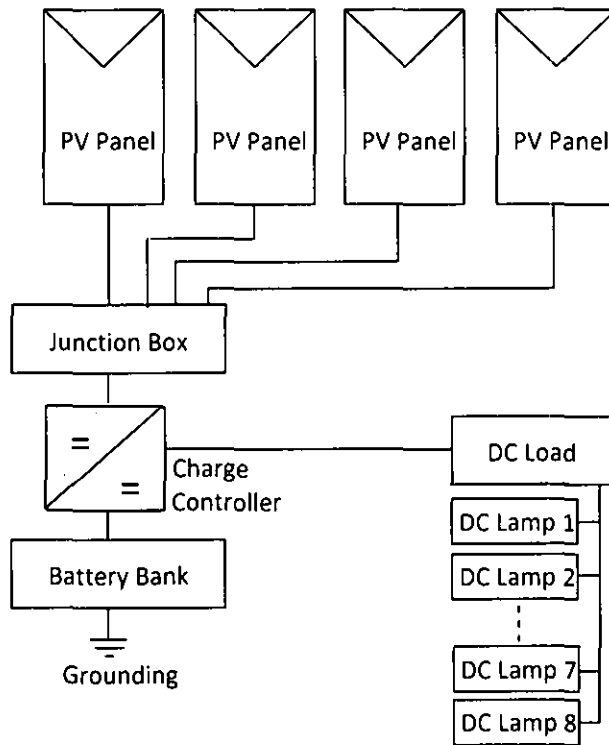


Figure 3.22: Solar Power System scheme

3.6.2 Load used in the experiment

The details of the experimental load are shown in Table 3.6 as follows:

Table 3.6: Experimental load list

No	Load type	Quantity	Total average measured current (A)	Total calculated power (Watt)
1	DC lamp @ (18 Watt _{rated})	10	5	60
2	Power Resistor I	1	2	25
3	Power Resistor II	1	3	35
	TOTAL		10	120

Residential lighting is only considered during the night assuming the house has good solar passive lighting during the day. In this research, lighting load during the night is assumed to be constant. In the experimental set-up, the load was controlled by automatic timer to work 10 to 12 hours during the night. The capacity of the load was changed to several conditions to observe system performance at different condition. The treatment details are described in Table 3.7.

Table 3.7: Load treatment list

No	Treatment	Total hours	Nominal DC voltage rated (V)	Total measured current (A)	Total energy (Wh)
1	Condition 1 (no load)	-	-	-	-
2	Condition 2	10	12	5	600
3	Condition 3	10	12	8	950
4	Condition 4	10	12	10	1200
5	Condition 5	12	12	10	1500

3.7 Measurement System Set-up

Measurement system is consists of data logger and sensors as described in Table 3.8. The data logger is PC based data logger and connected to sensors that measure weather and system parameter as seen in Fig. 3.23. The input and output power can be calculated using voltage and current data.

Table 3.8: Measurement system component list

No.	Equipment	General Specification
1	PicoLog 1216 Data logger	Single ended input, 16 Channel, 0-2.5V
2	PC	Desktop PC, Pentium 4, Windows XP
3	Pyranometer	Kipp & Zonen Pyranometer, SPLite
4	Current Sensor	HTFS 200-P/SP-2 LEM (Hall Effect)
5	Temperature Sensor	LM35
6	Humidity sensor	HIH-5030 Honeywell
7	Radiation shield	Handmade multi-plates radiation shield

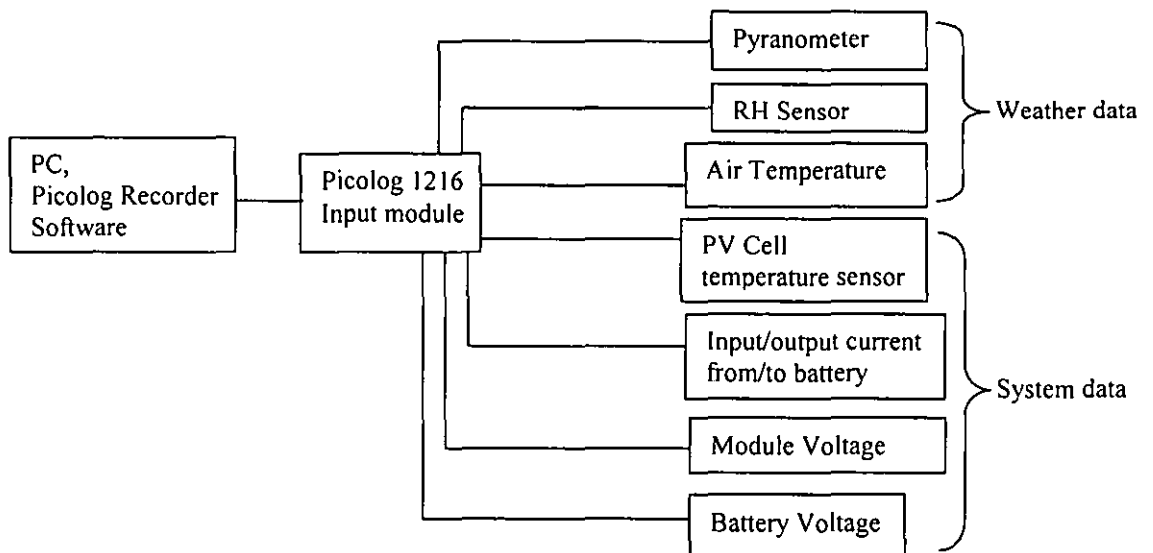


Figure 3.23: Measurement system configuration

3.7.1 Data logger

Picolog 1216 (Fig. 3.24) is multichannel data logger with 16 channels, single ended input. The data logger can record sensor output based on analog voltage. The voltage range is only 0-2.5V, while the sensor output can be at larger voltage or in the form of current, resistance etc. Therefore, the sensor output should be adjusted to meet the data logger requirement by install a signal conditioning circuit. The data logger does not have any memory. Therefore, the data is recorded in the PC via USB cable. The measurement setting is arranged through software in the PC.



Figure 3.24: Picolog 1216 input module

3.7.2 Sensors

There are seven sensors connected to the data logger. For Irradiation measurement, Kipp & Zonen pyranometer SPLite series was used (Fig. 3.25). The pyranometer was used to measure global horizontal solar irradiance in W/m^2 .

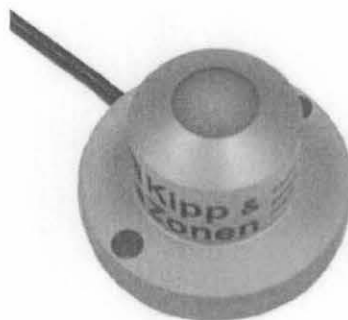


Figure 3.25: Kipp & Zonen Pyranometer SPLite series [122]

For RH measurement sensor HIH 5030 series was used. The HIH-5030 Series Low Voltage Humidity Sensors operate from 5.5V down to 2.7V, often ideal in battery-powered systems where the supply is a nominal 3V. USB voltage (5V) can be used as the power source. Direct input to a controller or other device is made possible by this sensor's near linear voltage output. Fig. 3.26 shows the picture of RH sensor and typical application circuit. Resistor of 15 kOhm was used as minimum load.

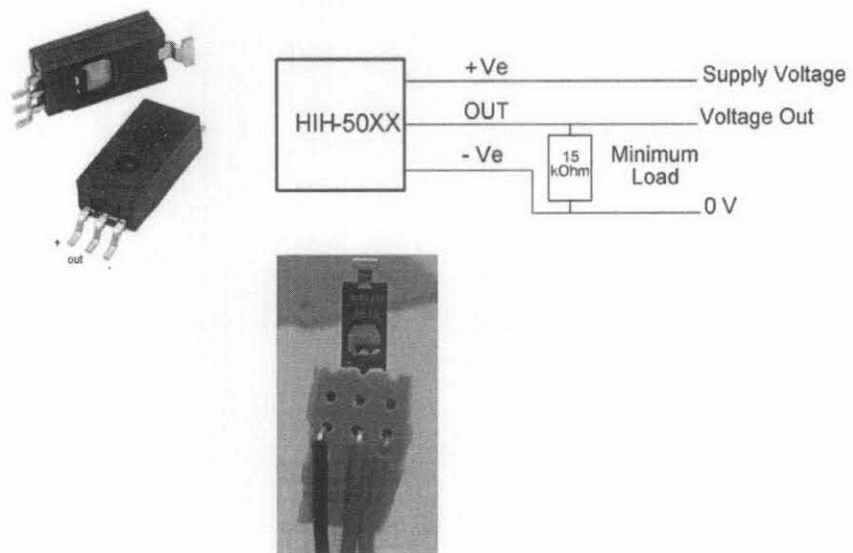


Figure 3.26: RH sensor and typical application circuit [123]

LM35 (Fig. 3.27) IC sensors were used to measure ambient and PV panels temperatures. The LM35 series are precision integrated-circuit temperature sensors, whose output voltage is linearly proportional to the Celsius (Centigrade) temperature.

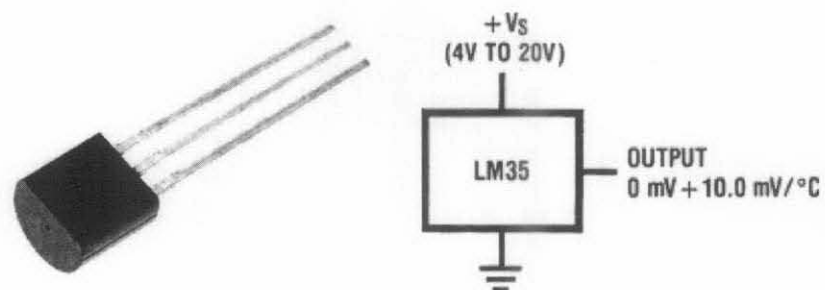


Figure 3.27: LM 35 Temperature sensor and typical application circuit [124]

The LM35 does not require any external calibration or trimming to provide typical accuracies of $\pm 1/4^{\circ}\text{C}$ at room temperature and $\pm 3/4^{\circ}\text{C}$ over a full -55 to $+150^{\circ}\text{C}$ temperature range [124]. LM 35 temperature sensor has been used for various applications that need low measurement range sensor (-55 to 150°C) [125 and 126].

To measure current in and out from battery Hall Effect Current transducer HTFS 200 series was used (Fig. 3.28). This sensor used the Hall Effect principle of the current that passing through the coil.

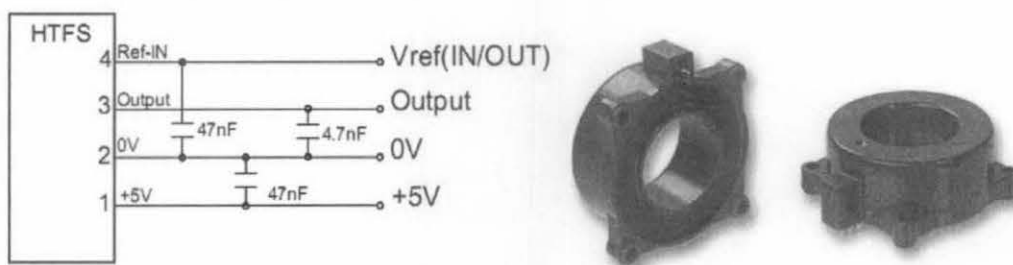


Figure 3.28: HTFS 200 current transducer and typical application scheme [127]

3.7.3 Power source

The RH sensor HIH 5030 and temperature sensor LM35 require external power source. The power source from USB port was used as a supply voltage of the sensor. The USB voltage value is 5V. There are 4 cables out from USB port, 2 cables for power supply and 2 cables for data transfer. For this application only power supply cable was used (pin number 1 and 4). Fig. 3.29 shows USB configuration.

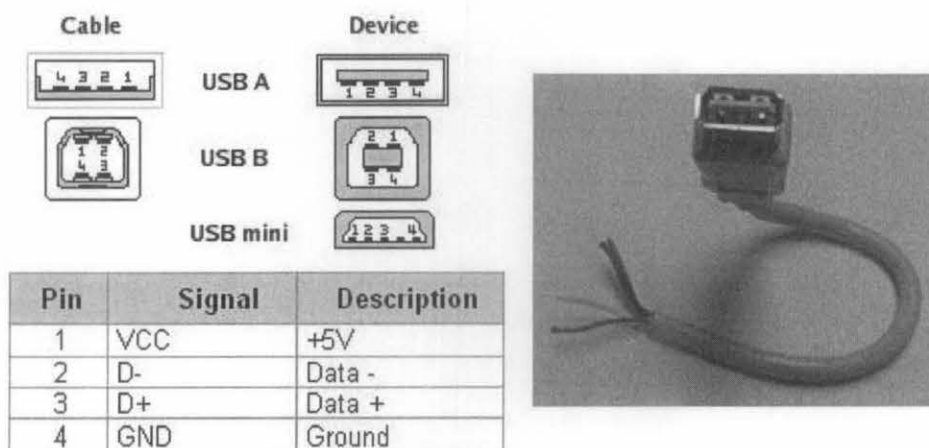


Figure 3.29: USB cable [128]

3.7.4 Ambient Temperature and Relative Humidity Sensor Circuit

Fig. 3.30 shows complete circuit used for RH and ambient temperature sensor which are placed in the hole inside the radiation shield, the air would flow through the space between the plastic plates but the sensor covered from direct radiation.

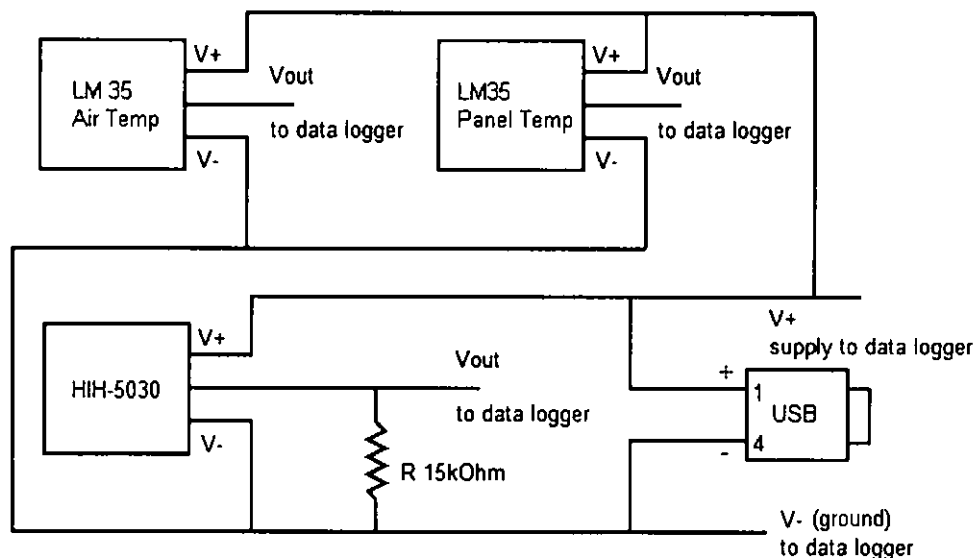


Figure 3.30: RH and ambient temperature sensors circuit configuration

3.7.5 Naturally aspirated solar radiation shields design

A radiation shield is required to minimize the radiation effect on air temperature and relative humidity measurement. Without a radiation shield, the temperature sensor will give relatively high measurement error during the day due to the huge amount of irradiance presence. Solar radiation would heat un-shielding temperature sensor and distract the measurement.

There are some types of the solar radiation shield. Naturally-aspirated and mechanically-aspirated radiation shield types are commonly used for air temperature measurement. Most of the weather station used multi-plated naturally aspirated radiation shields, because it is relatively low-cost and doesn't need an additional power. Julie M. Tarara et al. investigated several types of naturally aspirated and mechanically aspirated radiation shields. They found that aspirated shield indicates the smallest error measurement. Between naturally aspirated types, they found multi-

plates radiation shield indicates the smallest error than the other naturally aspirated types [131].

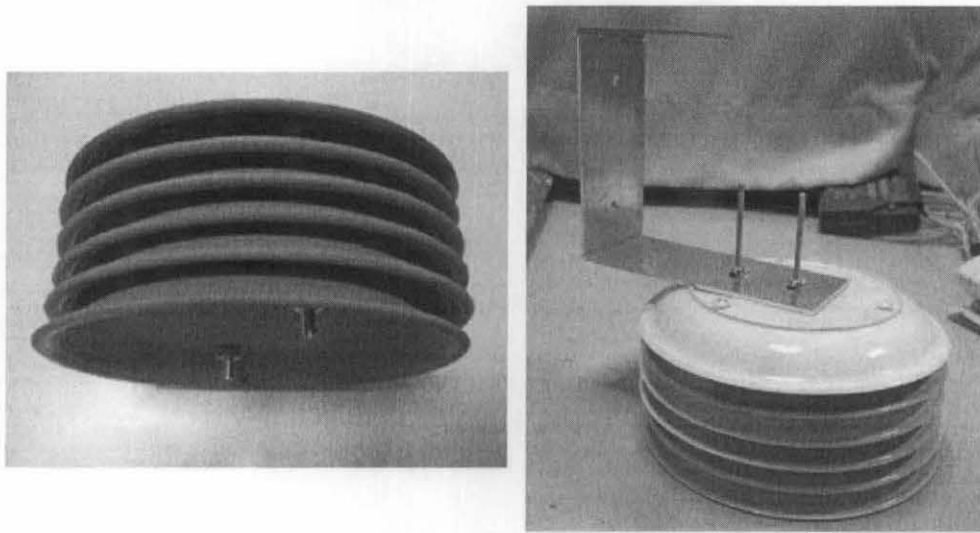


Figure 3.31: Hand-made radiation shields

The radiation shield made of 6 plastic plates arranged vertically as presented in Fig. 3.31. Fig. 3.32 shows the sensor placement inside the radiation shields. The shields painted with white paint to minimize heat absorption from the radiation.

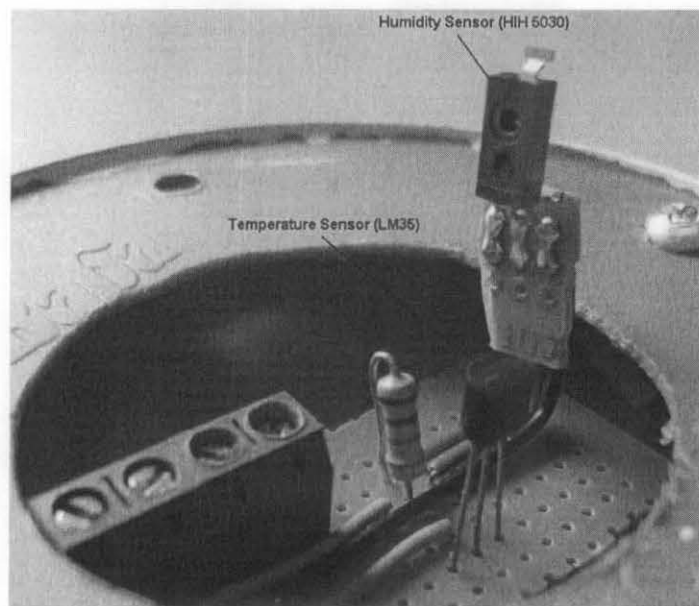


Figure 3.32: Sensor placement inside the radiation shield

3.8 PV panel efficiency calculation from measured data

Observation and analysis was carried out on experimental data. Standard Test Condition (STC) and actual PV panel efficiency can be calculated. PV panel efficiency at STC can be calculated from datasheet using Eq. 3-36 as follows:

$$\eta_{STC} = \frac{P_{PV}}{G_{STC} \cdot A_{PV}} \times 100\% \quad (3-36)$$

η_{STC} is efficiency at STC (Irradiance (G_{STC}) = 1000 W/m² and 25 °C ambient temperature) and A_{PV} is the area of each module.

To calculate efficiency in actual condition Eq. 3-37 was used as follows:

$$\eta_{actual} = \frac{P_{actual}}{G_{actual} A_{total}} \times 100\% \quad (3-37)$$

η_{actual} is actual efficiency, P is PV panel measured power output in Watt, G_{actual} is actual radiation received in W/m², A_{total} is total area of the PV panel.

3.9 Modeling and simulation

PV system is a complex system, mathematical modeling of each PV system's components is required to perform transient simulation. To simulate a standalone PV system, the following component's models are needed: Solar radiation model, PV panel, Charge Controller, Battery and Load.

Fig. 3.33 shows a typical diagram of the components involved in a standalone PV system. An inverter needs to be added if an AC load is utilized. However, this study only presents simulation of a standalone PV system with DC load.

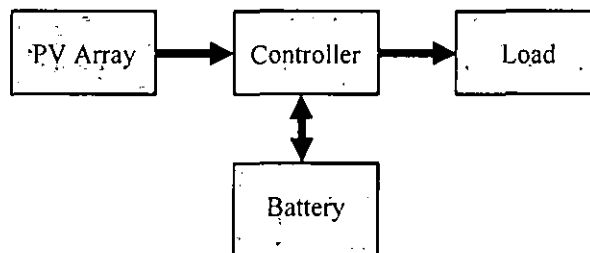


Figure 3.33: Standalone PV system components

In this study, TRNSYS 16 was used to build a model for standalone PV system. The following review is in accordance with the components available in the library of TRNSYS 16 [19].

3.9.1 Component selection

For the solar radiation model, type 109 (Combined data reader and solar radiation processor) was selected.

For PV array model, five parameters model should be used for better accuracy (Type 194). However, this type requires detailed weather data that is why it not always applicable. Therefore, type 94a (suitable for crystalline type PV panel) is used to determine the performance of PV array [19]. Type 94a is a four-parameter model. The data needed for this model is obtained from PV panel datasheet.

Type 48d is used as the controller model. In type48, both the regulator and inverter can operate in one of four modes. Modes 0 and 3 are based upon the "no battery/feedback system" and "direct charge system," respectively. Modes 1 and 2 are modifications of the "parallel maximum power tracker system" in the same reference [19].

Type 47c (Shepherd modified Hyman's battery model) was used as the battery model [19]. This model of a lead-acid storage battery operates in conjunction with solar cell array and power conditioning components. TRNSYS component Type 9 (Generic data files) was used to input the load profile data [19].

3.9.2 Simulation setting

Modeling and simulation has been carried out using TRNSYS 16. Figure 3.34 shows the component and connections between the components modeled in TRNSYS 16. Feng Shao modeled two SAPV systems TRNSYS models [86], the simulation shows some error and the validation only for small system. Same with L.K. Nkhonjera that

built the similar model for PV-battery systems, the simulation results shows some erroneous results, especially in battery voltage validation [87].

In this research, The TRNSYS model was validated using experimental data, and then the model used to test performance of designed SAPV using the Ipoh city weather data from which input file was created. Most weather stations provide hourly data as the smallest time series. Therefore, in the TRNSYS simulation, the simulation time step is set to hourly simulation. In this research, sub-hourly data were converted to hourly average data to reduce data quantity.

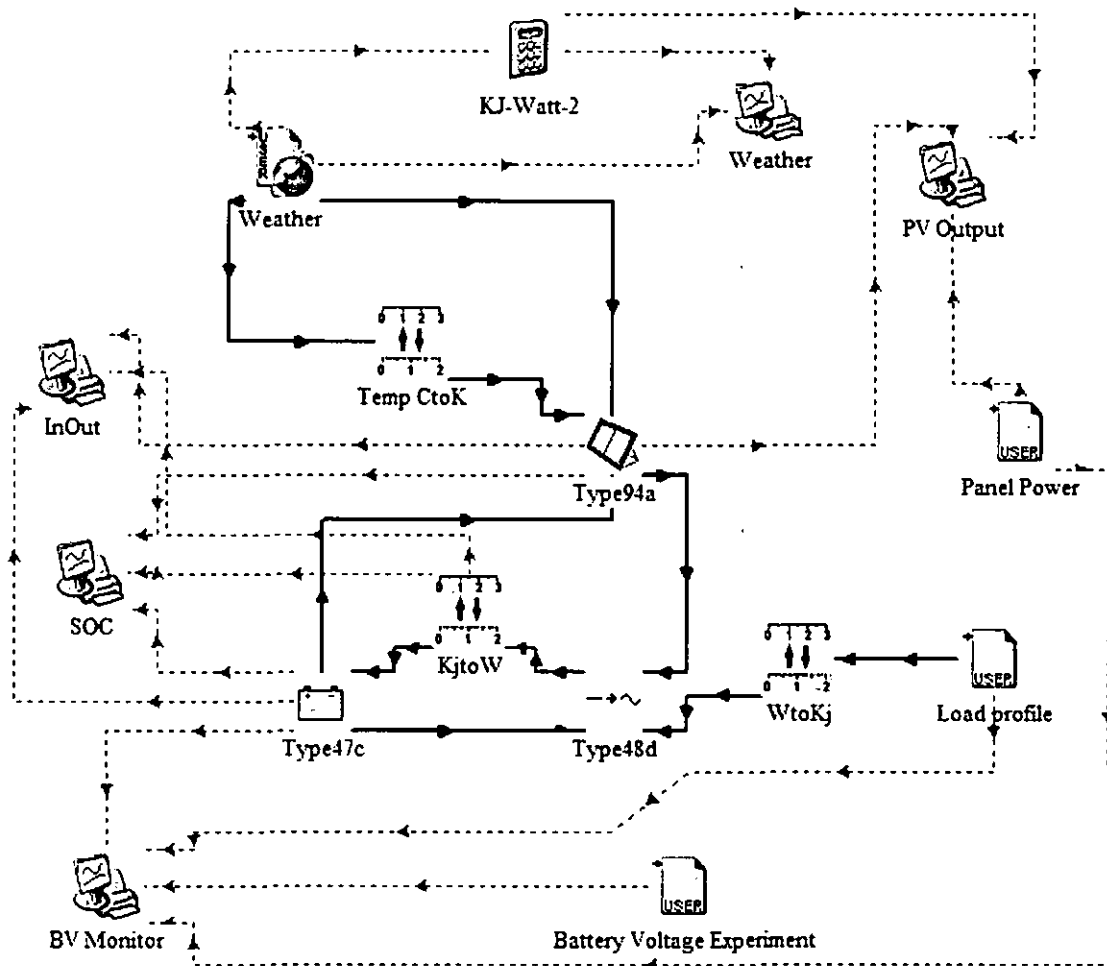


Figure 3.34: Solar Power System modeling in TRNSYS 16

Monitoring and measurement results of total global horizontal solar radiation, ambient temperature and relative humidity from the experimental setup site was used as input data for the type 109 solar radiation models. Parameter from the PV panel, controller and battery data sheet was also embedded into the TRNSYS model. If parameter data is unavailable, the default value in TRNSYS component was used. The

Load profile data was entered into a .txt file and implemented as an input for a type 9 data reader component. Plotters also have been connected and adjusted to displays the simulation results.

Variables are classified into parameters, inputs, and outputs in TRNSYS. Inputs and outputs are linked with data flow between components. There are some component's connections, which need a unit-converter component (Type 57-unit conversion routine) due to the differences of the parameter units between components, this unit conversion is also can be done by using equation component manually. Plotters were used to plot the simulation results on the screen or on the paper. The details of connection between component and component parameter setting are presented in the Appendix E.

3.10 Summary

This chapter presents in details, systematic methodology to carry out the research. Calculation procedure, experimental setup and simulation setting have been explained in details. Calculation procedure presented here includes deterministic method sizing, solar radiation data filling, daily-data based LPSP calculation procedure and optimization procedure. Experimental setup has been explained in details. PV system modeling procedure using TRNSYS 16 also has been explained.

CHAPTER 4
RESULTS AND DISCUSSIONS

4.1 Initial design results

This section deals with the data set that is used for calculation and the calculation's results. PV system sizing calculation results using the deterministic method are presented here. Solar radiation data from the global solar map, nearest weather station from location and direct measurement on the site were compared.

4.1.1 Solar radiation availability data

In this study, besides global solar map observation, one-year weather data from Ipoh weather station located at 30 km from the site was obtained. On-site measurements of weather parameters have been carried out for eight months before the analysis is made. Fig. 4.1 shows Ipoh weather station data while Fig. 4.2 shows on-site measurement from May to December 2010.

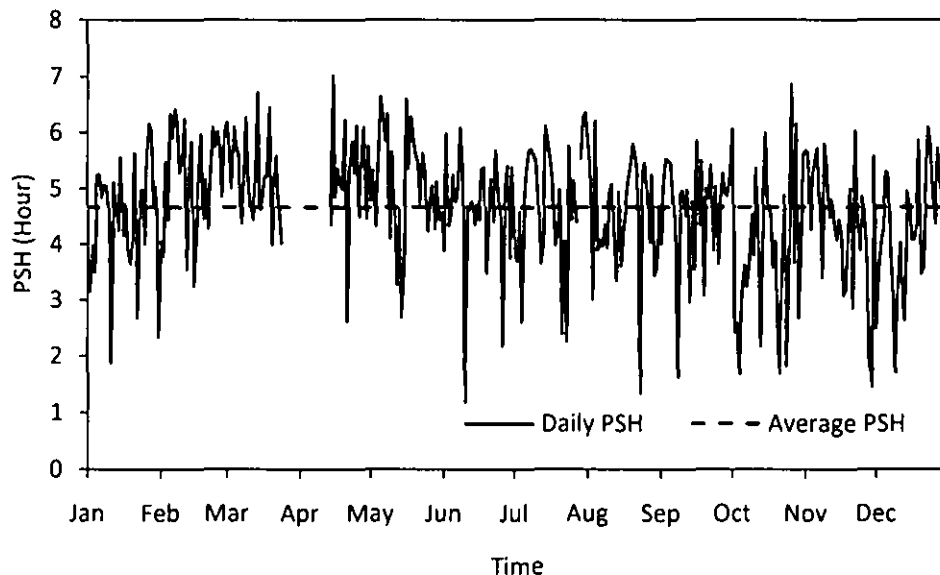


Figure 4.1: Measured PSH from Ipoh weather station on 2003

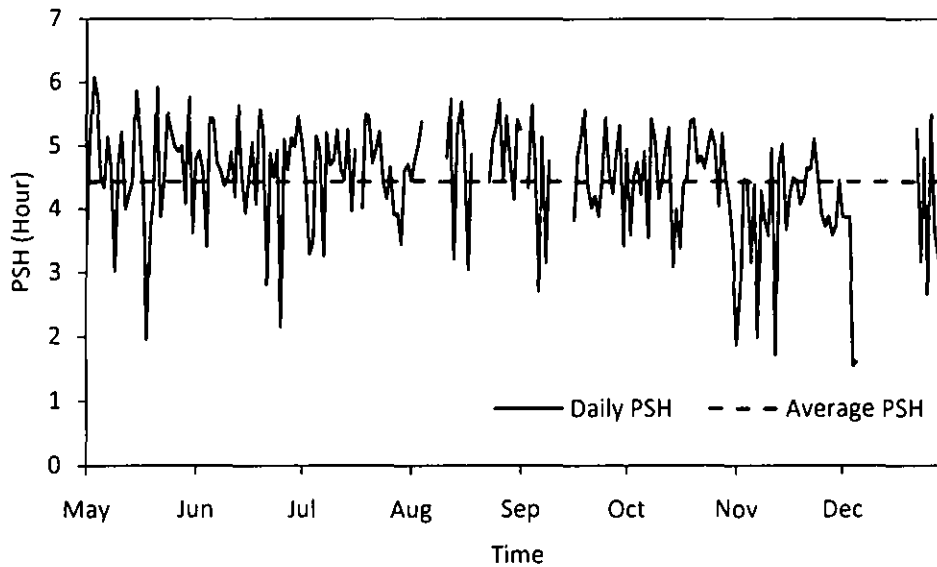


Figure 4.2: Measured PSH in Bandar Seri Iskandar from May to December 2010

The Ipoh weather station data and the on-site measured data show similar average PSH value as that of presented in the Global Solar Energy Map, ranging from 4-5 hours (Fig. 3.1). Ipoh data shows averaged PSH value of 4.67 for one-year data (2003) and on-site data shows averaged PSH value of 4.43 for eight month data (May to December 2010).

According to Ipoh weather station data, maximum recorded consecutive days with PSH lower than 4 hours is 7 days and with PSH lower than 3 hours is 3 days, both were occurred on the month of October. On-site measurement results show maximum-recorded consecutive days with PSH lower than 4 hours during the period are 3 days that are occurred in the month of July and October 2010 and 5 consecutive days, which occurred on November and December 2010. Maximum-recorded consecutive days with PSH lower than 3 hours are 2 days that are occurred on the month of November and December 2010.

According to the measured data, monthly averaged PSH value for the site in the month of May to December 2010 consecutively 4.62, 4.63, 4.55, 4.85, 4.52, 4.54, 3.95 and 3.43 hours. Fig. 4.3 shows the comparison between Ipoh and Bandar Seri Iskandar monthly averaged PSH value. Since Malaysia is situated near equator, average solar irradiation is not changing drastically over the year. Seasonal cycle

causes only a relatively small change in solar radiation value compared to the subtropical region.

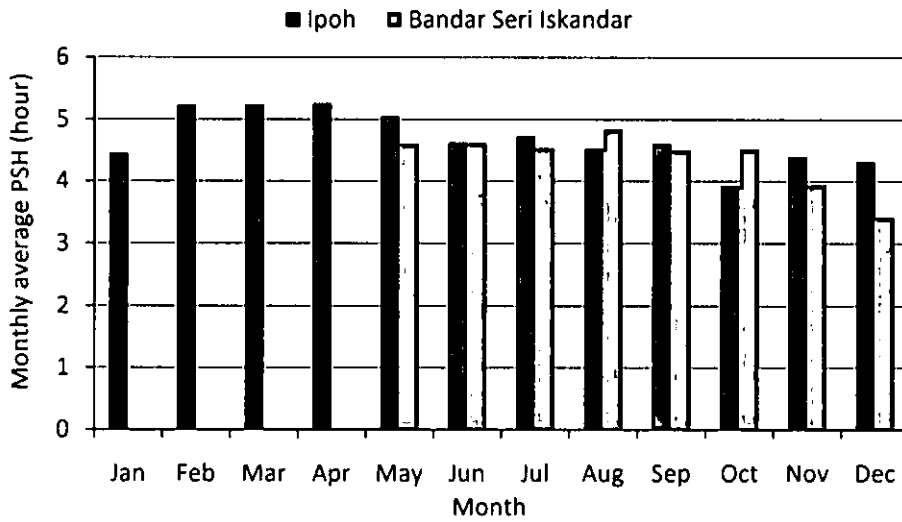


Figure 4.3: Monthly averaged PSH value comparison between Ipoh data and Bandar Seri Iskandar on-site measurement

4.1.2 Calculation results

Deterministic method, as described in section 3.1, has been used to calculate initial capacity of PV panel and battery. PV panel capacity calculation has been carried out and the sizing curves for various PSH values were presented in Fig. 4.4.

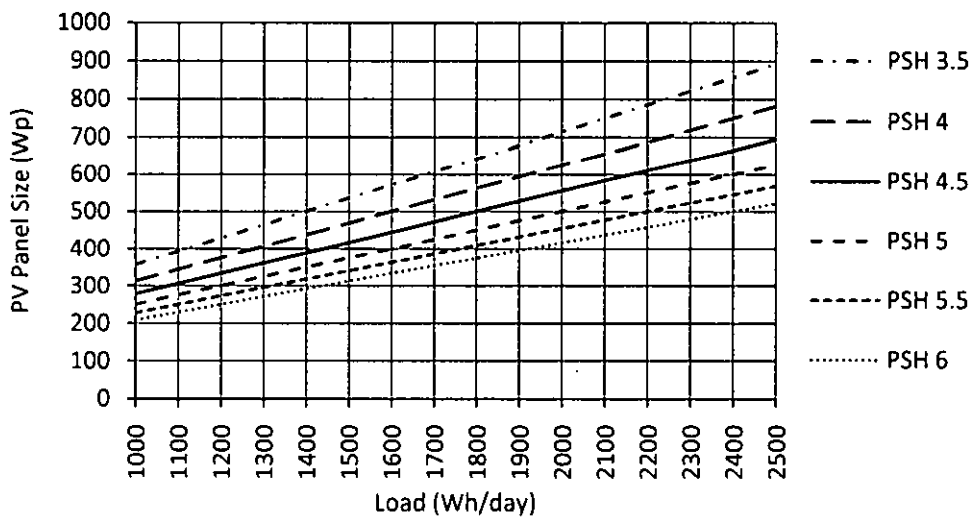


Figure 4.4: PV panel sizing curves based on deterministic method using different Peak Sun Hour (PSH) value

From Fig. 4.4, it is observed that the higher solar energy availability (by mean of PSH) will results smaller PV panel requirement. In a lower PSH value, the PV panel requirement will increase more significantly with load increasing rather than in higher PSH value. For the location at Bandar Seri Iskandar, PSH value of 4.5 was chosen based on the available data. Table 4.1 presents the minimum PV panel size for lighting loads case in Table 3.1 that is 23% from the average total load of the typical Malaysian terraced house (about 6kWh) and for 25% of average total load.

Table 4.1: PV panel size calculation

No	Note	Load (Wh/Day)	PV panel Size (Wp)				
			PSH=4	PSH=4.5	PSH=5	PSH=5.5	PSH=6
1	23% of total average load	1364	426.25	378.89	341	310	284.17
2	25% of total average load	1500	468.75	416.67	375	340.91	312.5

Battery capacity calculation has been carried out using deterministic method. Fig. 4.5 shows sizing curve of battery capacity with variation of number of autonomy days (N_a).

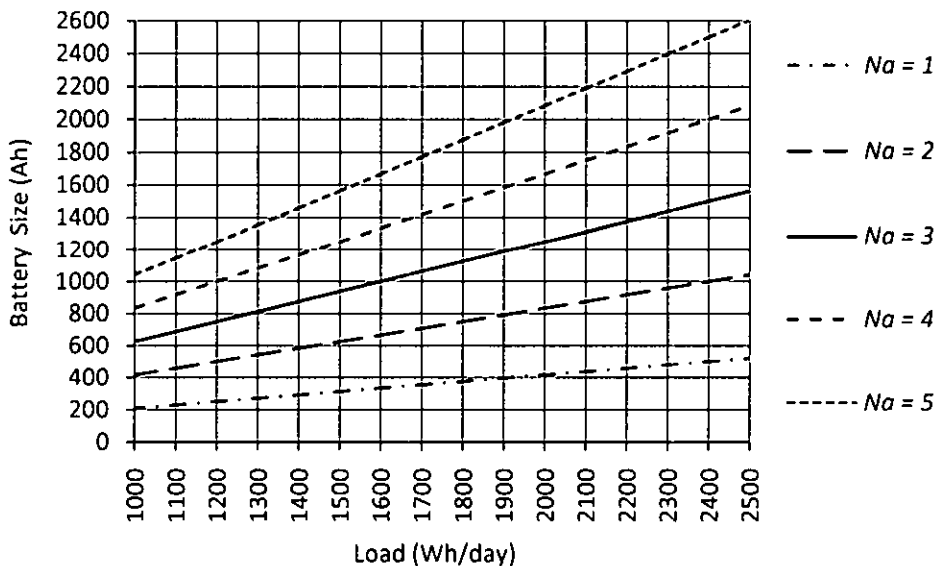


Figure 4.5: Battery sizing curve for DoD = 50% and $V_{rated} = 12V$

Table 4.2 shows the battery sizing calculation results. Then, after both PV panel and battery sizing curve were obtained, the configuration can be determined. From the calculation above, for a typical house in Malaysia that has a constant lighting load of

about 1364 Wh/day, with system efficiency 80%, the PV panel required for the system is 400 Wp with battery storage of about 852.5 Ah for a 12V system.

Table 4.2: Battery Size Calculation

No	Load (Wh/Day)	Battery Capacity (Ah)				
		$N_a=1$	$N_a=2$	$N_a=3$	$N_a=4$	$N_a=5$
1	1364	284.17	568.33	852.50	1136.67	1420.83
2	1500	312.50	625.00	937.50	1250.00	1562.50

From the data observation, it is observed that the value from measurement is almost the same with the value presented in Global Solar Map. Deterministic method use average value of solar radiation availability to calculate PV panel and battery capacity. Using this method, the sizing calculation can be carried out quickly with a simple procedure, as described in section 3.1. However, the performance prediction of the system cannot be observed using this method. As observed from the solar radiation data, there are seasonal, monthly and daily variations of solar radiation. Deterministic method does not incorporate these variations into the calculation.

4.2 Missing data estimation results

Missing data estimation has been carried out using Method 1 and 2 (refer to section 3.2). Calculation results of both the methods are presented in this section. A comparison of both the methods and existing method with that of statistical analysis is also a part of discussion in this section.

4.2.1 Calculation results and statistical analysis

Solar radiation estimation has been carried out using Method 1 and Method 2. Both of the methods use decomposition technique to predict beam and diffuse components of global solar radiation. Method 1 uses decision matrix to determine the beam transmittance value. Method 2, which uses correlation, is split into three parts: linear (2a), quadratic (2b) and cubic (2c). Fig. 4.6 shows scatter plot of measured and predicted value of both the methods.

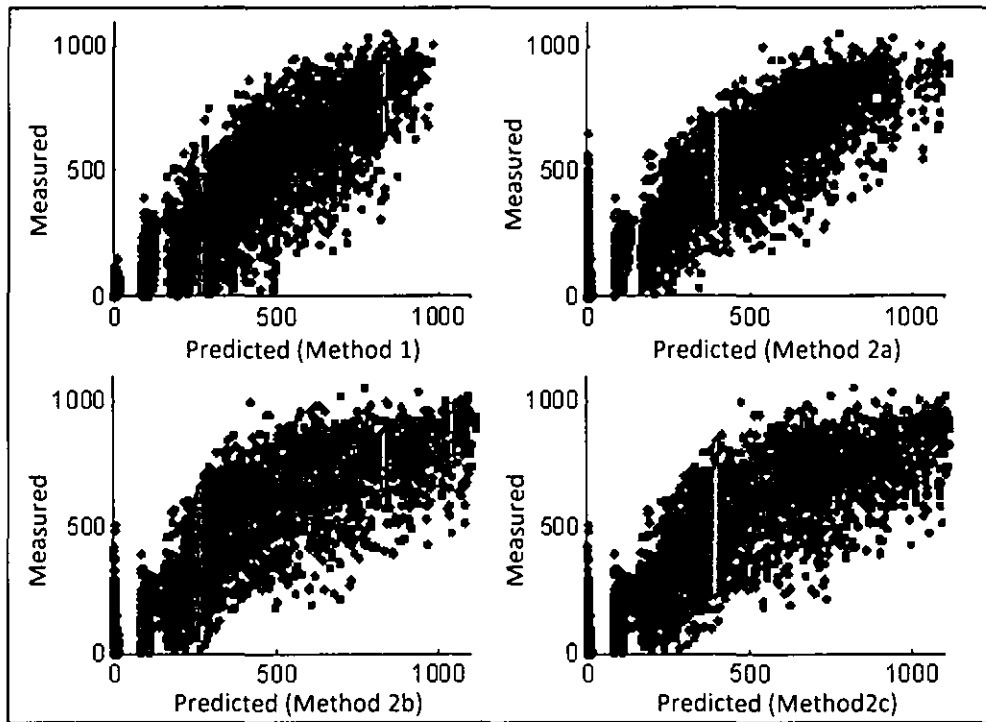


Figure 4.6: Scatter plot of measured and predicted solar radiation

Table 4.3 shows the statistical-analysis result's comparison between proposed method and existing temperature based method (Hargreaves and Samani/H-S and Hargreaves, Samani and Annandale/H-S-A). The minimum RMSE value of 87.6 W/m^2 was obtained with 0.95 of correlation coefficient value and 0.97 index of agreement value. Previous method that used precipitation data obtained averaged index of agreement of 0.95, thus the model presented in this study also performed well. It is concluded from statistical analysis results that Method 1 gives the best estimation results compared to other methods.

Table 4.3: Statistical analysis results comparison

No.	Method	Statistical parameter			
		RMSE (W/m^2)	NRMSE (%)	$d^{a)}$	$r^{b)}$
1	Method 1	87.6	8.29	0.97	0.95
2	Method 2				
	a. Linear	101.94	9.63	0.96	0.93
	b. Quadratic	109.17	10.32	0.96	0.92
	c. Cubic	103.69	9.8	0.96	0.93
3	H-S method ($K_f=0.175$)	106.45	10.06	0.96	0.88
4	H-S-A method ($K_f=0.172$)	106.44	10.06	0.96	0.88

Note:

a) Index of Agreement (d)

b) Correlation Coefficient ($r=\sqrt{R^2}$)

4.2.2 Selected results (Method 1)

Based on statistical analysis results presented in previous section, Method 1 has been selected to be a better method of solar radiation estimation. Fig. 4.7 shows the example of estimation results of each solar radiation component on random dates using Method 1. Predicted global solar radiation is the total sum of beam and diffuse radiation components.

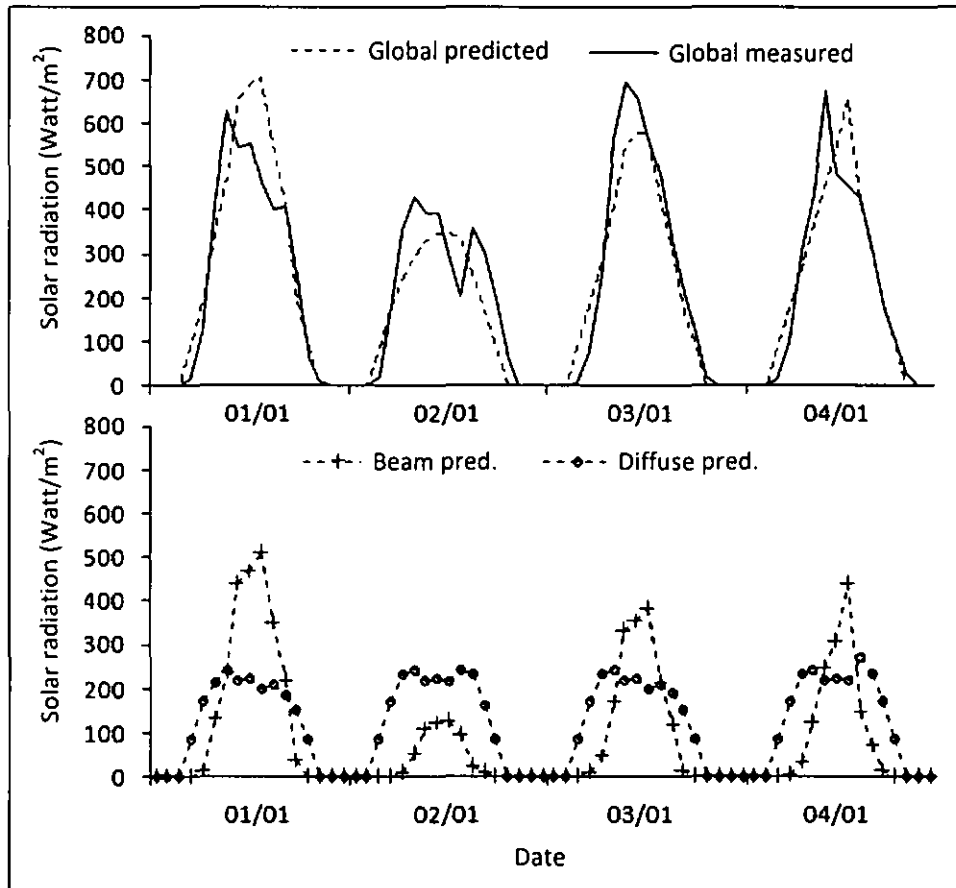
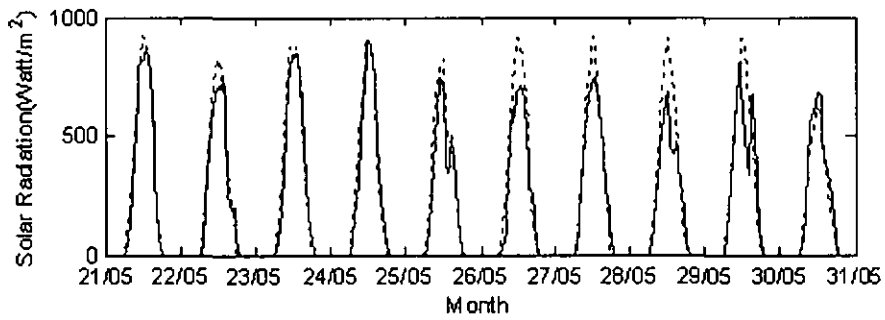
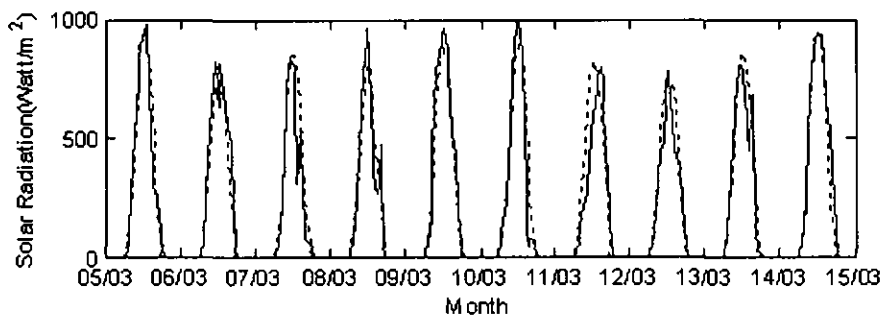
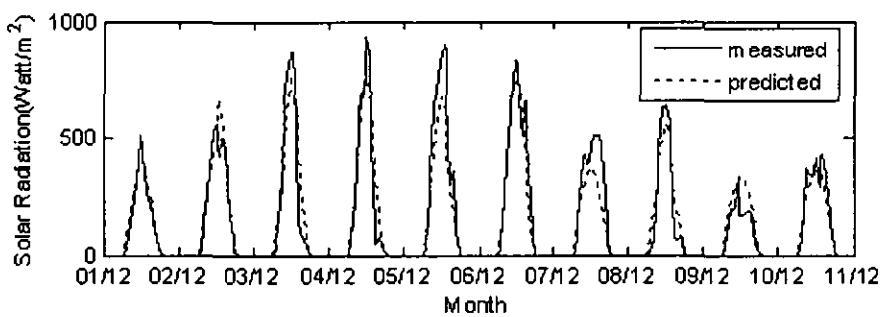
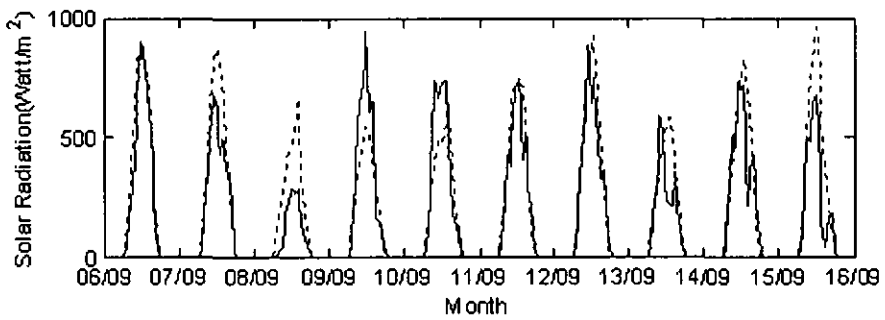


Figure 4.7: Graphical comparison of predicted (all solar radiation components) and measured solar radiation on random dates using Method 1

Fig. 4.8 shows the graphical comparison of measured and predicted solar radiation for random dates in dry season (a) and rainy season (b). It is observed from Fig. 4.8 (a) that during the dry season, the solar radiation is mostly high and the estimation results show good compromise with the measured results. Some estimation errors are observed from 26-29 May, it is probably caused by cloudy sky, which clouds sometimes suddenly come and disappear, whereas the relative humidity and temperature measurement (which were used for estimation) are not as responsive as solar radiation measurement.



a) Dry season



b) Rainy season

Figure 4.8: Graphical comparison measured and predicted (Method 1)

More errors are observed from estimation during the rainy season (Fig. 4.8 (b)). Sometimes the estimation result is overestimating the solar radiation and sometimes

underestimates the solar radiation. Again, it is probably caused by the cloudy sky which cloud sometimes suddenly comes and disappears. In rainy season, normally the intensity of the cloud is higher than dry season. That is why more errors are observed in rainy season. However, the results using Method 1 are the best compared to the other method and the results are used to fill the missing solar radiation data in this study.

4.2.3 Final estimation results and discussion

After the prediction results of Method 1 have been validated using available data, the results for the missing data days can be used with confidence. Fig. 4.9 shows prediction results in the days when the solar radiation measurements were absent. There are 23 days missing data in the presented data set. To fill the missing data, Method 1 result was used and the complete data set is presented in Fig. 4.10. This complete data set is one-year full hourly global horizontal solar radiation. Solar radiation on the tilted surface estimation results will be presented in the next section.

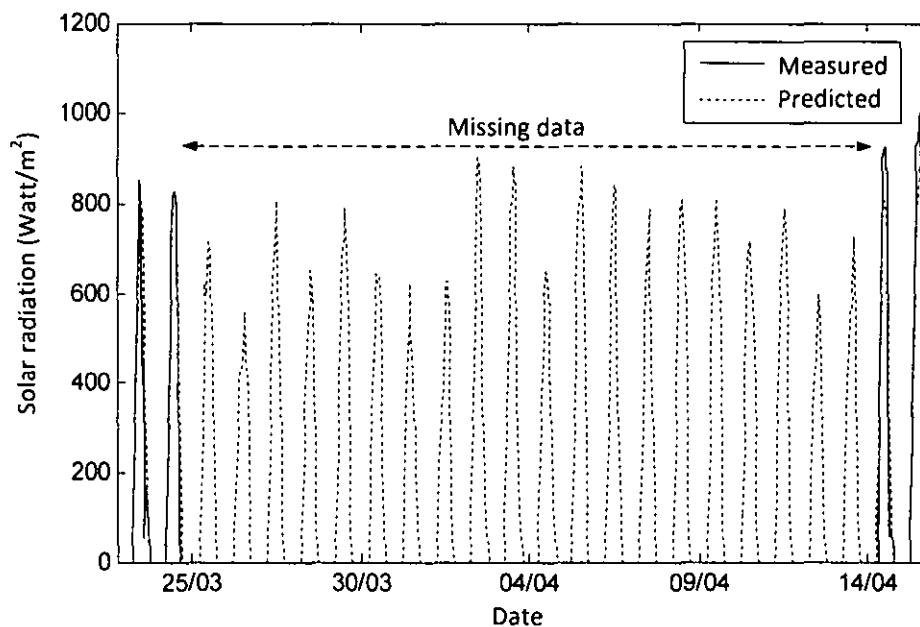


Figure 4.9: Estimation results of missing measured data on 25 March – 13 April (Method 1)

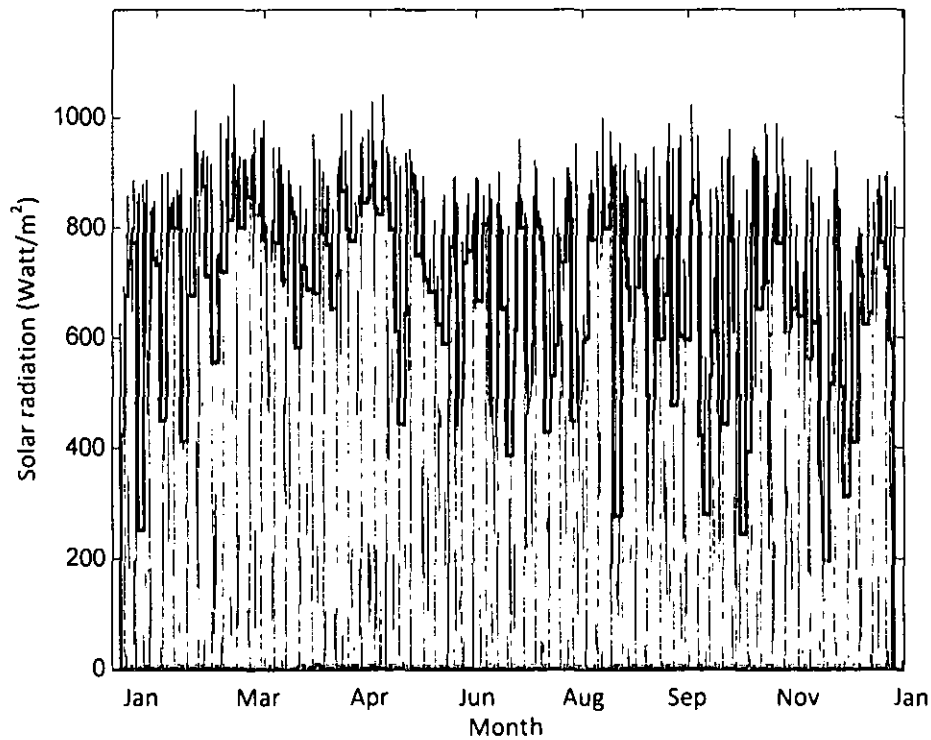


Figure 4.10: Complete one-year hourly solar radiation data set

Although the data filling methodology is good for the location in this study, it also can be utilized for data estimation in other geo-locations with notes, for first method the assignment criteria of atmospheric transmittance using RH and ambient temperature should be adjusted to the available solar radiation data of the area to get the minimum error. To generate general criteria of atmospheric transmittance assignment using RH and ambient temperature further research is required with a sufficient large amount of data for various areas. For the second method, the correlation should be built based on available measurement nearest from the location to give satisfactory estimation results.

4.3 Solar radiation on the tilted surface calculation results

To incorporate the tilt angle effect on LPSP calculation, solar radiation on the tilted surface needs to be calculated. This section presents solar radiation on the tilted surface simulation results and selection of optimum tilt angle for the location. Then, PSH on the selected tilted angle is used as input for LPSP calculations. The input data

is complete one-year hourly global horizontal solar radiation, ambient temperature and relative humidity for the city of Ipoh with latitude of 4.34° and longitude of -101.06° . The best tilt angle for the location was determined by performing transient simulation using the weather simulator (type 109) in the TRNSYS 16's library. The detail of the method to perform the calculation was presented in Chapter 3. The simulation was carried out using Reindl and Perez model for tilt angle -6 to 15° facing equator (south). The negative value means the PV panel facing towards North. Fig. 4.11 shows the comparison between total solar radiation received on the tilted surface for one year using Reindl and Perez model simulation.

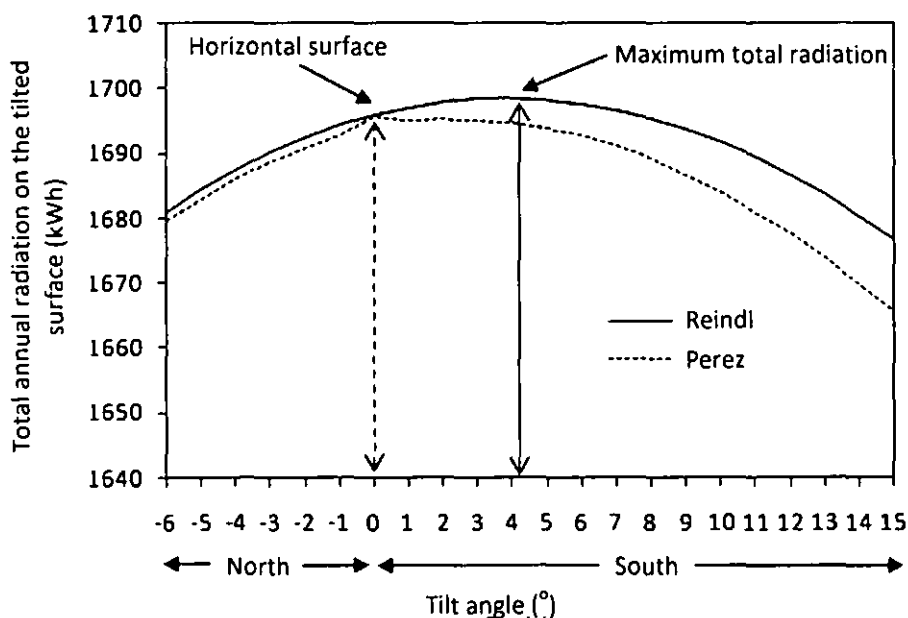


Figure 4.11: TRNSYS simulation results for total solar radiation received on the tilted surface for one year using Reindl and Perez model

For horizontal surfaces, the program is not calculating the solar radiation because the surface is in zero tilt angles. That is why for horizontal surfaces, both models give the same output as input data. For Reindl model, the maximum total radiation received on the tilted surface was found to be at a tilt angle of $4-5^\circ$. Perez model underestimated the solar radiation received on the tilted surface, this, result maximum total radiation to be at the horizontal surface (0°). Normally, the tilt angle of PV panel is facing equator (south) if the location on the northern hemisphere. In this study, it was decided to use Reindl model because the simulation results using Reindl model make more sense than Perez model for the above case.

Climatic cycle effect analysis is required to determine the best tilt angle for the location. It is carried out by observing monthly total radiation for various tilt angles. The calculations were carried out for 5°, 0°, 10° and 15° to simplify the observation and installation after the tilted angle is selected. Table 4.4 shows monthly total radiation on respective tilted angles. The highest average total irradiation value was obtained on 5° facing south. Fig. 4.12 shows graphical version of Table 4.4.

Table 4.4: Monthly total irradiation on the tilted surfaces (simulation results) using Reindl model

Month	Total Radiation on the tilted surface (kWh/m ²)				
	-5°	0°	5°	10°	15°
January	131.53	137.31	142.38	146.69	150.24
February	141.24	145.44	148.87	151.50	153.34
March	155.90	157.65	158.57	158.66	157.94
April	155.86	154.65	152.59	149.73	146.09
May	158.69	155.29	151.06	146.03	140.26
June	141.71	137.69	132.92	127.47	121.43
July	149.29	145.70	141.34	136.25	130.57
August	141.27	139.26	136.53	133.09	128.99
September	136.82	137.27	137.02	136.07	134.44
October	118.28	120.76	122.64	123.90	124.55
November	126.38	131.22	135.36	138.78	141.47
December	127.43	133.53	138.92	143.57	147.47
Average	140.37	141.31	141.52	140.98	139.73

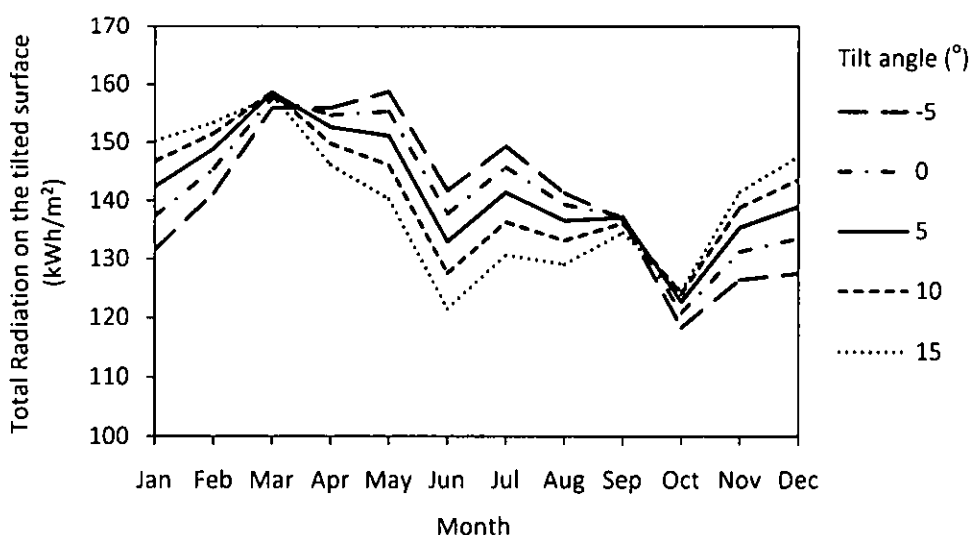


Figure 4.12: Monthly total radiation on the tilted surface

Since 5° tilted surface collected highest average total solar radiation, it was chosen as the best tilt angle for the location. Then hourly global horizontal solar radiation processed using TRNSYS simulation with 5° tilted surface facing south using Reindl model to obtain hourly solar radiation on 5° tilted surface data. Since the LPSP calculation requires daily solar radiation data (PSH value), whereas the TRNSYS output is hourly based, data processing is required to obtain daily solar radiation data on the tilted surface. The TRNSYS output results are then processed using Eq. 2-29 to obtain daily peak sun hour data on the tilted surface (PSH_t). Fig. 4.13 shows PSH on 5° tilted surface (PSH_t) for one year that is used for LPSP calculation.

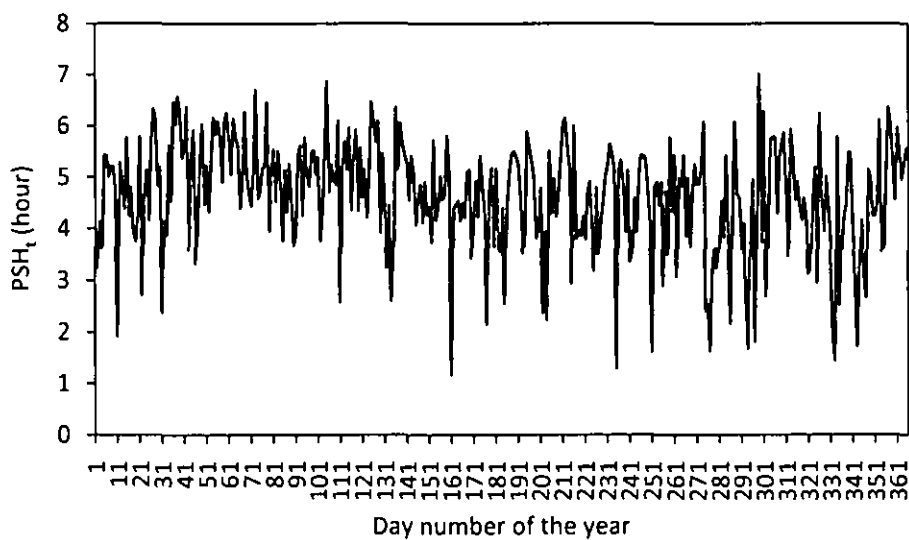


Figure 4.13: PSH on the tilted surface

In this study, the PV panel is installed at 5° . However, in actual application the PV panel tilt angle and orientation are not always in optimum because of appropriate installation in building architecture to maintain the aesthetic of the building. In this case, the solar radiation received on the tilted surface are directly calculated using TRNSYS without determining the optimum tilt angle.

4.4 Sizing and optimization results

Stochastic methods by LPSP calculations have been used for the sizing calculation. From the calculation methodology that is presented in section 3.3, sizing parameters include LPSP, Capital Cost, Life Cycle Cost and Excess Energy are obtained and presented here. Optimization results using two parameters (LPSP-CC and LPSP-LCC)

and using four parameters (design space) are compared. Economic analysis is also presented in this section.

4.4.1 Calculation results

The calculation algorithm described in section 3.3 was implemented to obtain LPSP value in the range of 0-990 Wp PV panel capacity and 0-990 Ah battery capacity. Matlab was used to plot the calculation results. Fig. 4.14-17 shows LPSP, Excess Energy, Capital Cost and LCC surface graphic, respectively. The surface graphic can be easily edited using Matlab, to perform analysis of LPSP, Excess energy, capital cost, and LCC value within the graphic range (0-990 Wp of PV panel and 0-990 Ah of battery capacity).

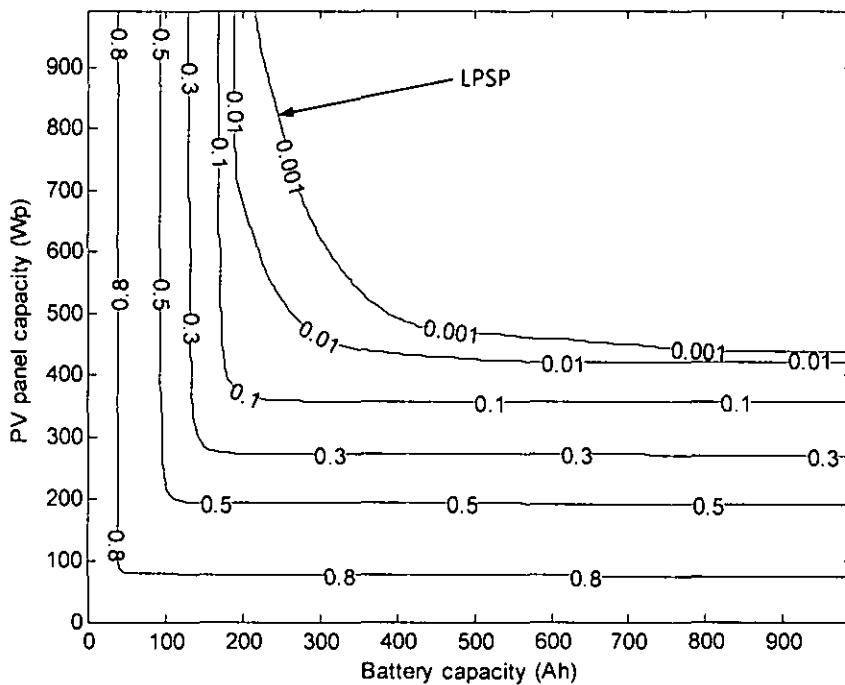


Figure 4.14: LPSP surface graphic

LPSP value is an indicator of PV system’s performance. Lower LPSP value indicates better system’s performance. LPSP value of zero is the best, but it would be difficult to determine the configuration with this value since zero in the LPSP surface graphic is an area not the line. That is why LPSP value 0.001 is chosen to represent the limit for the design space. Lower LPSP is obtained at larger PV panel and battery capacity as seen in Fig. 4.14.

Excess energy is an indicator of PV panel over design. It is occurred during the day when the battery energy level is at maximum and solar radiation still presents. Charge controllers will disconnect PV panel-battery's connection, and the excess energy will be wasted. It is unavoidable and necessary to compensate the lack of solar energy in the rainy season. 30% excess energy value is chosen as the limitation since it meets the required LPSP value. Fig. 4.15 presents excess energy surface graphic.

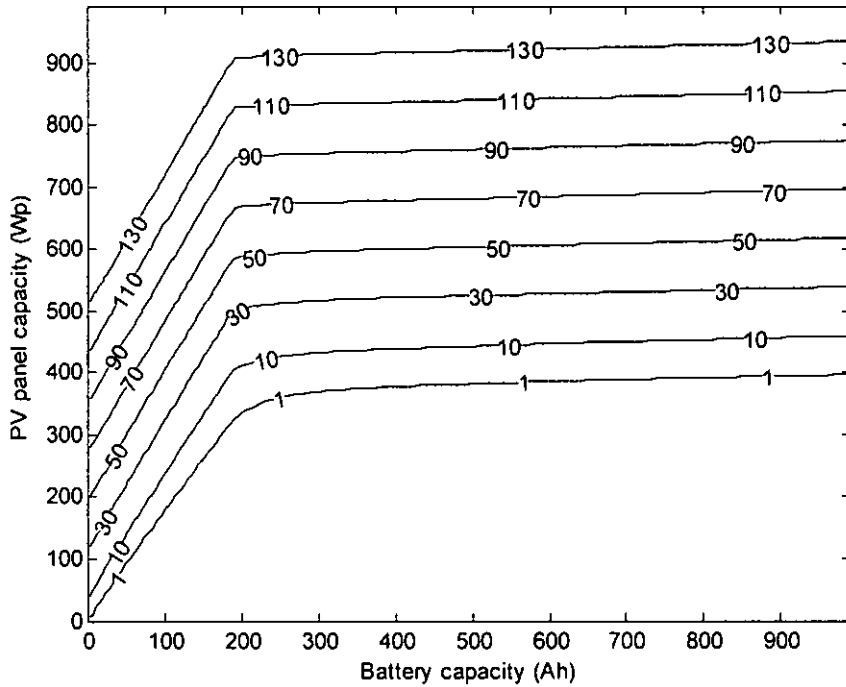


Figure 4.15: Excess energy surface graphic

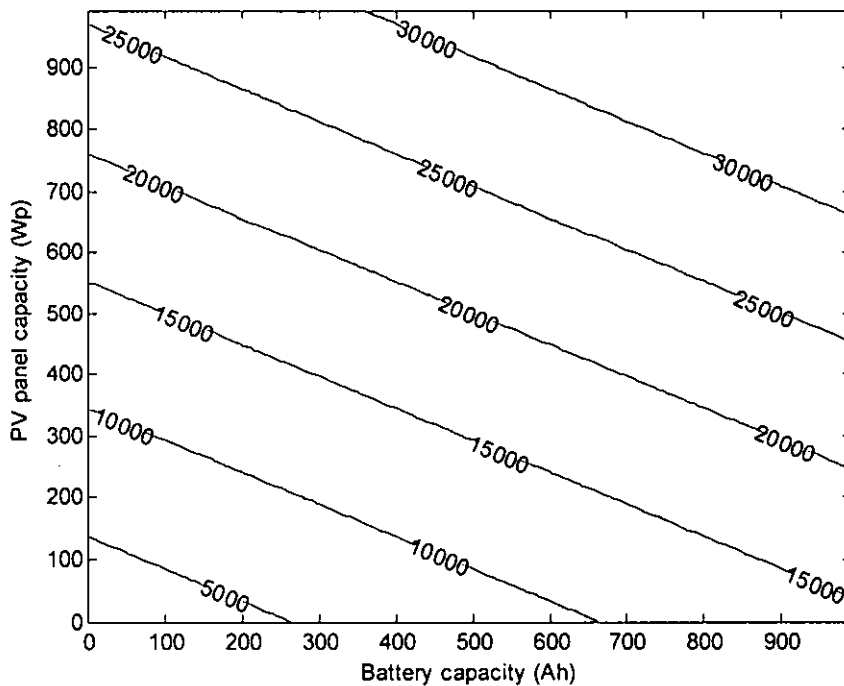


Figure 4.16: Capital cost surface graphic

For size optimization, system cost surface graphics, consist of Capital Cost (CC) and Life Cycle Cost (LCC), were also plotted (Fig. 4.16 and 4.17). The CC and LCC surface graphic are linear and increase with PV panel and battery capacity.

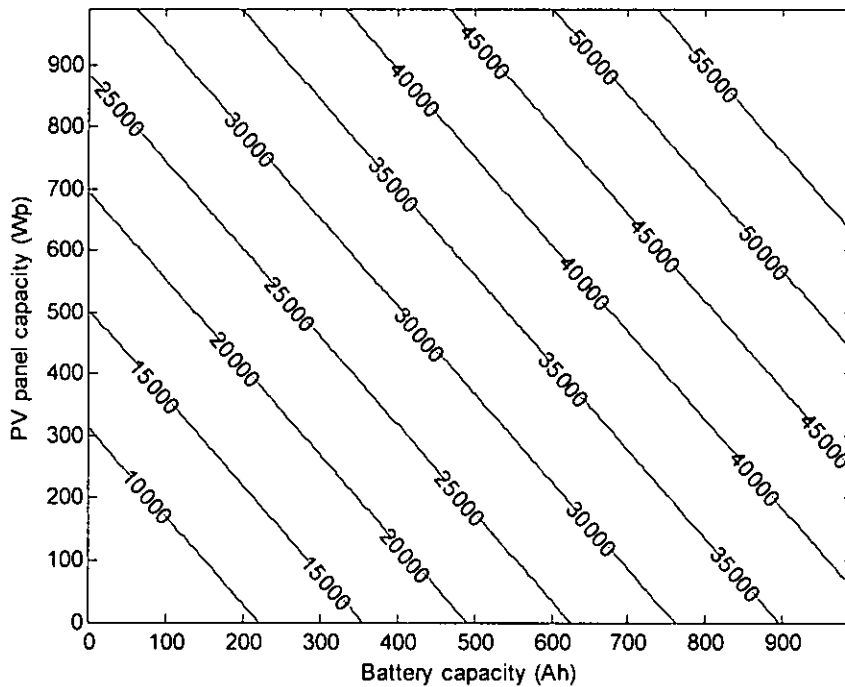


Figure 4.17: LCC surface graphic

4.4.2 Sizing curve and selection of the PV-battery configuration

Sizing optimization has been carried out using two parameters approaches by mean of minimum Capital Cost for selected LPSP value (LPSP-CC), minimum Life Cycle Cost for selected LPSP value (LPSP-LCC) and by using four parameters approach (design space). Then, the results of all the approaches are compared with deterministic method results.

Fig. 4.18 shows the comparison between sizing results by using the deterministic method (initial design), by minimum capital cost and by mean of LCC. It is observed from Fig. 4.18 that deterministic method result is undersize the PV panel capacity and oversize battery capacity. LPSP value of deterministic method is higher than other methods. It is means the performance of the system is worse. Small LPSP value

indicates better system performance. There is only little difference between the results using minimum CC and minimum LCC. If the investor prioritizes small CC, then the configuration with smaller PV panel and larger battery capacity is selected. If LCC is prioritized, then the configuration with larger PV panel and smaller battery capacity is selected.

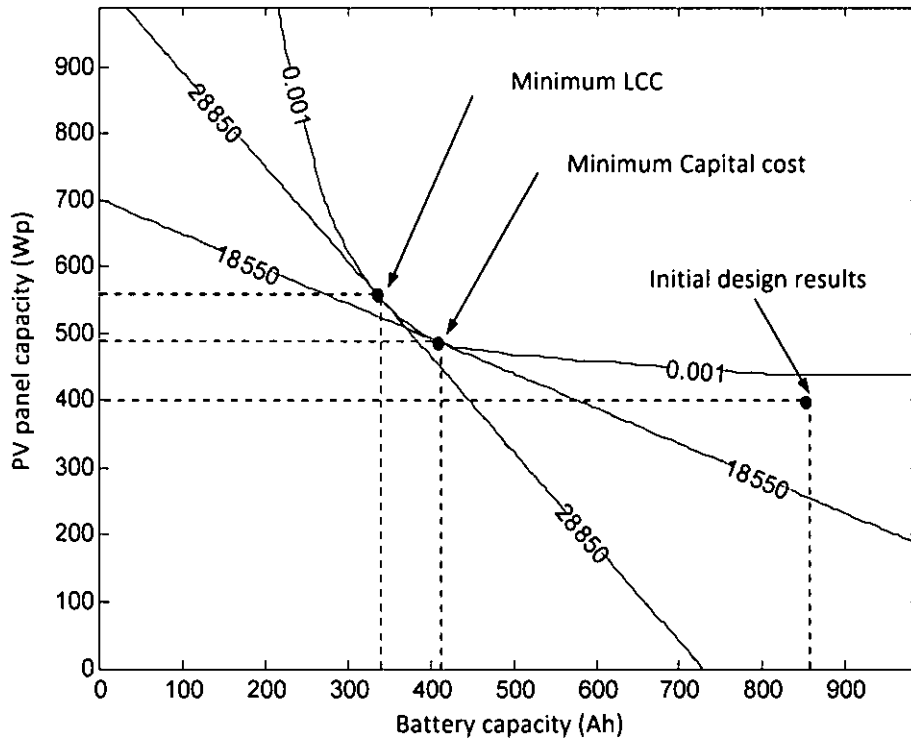


Figure 4.18: Sizing curve based on minimum Capital cost and LCC on desired LPSP

For design space approach, sizing optimization was performed by determine design area using limitation of minimum LPSP value, maximum excess energy and maximum capital cost and maximum LCC. Design area for LPSP is determined between 0-0.001 LPSP. Generally, the lower LPSP choice is better. Design area for excess energy is 0-30% excess energy and design area for LCC is below RM 32,000 with a capital cost below RM 20,000. PV panel and battery capacity for design space approach are selected based on values that are multiples of the available commercial capacity in the market, in this study it was assumed that commercial capacities of PV panel available in the market are 100 Wp, and commercial capacity of battery for 12V nominal are 50 and 100 Ah. Fig. 4.19 shows the design space approach and Fig. 4.20 shows the zoom in of Fig. 4.19 and size selection (option 1 and 2).

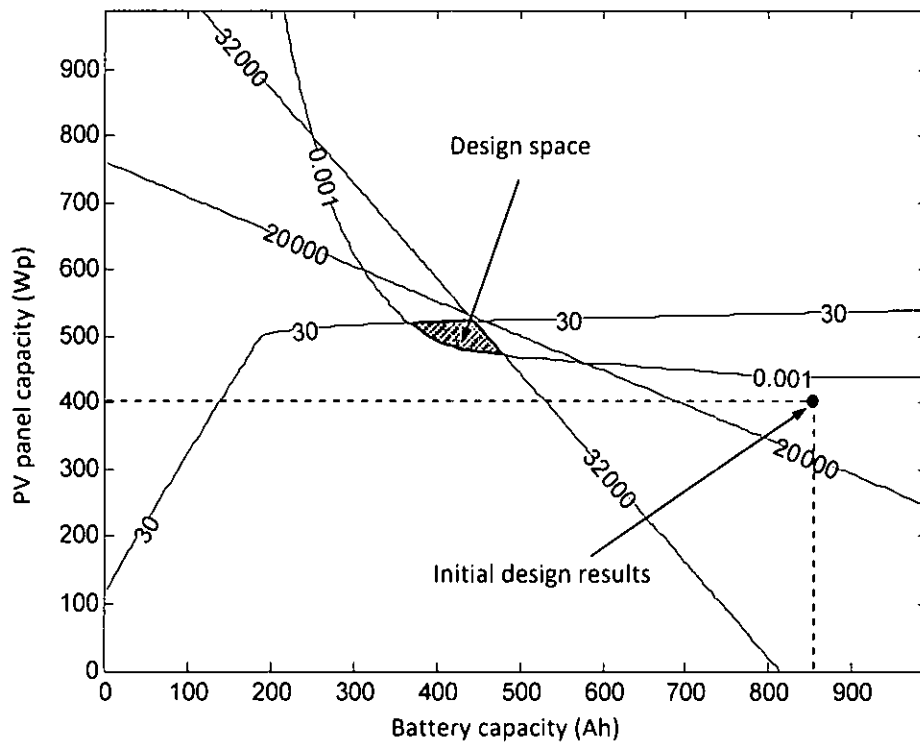


Figure 4.19: Design space approach results

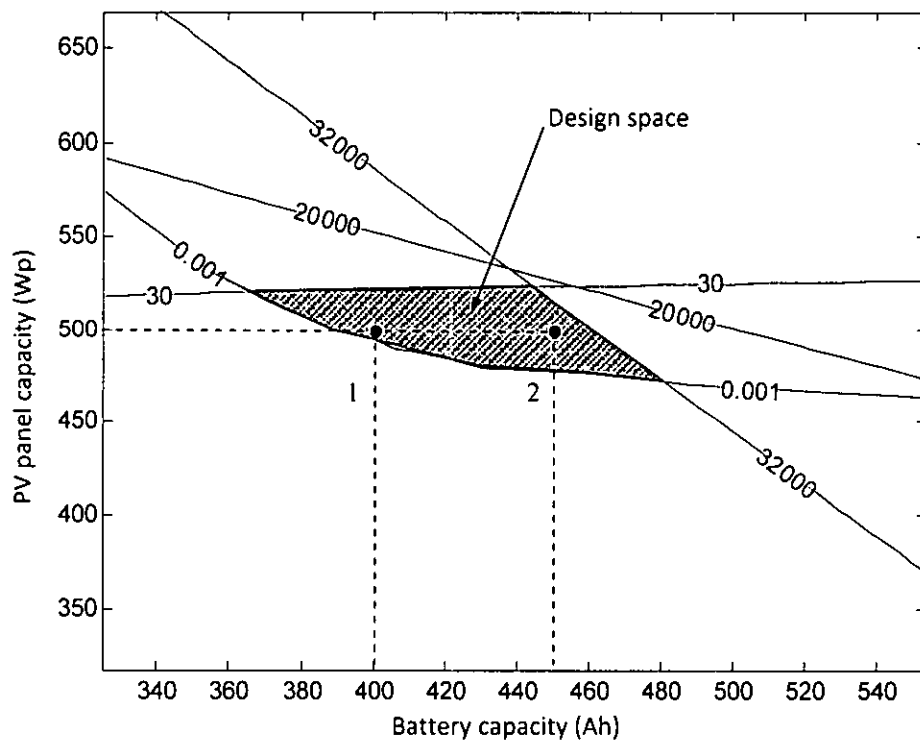


Figure 4.20: Design space (zoom-in) option 1 and 2

Table 4.5 shows comparison of sizing optimization results. As seen from the results, deterministic method shows higher LPSP value, underestimate PV panel capacity and overestimate battery capacity. This method also results higher capital cost and LCC than proposed daily based LPSP calculation method.

Table 4.5: Comparison of sizing optimization results

No.	Method	System Configuration		Considered parameters			
		PV panel (Wp)	Battery (Ah)	LPSP	Excess Energy (%)	Capital Cost (RM)	LCC (RM)
1	Initial design (Deterministic method)	400	864	0.031	1.5	22118	44296
2	Minimum capital cost on 0.001 LPSP	495	405	0.001	23	18675	29793
3	Minimum LCC on 0.001 LPSP	560	340	0.001	40	19427	29086
4	Design space approach option 1	500	400	0.001	24	18733	29738
5	Design space approach option 2	500	450	0.0002	24	19357	31589

Size optimization using minimum capital cost on 0.001 LPSP shows results that are more reasonable and size optimization using minimum LCC shows a higher capital cost. PV panel and battery capacity value that are more rational and applicable can be obtained using design space approach by considering the PV panel and battery capacity unit that is available in the market. Design space approach option 1 shows lower capital cost and LCC than option 2, while option 2 shows lower LPSP value. It is up to investor priority to select PV panel and battery configuration. Option 1 is preferable for lower system cost, while option 2 is preferable for better system performance by mean of lower LPSP value. However, for the above case, option 1 is selected since the LPSP value indicates enough desired performance.

4.4.3 Analysis of the selected configuration

Analysis of selected PV-battery configurations from previous section were presented here and compared with deterministic method results. One-year energy balance analysis is carried out by using calculation results from proposed daily-based LPSP calculation algorithm (section 3.3). Energy balance by mean of energy excess and losses were observed from the calculation results. Daily battery status also observed.

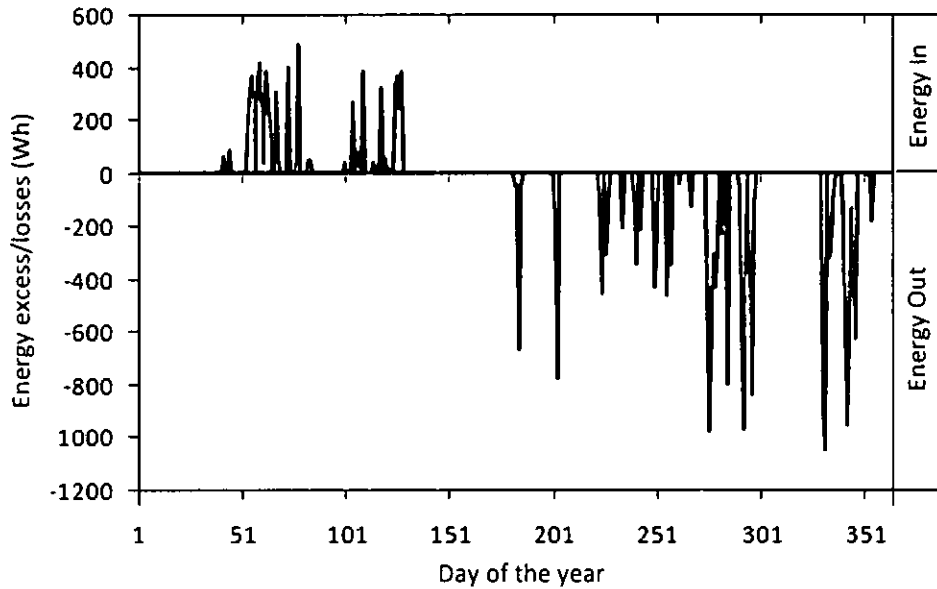


Figure 4.21: Daily excess and losses energy for 400 Wp PV panel and 864 Ah Battery capacities (deterministic method)

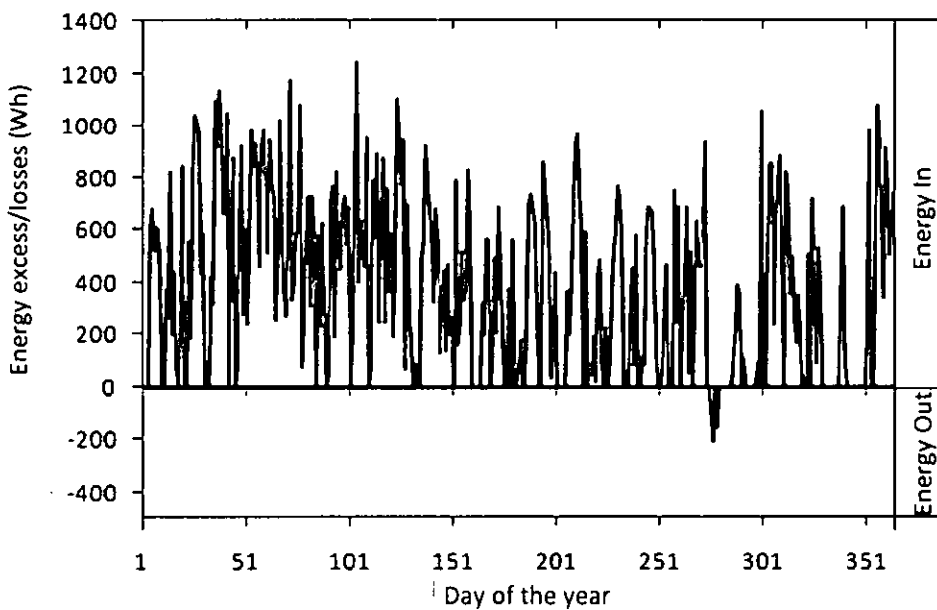


Figure 4.22: Daily excess and losses energy for 500 Wp PV panel and 400 Ah battery capacities (Design space approach option 1)

Fig. 4.21 shows daily excess energy and losses energy throughout the year for deterministic method results. It is observed from Fig. 4.21 the excess energy is small, occurred only during dry season period. The energy loss is occurred during the rainy season. Fig. 4.22 shows energy balance throughout the year for design space approach (option 1) size configuration. There is more excess energy throughout the year than deterministic method results and only small losses.

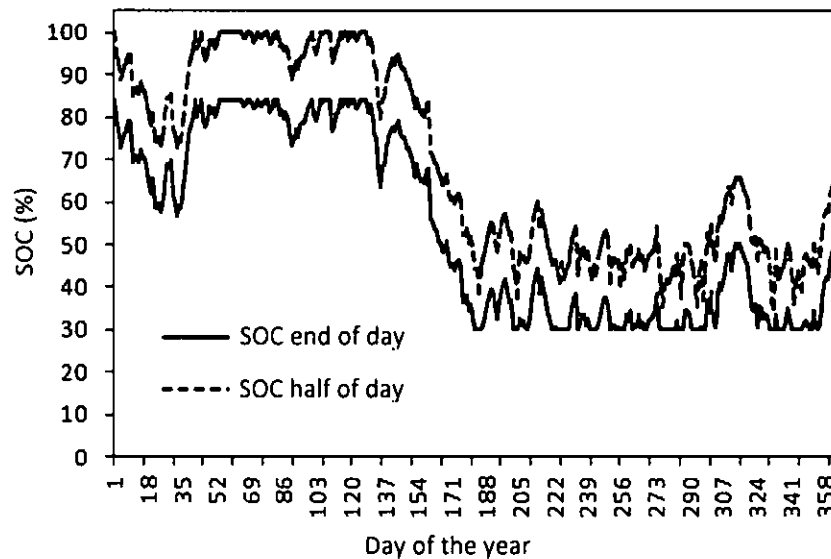


Figure 4.23: Daily SOC of the battery for 400 Wp PV panel and 864 Ah Battery capacities (deterministic method)

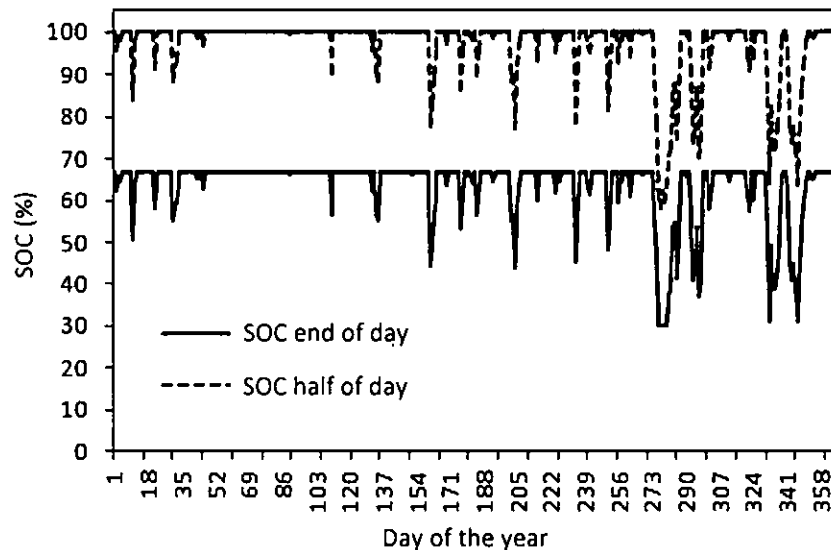


Figure 4.24: Daily SOC of the battery for 500 Wp PV panel and 400 Ah battery capacities (Design space approach option 1)

Fig. 4.23 shows daily battery SOC (on half day and full day) throughout the year for deterministic method configuration. As seen from Fig. 4.23 for deterministic method results, even though the battery capacity relatively larger than design space results, the battery mostly operates near 30% of SOC (minimum design SOC) which is occurred on the rainy season. This is because the PV panel capacity is undersized. Fig. 4.24 shows the daily battery SOC (on half day and full day) throughout the year for selected configuration (design space approach option 1). It is observed in selected configuration results even though the battery size is smaller than deterministic method results, the battery mostly operate on SOC about 68%, and only several days operate near 30% of SOC. This is because the configuration between PV panel size and battery is balance.

4.4.4 Economic evaluations

The Capital Cost and Life Cycle Cost calculation results have been presented in Table 4.6. This section presents a further economic analysis, including Annual Life Cycle Cost (ALCC), Payback Period (PBP) and Cost of Energy (COE). Annual Cash Flow (ACF) for conventional grid electricity is calculated by multiplying Annual Energy Service (AES) with respective Electricity Tariff (ET) as follows:

$$ACF = AES \times ET$$

Payback period (PBP) is calculated as follow:

$$PBP = \frac{ALCC}{ACF}$$

Table 4.6 shows calculation results of AES, ALCC, COE and PBP for each configuration. From the results, it is noted that solar energy is still expensive as compared to grid electricity. Cost of electricity energy generated from PV system is almost ten times of conventional grid electricity (about 0.22-0.33 RM/kWh). This is because grid electricity has a subsidy from the government and PV system technology still considered as an expensive technology. However, PV technology has been

developing, and the PV cost is decreasing day by day. On the other hand, the cost of grid electricity that generated from fossil fuel is increasing.

Table 4.6: Economic analysis results

No.	Method	AES (kWh/year)	ALCC (RM)	COE (RM)	PBP (year)
1	Initial design (Deterministic method) (400 W _p , 864 Ah)	550.274	1996	3.25	16.6
2	Minimum capital cost on 0.001 LPSP (495 W _p , 405 Ah)	567.301	1685	2.97	13.6
3	Minimum LCC on 0.001 LPSP (560 W _p , 340 Ah)	567.287	1753	3.09	14.1
4	Design space approach option 1 (500 W _p , 400 Ah)	567.322	1690	2.98	13.6
5	Design space approach option 2 (500 W _p , 450 Ah)	567.635	1746	3.08	14.1

4.5 Experimental results

Experimental results, including PV panel's I-V curve under experimental condition, PV panel's efficiency monitoring and standalone PV system with lighting load monitoring results are presented here. Controller performance was evaluated in PV panel's P-V curve. Measured weather and system parameters of standalone PV systems also presented in this section. Fig. 4.25 shows the schematic diagram of SAPV system. Experimental setup for this study only used DC load.

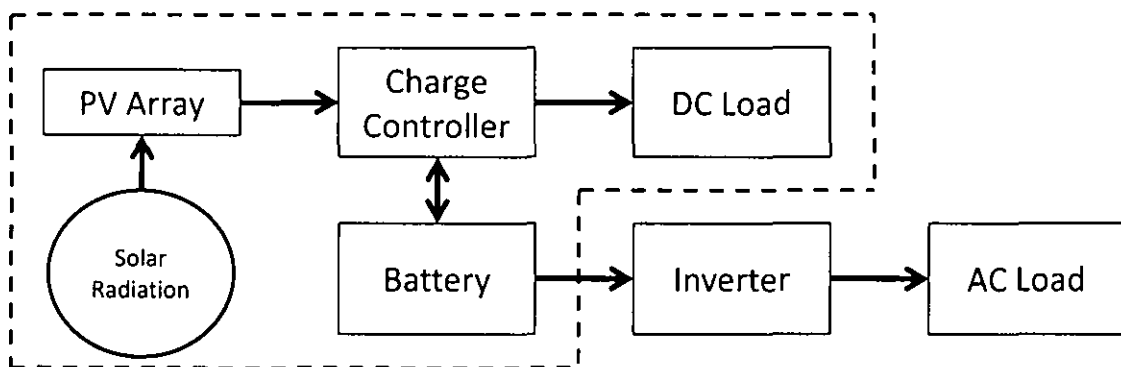


Figure 4.25: Schematic Diagram of Standalone PV System

4.5.1 PV panel's I-V curve

Several power resistors with different values and power ratings were used to take data for I-V curve plotting, as explained in section 3.5. Two standard multi-meters were used to measure current and voltage of PV panel during an on-site generation. Kipp & Zonen pyranometer (SP-LITE series) was used to measure solar irradiation. The pyranometer and J-type thermocouples connected with the FLUKE Hydra logger 2620A were used to measure air temperature and PV panel surface temperature. The variable resistor value was changed several times in different irradiance to get paired value of current (I) and voltage (V) on respected solar radiation value.

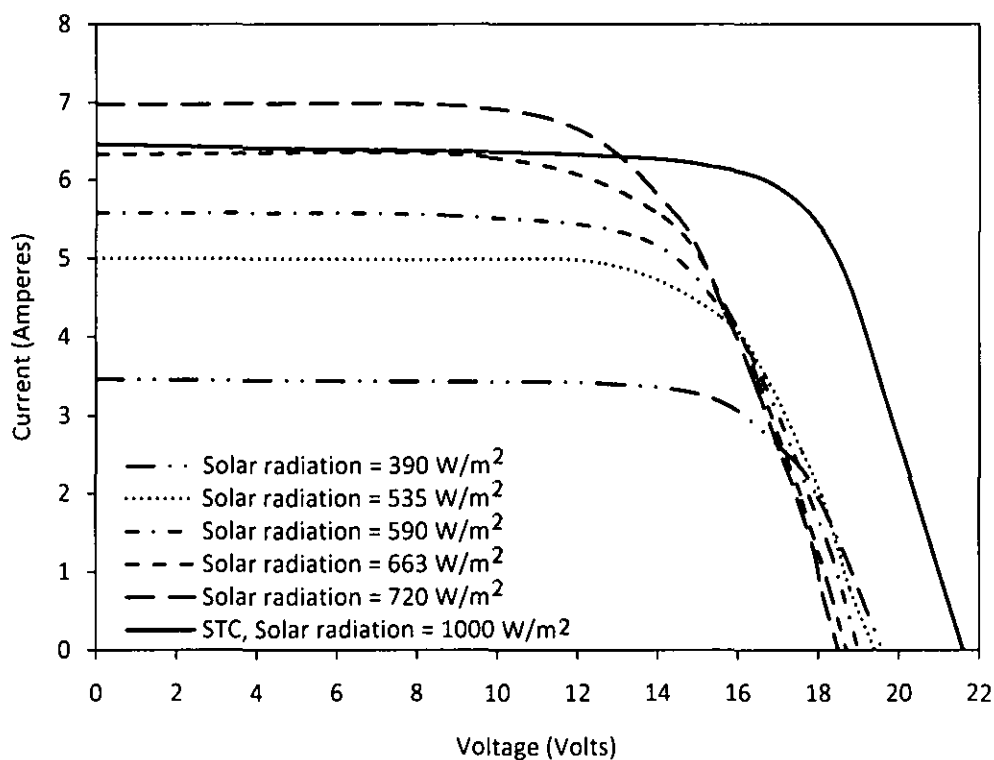


Figure 4.26: I-V curve characteristics of PV panel for different solar radiation level

Fig. 4.26 shows I-V curve characteristic of PV panel from experimental data compared with I-V curve from PV panel datasheet (at STC). The measurements show that actual output of the PV panel is lower than the output at STC. As shown in Fig. 4.26, the short circuit current of the PV panel increased with irradiance. It increased from 3.4 Amperes at $390 W/m^2$ to 6.9 Amperes at $720 W/m^2$. The open circuit voltage decreases with the increase of the irradiance that increases cell temperature.

The maximum power of the PV panel is shifted to a lower voltage as irradiance increases as presented in Fig. 4.27. The maximum power output at 720 W/m² irradiance is about 80 Watt, with 14 Volt operation voltages. For a charging voltage at about 15-16 Volts, power losses due to the shifting of maximum power point were observed. For 390 W/m² irradiance, maximum power occurred at 15.4 Volt. For 663 W/m² irradiance, maximum power occurred at 14.1 Volts.

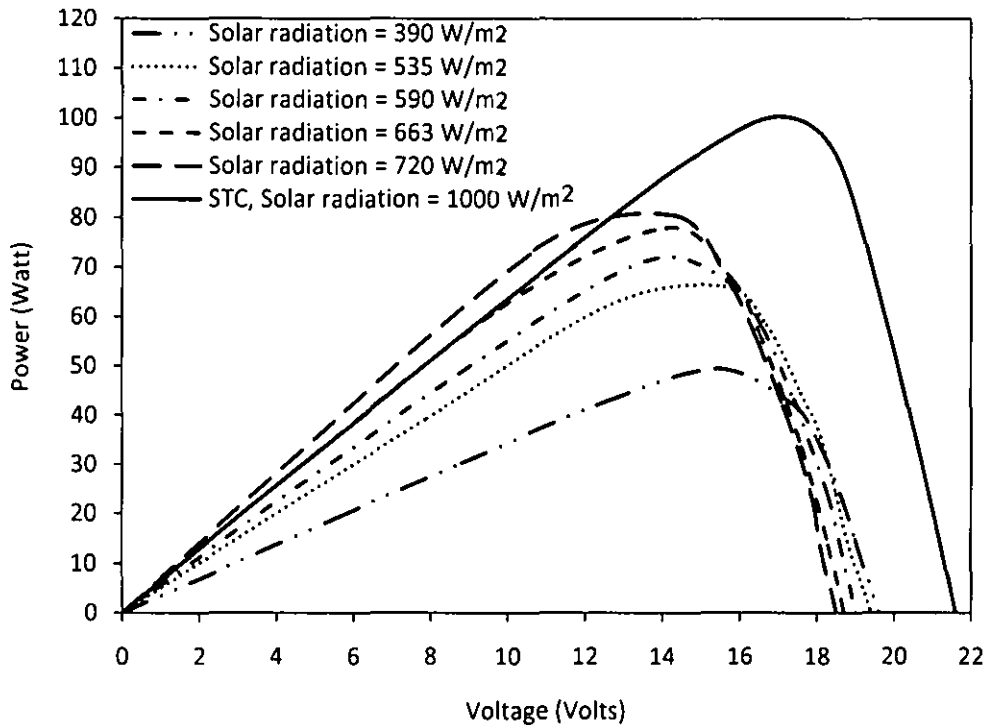


Figure 4.27: Power curve characteristics of PV panel for different solar radiation level

Power loss due to the shifting of the maximum power point occurred because the controller does not support Maximum Power Point Tracking (MPPT). Charge controller operation voltage is recommended to be set at about 15 Volt considering the shifting in maximum power point and to make sure that the operation voltage is always above the battery voltage. Maximum battery voltage when it is 100% charged is about 13.8 Volt, so the controller operation voltage should be above this value.

4.5.2 Charge Controller performance

The main function of the solar charge controller is to regulate the charging voltage to extract maximum power from PV panel and to prevent overcharging and over

discharging. In the experiment, Pulse Width Modulation (PWM)-type charge controller was installed. Fig. 4.28 shows power output of the controller from 26-30 June 2010 as compared to actual power curve and STC power curve. The data was recorded in 5 minutes time step during the day. The controller works well in high solar radiation and there are some inefficient results under low solar radiation. Average measured conversion efficiency during the period is 11.05%. This system efficiency is total system's efficiency, include PV panel's efficiency, controller efficiency, and losses due to power dissipation in the cable, dust, etc.

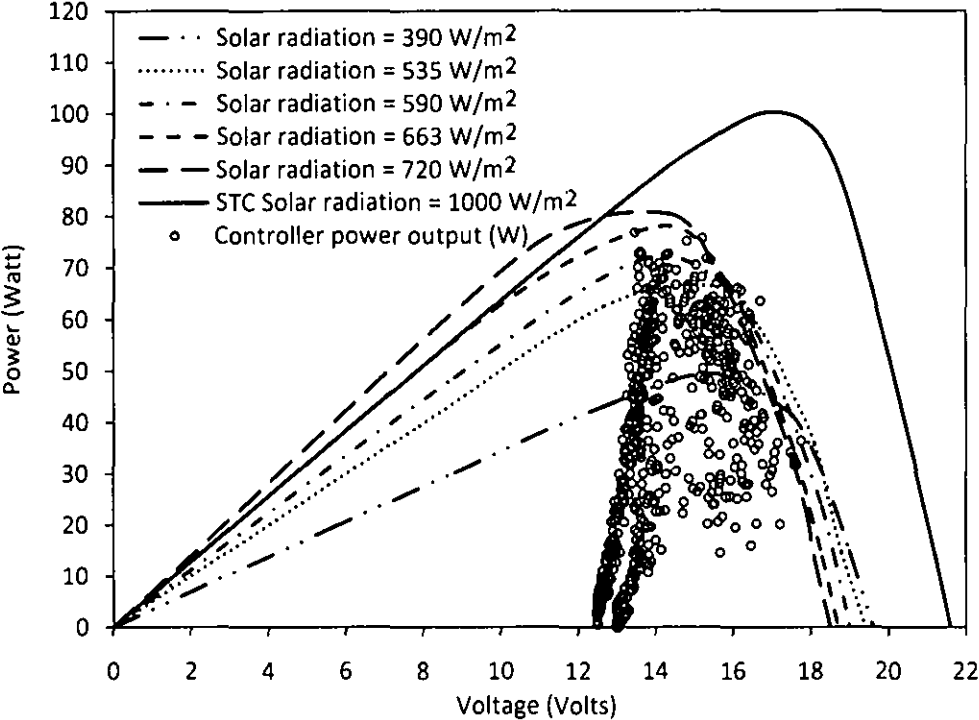


Figure 4.28: Solar Charge Controller output compared with power curve

4.5.3 PV panel efficiency

PV panel efficiency measurement has been carried out and compared with PV panel efficiency calculated from the datasheet. According to the manufacturer's datasheet, P_{peak} of each module used in the experiment is 100 Wp and the area of each module (A) is $1.15m \times 0.655m = 0.75325 \text{ m}^2$, STC condition is test condition at 1000 W/m^2 of solar radiation level and $25 \text{ }^\circ\text{C}$ ambient temperature. PV panel's efficiency at STC is calculated from datasheet as follow:

$$\eta_{STC} = \frac{100}{1000 \times 0.75325} \times 100\% = 13.27\%$$

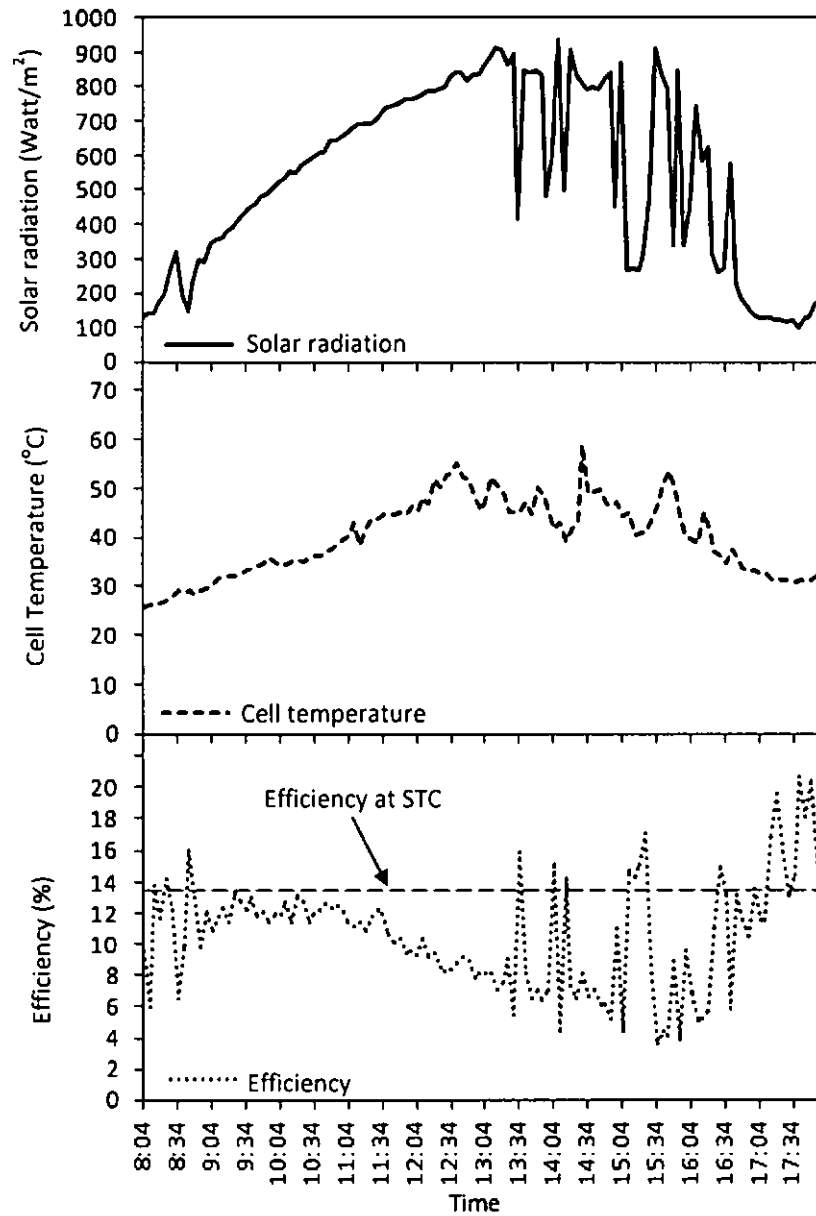


Figure 4.29: Effect of Solar radiation and cell temperature on PV panel Efficiency (30 June 2010)

Data monitored during the experiment were used to calculate PV panel efficiency during the day. It is observed from the graphic, the increasing of solar radiation increase the PV panel surface temperature and decrease PV panel's efficiency. In the afternoon, the sky is clear there are only small fluctuations in solar radiation and the measurement was performed correctly, during the afternoon the cloud caused a fluctuation in solar radiation and PV panel output. However, the efficiency-changing pattern during the day can be observed by looking at data trend in Fig. 4.29.

4.5.4 Weather parameter, Power input and output of the system

Monitoring of weather and system parameters of standalone PV system have been carried out for several load levels. Five consecutive day's data (1-5 July 2010) have been monitored and presented here. Fig. 4.30 and 4.31 shows monitored solar radiation, Relative Humidity (RH) and ambient temperature on 1-5 July 2010. During the period, the weather is cloudy and there was a rain on 3 July 2010 in the afternoon. The PSH values for the five days are 3.85, 3.40, 2.49, 2.64 and 3.91 respectively. The ambient temperature is fluctuated ranging from 24-37 °C. High RH values were observed during the night and during the rain.

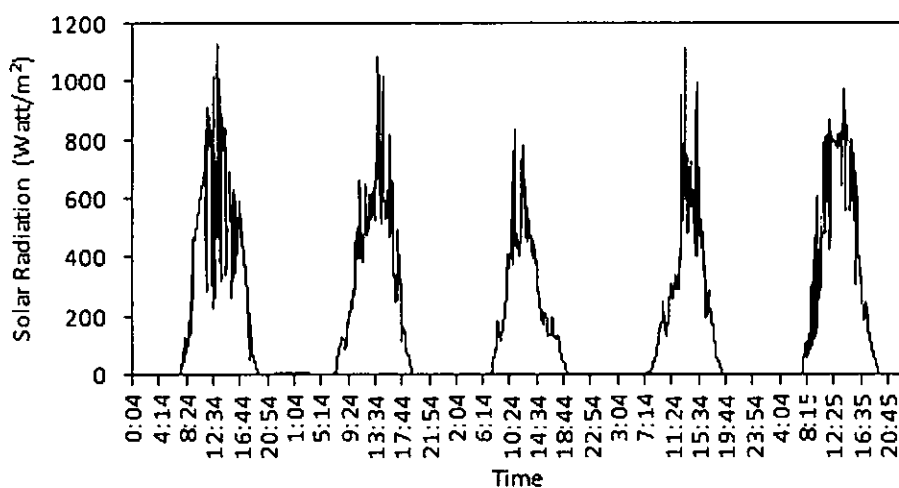


Figure 4.30: Monitored solar radiation on the site 1-5 July 2010 (5 min. time step)

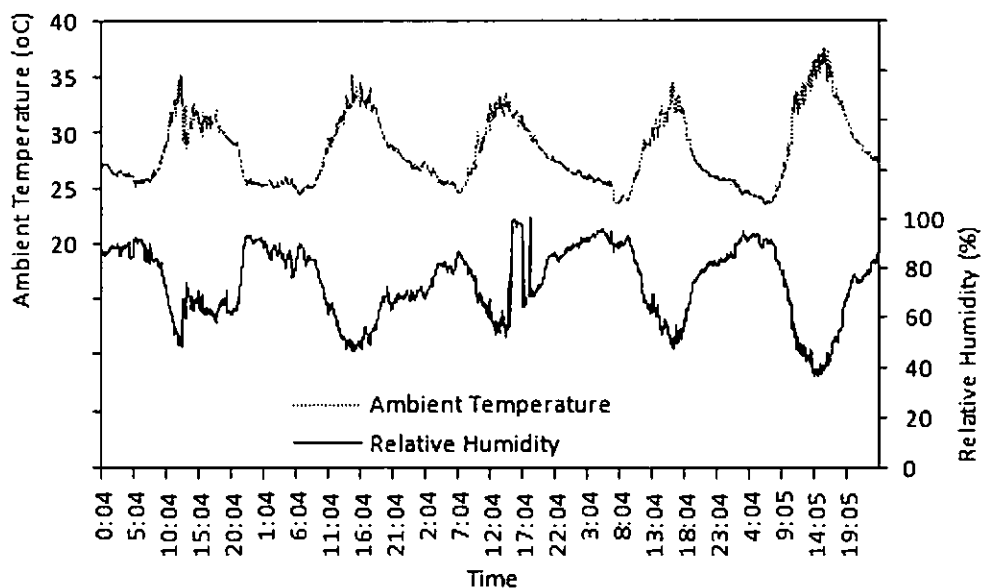


Figure 4.31: Monitored Ambient Temperature and Relative Humidity on the site, 1-5 July 2010 (5 min. time step)

The results presented in this section are for total load of 1200 Wh/day, further details are presented in Appendix F. Fig. 4.32 shows the monitored results of the power-in and out of the battery. Power in to the battery (from the PV panels) is indicated by positive values and the power out from the battery due to the loading is indicated by negative values. The input energy is fluctuated during the day dependent on the solar radiation level. The calculated energy inputs consecutively are 1537.63 Wh, 1377.3 Wh, 1192.64 Wh, 1229.98 Wh and 1528.15 Wh. The load was about 120 Watt in the 10-hour duration during the night. Therefore, the total lighting equivalent load for each day was approximately 1200 Wh per day. The total energy supplied by the battery (full night data only) consecutively are -1194.48 Wh, -1188.74 Wh, -1165.68 Wh and -1147.7 Wh as shown in Fig. 4.32. From the calculated energy input and output, since the observed energy input is always higher than energy output, the system is meeting the required daily energy.

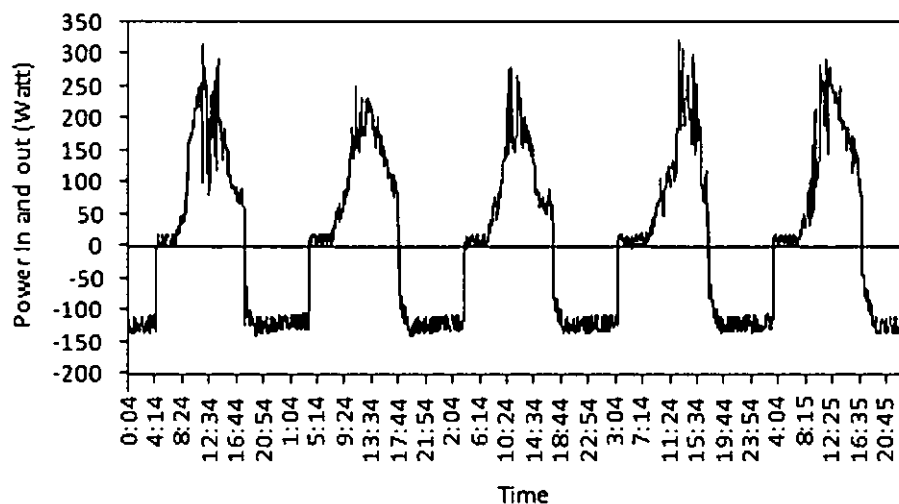


Figure 4.32: Power in and out of the battery, 1-5 July 2010 (5 min. time step)

4.5.5 PV panel and Battery voltage monitoring

PV panel voltage and battery have been monitored as presented in Fig. 4.33. During the charging period, PV panel voltage is higher than battery voltage, while during the night the PV panel voltage drops to zero. PV panel voltage was fluctuated dependent on solar radiation and cell temperature. The controller will cut off the PV panel-battery's connection if the battery in full charge condition. In this case, the observed

value of PV panel voltage is V_{oc} (open circuit). The charging process is controlled by PWM charge controller.

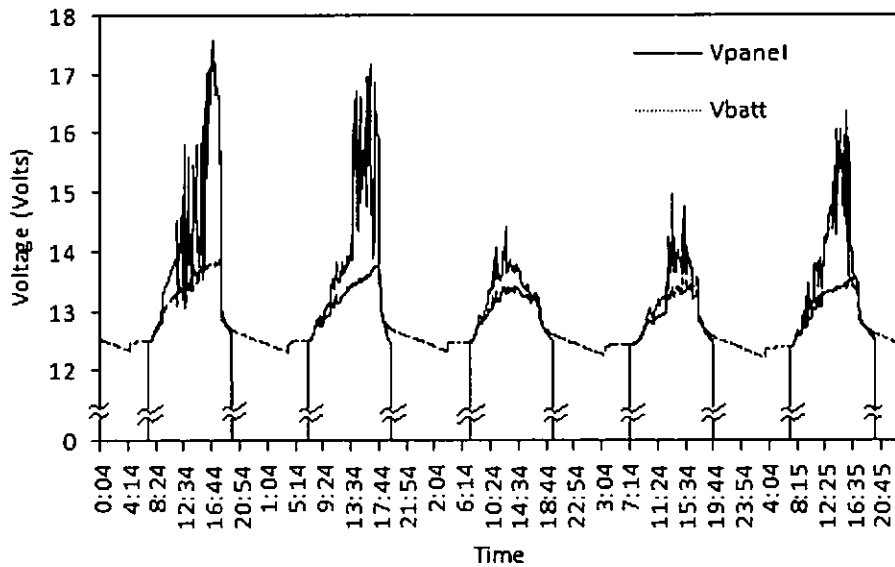


Figure 4.33: PV panel and battery voltage, 1-5 July 2010 (5 min. time step)

Battery voltage level during charging and discharging can be observed in more detail in Fig. 4.34. The controller maintained the battery voltage below 14.5 Volts to avoid overcharging. During discharging, the battery level drops linearly due to the constant loading. In the afternoon, the battery level drops to about 13.2 Volts, this is because the charge process over and the discharge process is started.

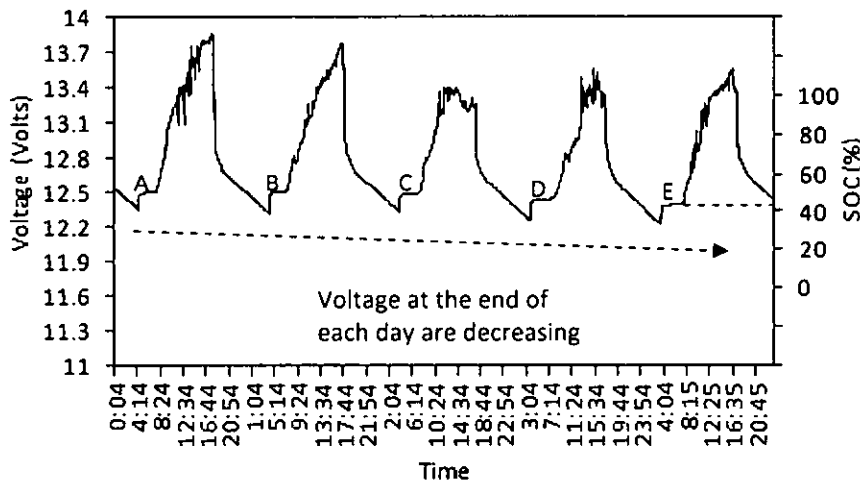


Figure 4.34: Battery voltage, 1-5 July 2010 (5 min. time step)

The state of charge of the batteries was observed by monitoring their open circuit voltage [98]. The SOC scale in Fig. 4.34 is based on open circuit voltage while the measured voltage presented here is closed circuit voltage. It is difficult to monitor open circuit voltage of the battery during charge and discharge process. However,

SOC of the battery can be estimated by observing the battery condition during the unloading period and before the charging is started. Daily battery SOC level is predicted by observing data monitored at points A-E as shown in Fig. 4.34. It is observed from the figure that the battery voltage at the end of each day in the period is decreasing. It is indicating that the energy level in the battery is decreasing or the SOC is decreasing. Whereas, the input and output energy observation in Fig. 4.32 shows that the daily input energy is higher than output energy. It is concluded that the measured input energy was not efficiently stored in the battery during the charging process, it means the charging efficiency is not 100% and there is self-discharge factor of the battery. That is why the voltage level of the battery is decreasing, which indicates that the actual input energy is lower than the output energy.

4.6 Simulation results

Standalone PV system modeling has been carried out using TRNSYS 16. The detail of the model was presented in section 3.9. This section presents simulation validation results and one-year simulation results for selected PV-battery configuration.

4.6.1 Simulation validation results

Five minutes time step experimental data were collected and converted to hourly averaged data as input for the simulation (weather data) and to validate the simulation model (system data). The data are ten days experimental data from 1-10 July 2010. Fig. 4.35 shows hourly weather data input for the simulation consist of solar radiation, ambient temperature and RH data. System data were presented in Fig 3.36 and 3.37. Fig. 3.36 shows hourly data of the power input and output to and from the battery. Power input and output are separated into two hourly data, called Power Input (PV panel output) and Power Output (Load) in positive value. In the simulation, this load value will automatically be converted to negative since it is the energy output. Fig. 4.37 shows the hourly battery voltage during charging and discharging process from 1-10 July 2010.

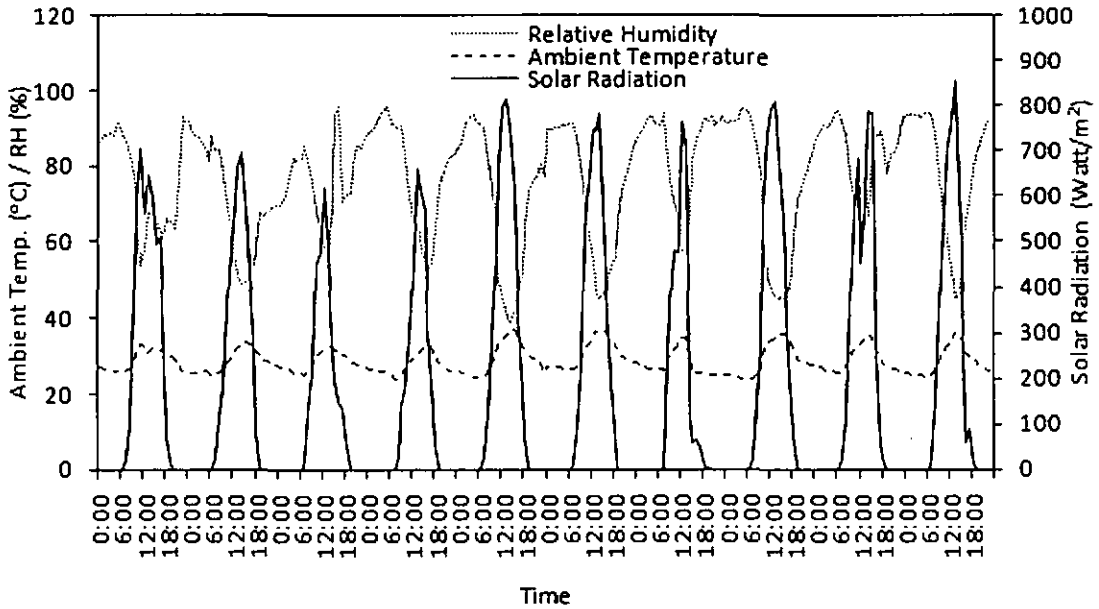


Figure 4.35: Weather data used as the input for simulation

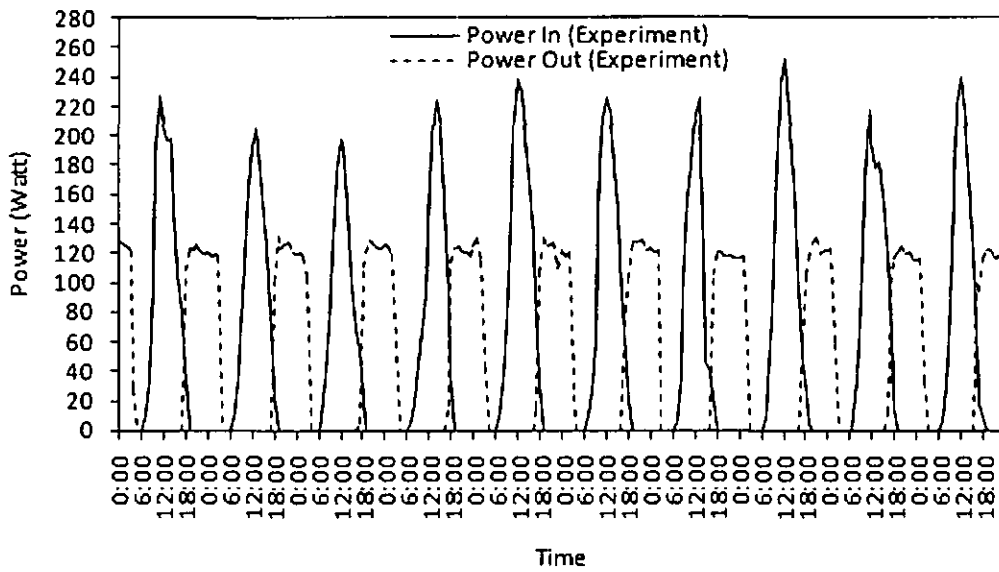


Figure 4.36: Measured Power in and out to/from battery to validate the simulation

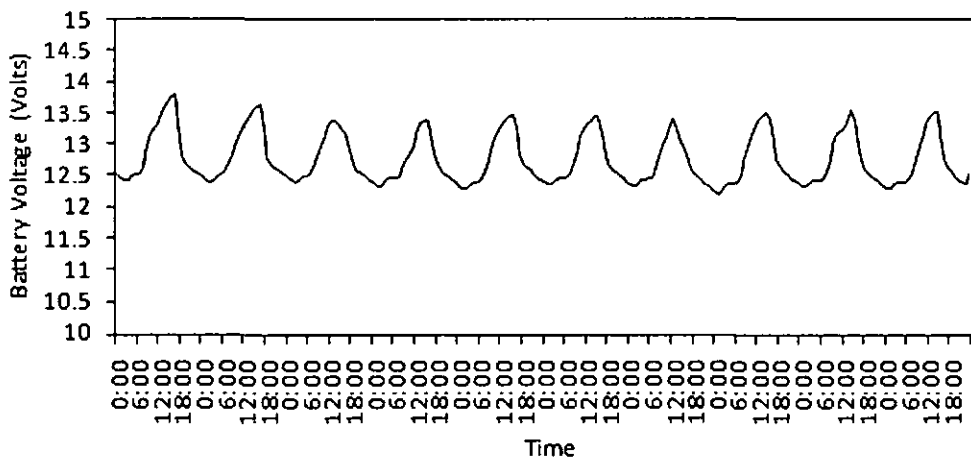


Figure 4.37: Measured battery voltage to validate the simulation

After the input is configured and entered in the TRNSYS component, then the component parameters are configured as explained in section 3.9. An image of parameters setting of PV panel is shown in Fig. 4.38. The parameters are configured according to the PV panel's datasheet. The simulation is performed in TRNSYS simulation studio as presented in Fig. 4.39. The simulation results data can be exported into .txt file and processed in Excel spreadsheet.

(Complete System July 1:5 edit.tpf) Type94a

Parameter	Input	Output	Derivative	Special Cards	External Files	Comment
1	<input type="checkbox"/>	<input type="checkbox"/>	<input type="checkbox"/>	<input type="checkbox"/>	<input type="checkbox"/>	<input type="checkbox"/>
Module short-circuit current at reference conditions	6.3	amperes	More...			
2	<input type="checkbox"/>	<input type="checkbox"/>	<input type="checkbox"/>	<input type="checkbox"/>	<input type="checkbox"/>	<input type="checkbox"/>
Module open-circuit voltage at reference conditions	21.6	V	More...			
3	<input type="checkbox"/>	<input type="checkbox"/>	<input type="checkbox"/>	<input type="checkbox"/>	<input type="checkbox"/>	<input type="checkbox"/>
Reference temperature	298	K	More...			
4	<input type="checkbox"/>	<input type="checkbox"/>	<input type="checkbox"/>	<input type="checkbox"/>	<input type="checkbox"/>	<input type="checkbox"/>
Reference insolation	1000	W/m ²	More...			
5	<input type="checkbox"/>	<input type="checkbox"/>	<input type="checkbox"/>	<input type="checkbox"/>	<input type="checkbox"/>	<input type="checkbox"/>
Module voltage at max power point and reference conditions	17.7	V	More...			
6	<input type="checkbox"/>	<input type="checkbox"/>	<input type="checkbox"/>	<input type="checkbox"/>	<input type="checkbox"/>	<input type="checkbox"/>
Module current at max power point and reference conditions	5.7	amperes	More...			
7	<input type="checkbox"/>	<input type="checkbox"/>	<input type="checkbox"/>	<input type="checkbox"/>	<input type="checkbox"/>	<input type="checkbox"/>
Temperature coefficient of Isc at (ref. cond)	0.0028	any	More...			
8	<input type="checkbox"/>	<input type="checkbox"/>	<input type="checkbox"/>	<input type="checkbox"/>	<input type="checkbox"/>	<input type="checkbox"/>
Temperature coefficient of Voc (ref. cond)	-0.074	any	More...			

Figure 4.38: Parameter setting in TRNSYS 16 simulation studio

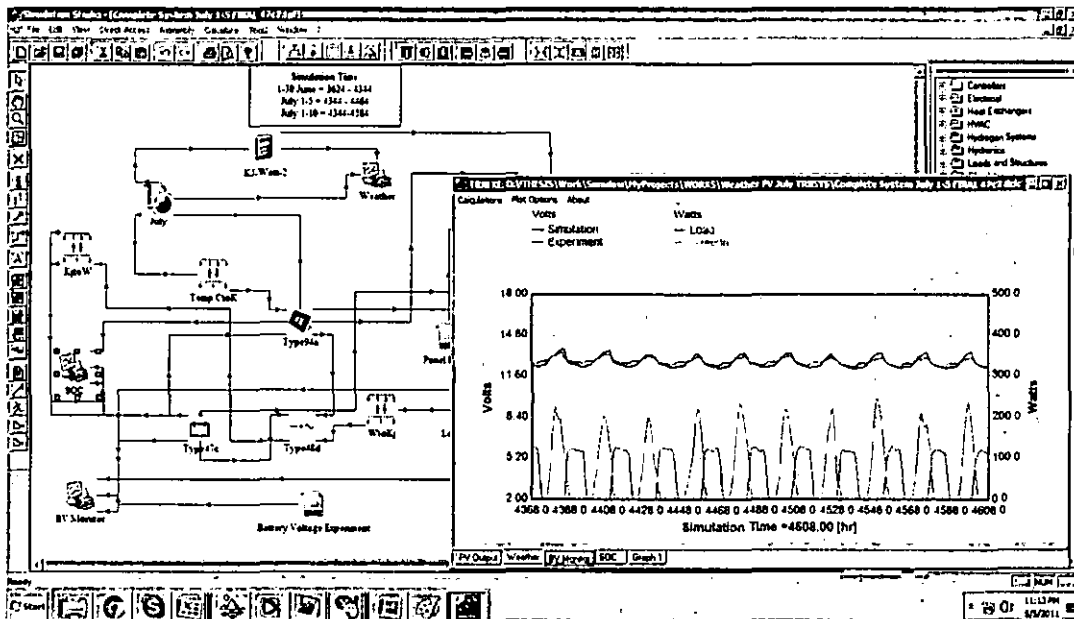


Figure 4.39: Running simulation in TRNSYS 16 simulation studio

Fig. 4.40 shows the PV arrays power output comparison between the measured and simulated results. It is observed that the data trend shows good compromise between measured and simulated data.

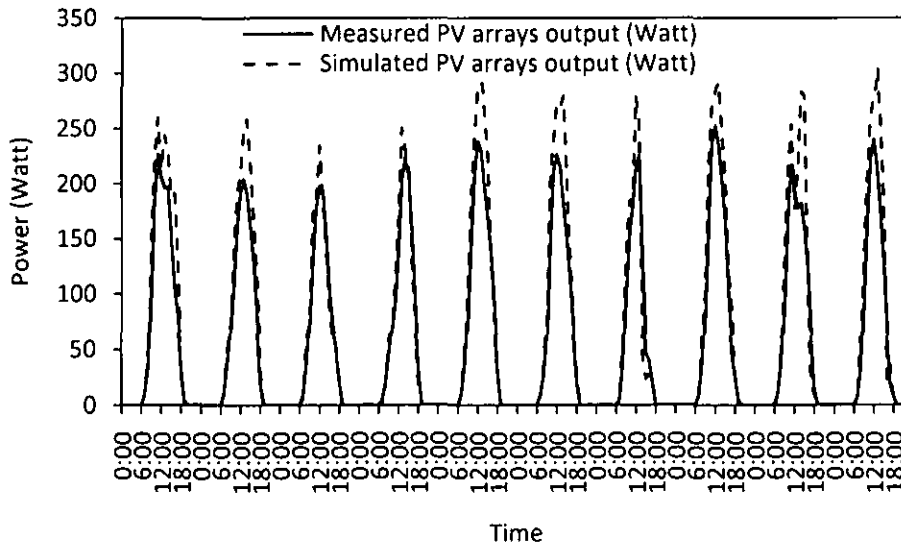


Figure 4.40: Comparison between measured and simulated PV arrays output

Scatter plot of simulated and experiment results of PV arrays output are presented in Fig. 4.41. The coefficient of determination (R^2) is very good about 0.96. Root mean square error (RMSE) is 27.8W and Normalized root mean square error (NRMSE) is 11%. With this result, PV arrays model has been validated and can be used for further simulation.

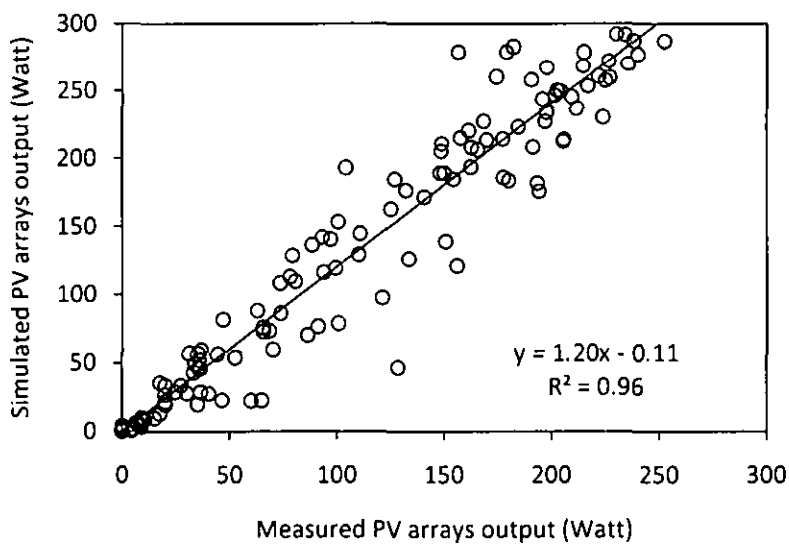


Figure 4.41: Scatter plot of measured and simulated arrays output

Graphical comparison between simulation and experiment battery voltage are presented in Fig. 4.42. The trend of the data shows good compromise between measured and simulated battery voltage value.

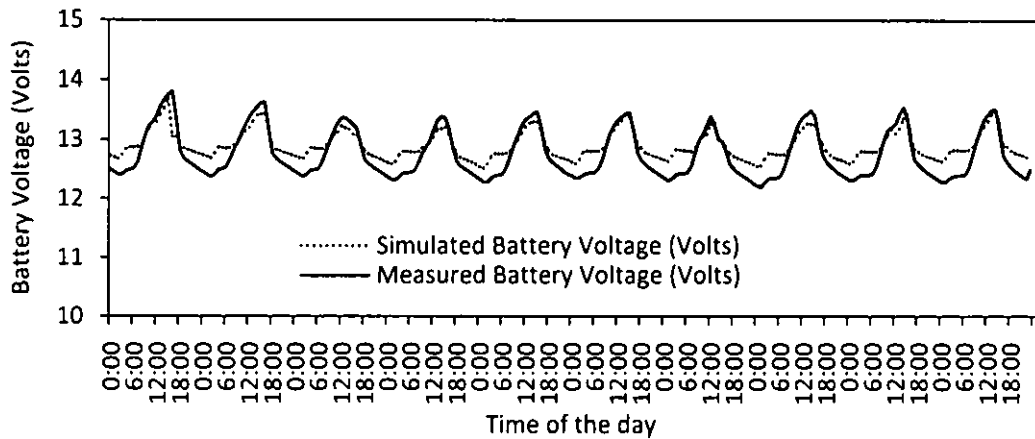


Figure 4.42: Comparison between measured and simulated battery voltage

Fig. 4.43 shows the scatter plot of simulated and measured battery voltage. The simulation results of battery voltage is good with $R^2=0.904$, $RMSE=0.24V$ and $NRMSE=15.6\%$. This result is better from previous researches that were done by F. Shao [86] and L.K. Nkhonjera ($RMSE=0.49V$) [87], it is because they used different battery component type. With this result, the battery component has been validated.

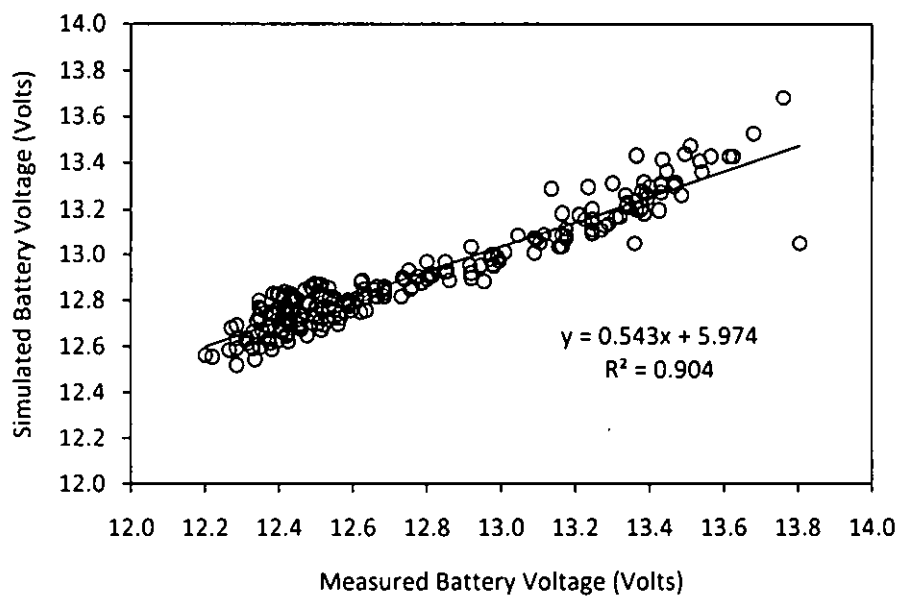


Figure 4.43: Scatter plot of measured and simulated battery voltage

Simulation results of Fractional State of Charge (FSOC) of the battery are presented in Fig. 4.44. The results show that the FSOC of the battery is decreasing during the period. This is the same with data observation in Fig. 4.34. In Fig. 4.44, at point E (5 July 2010, morning), battery FSOC is observed at about 0.39 (SOC=39%), compared to Fig. 4.34 the SOC prediction at the same period is about 41% (FSOC=0.41) SOC, these results shows similar results between measured and simulated value.

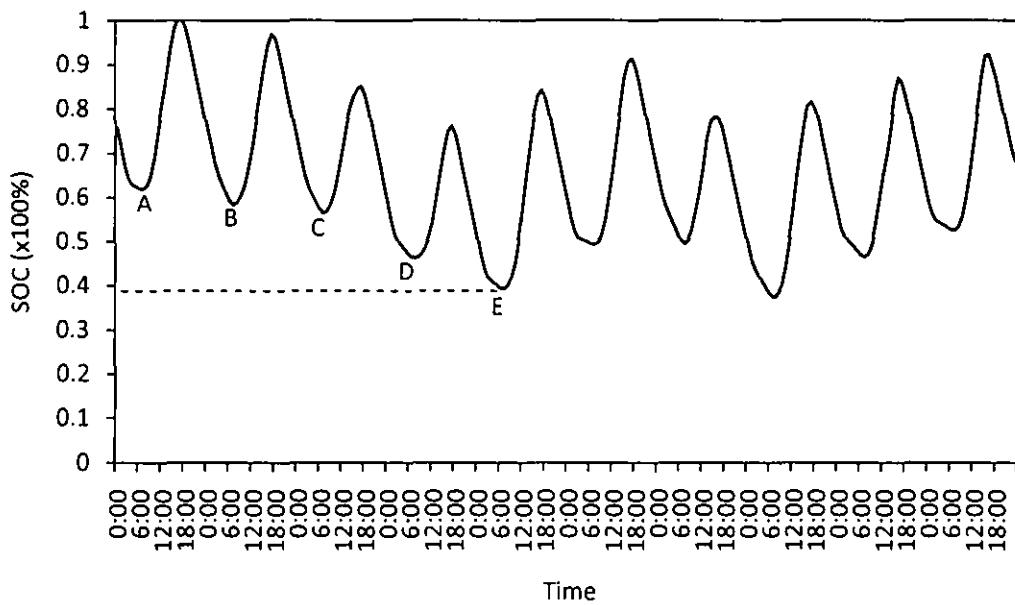


Figure 4.44: Simulation results of FSOC (A-E points refer to Fig. 4.34)

Simulation validation has been carried out, and the results show good compromise in every component model of the simulation. Especially in battery voltage, the simulation result shows improvement from previous research work. The results indicated that Root Mean Square Error (RMSE) between simulated and measured battery voltage has decreased by 50% compared to previous work [87]. With these results, the simulation model has been validated and can be used to simulate other configuration of standalone PV-battery system with confidence. To simulate other configuration of the PV and battery capacities, PV panel and battery component setting need to be changed according to the desired configuration.

4.6.2 Simulation results for selected configuration

Simulation has been carried out for selected configuration (500Wp PV panel and 400Ah battery capacities at 12V system voltage). Fig. 4.45 shows the print screen of TRNSYS 16's simulation studio and the configuration of the simulation. The component is linked, and the connections have been configured according to section 3.9. The details of parameters setting and component's connections are presented in the Appendix E. The simulation control card was adjusted to simulate the system in hourly time step for one year (8760 hour). Weather data consist of Global horizontal solar radiation, ambient temperature, and Relative Humidity from Ipoh meteorological station was used as input for the simulation model.

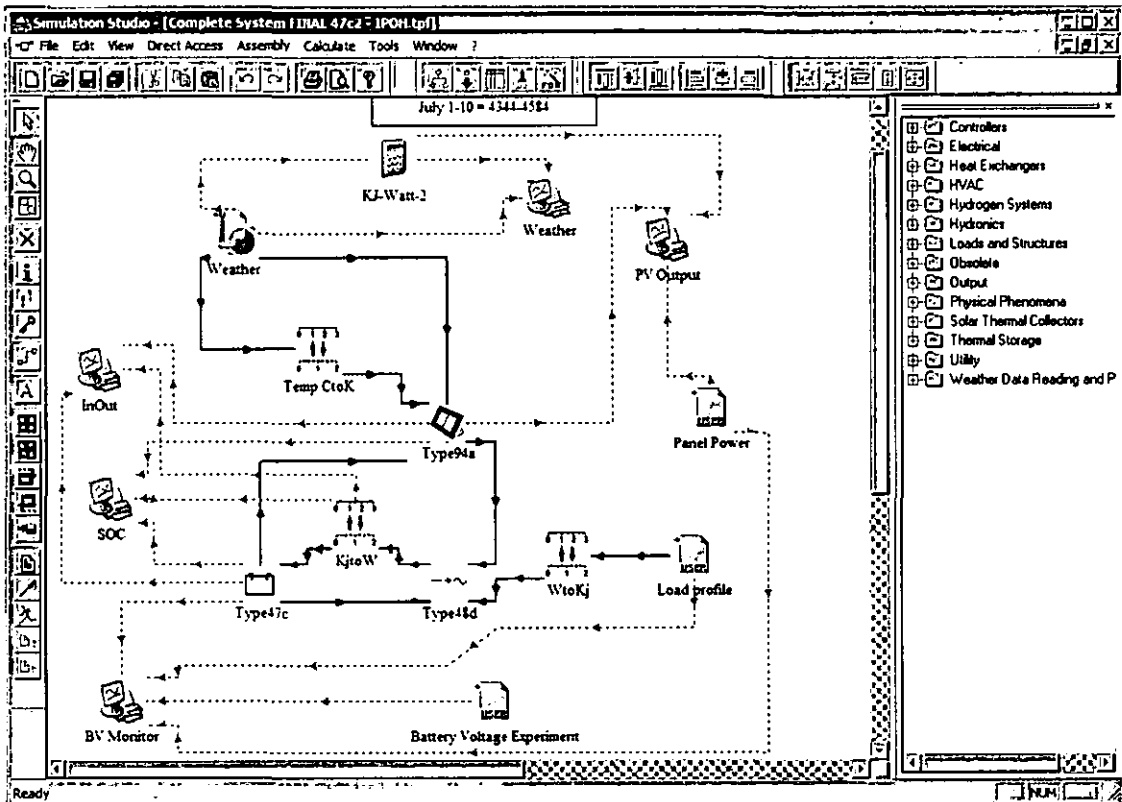


Figure 4.45: Print screens of TRNSYS 16 simulation studios

Fig. 4.46 shows simulation results for PV panel output power in Watts. The parameters in PV panel component model were adjusted as that of experimental PV panel datasheet. The total nominal Watt peak of PV panel is 500Wp. In actual

condition the output always below 500 Watts because hourly average solar radiation never reach 1000 W/m^2 and the PV panel temperature always above 25°C during the day in the presence of solar radiation. A zoom in graphic is shown in Fig 4.47.

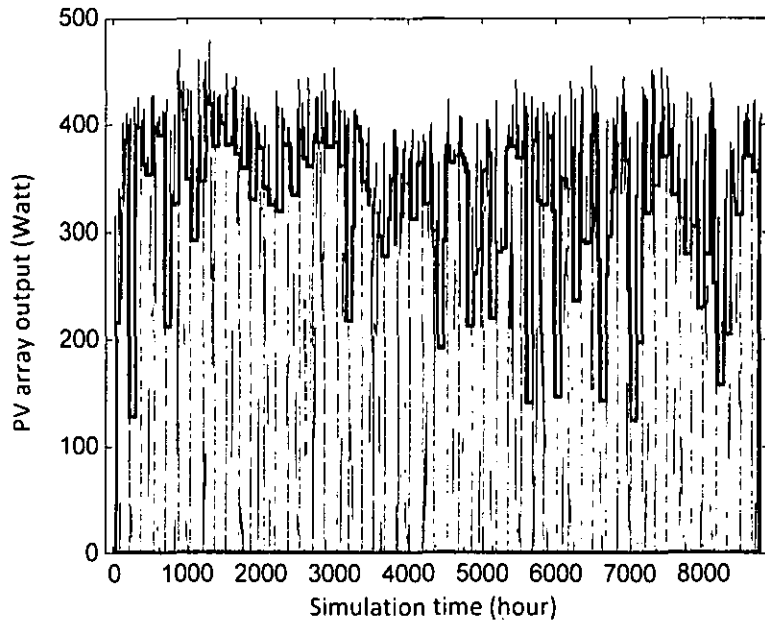


Figure 4.46: Simulation results: PV array output (Full simulation)

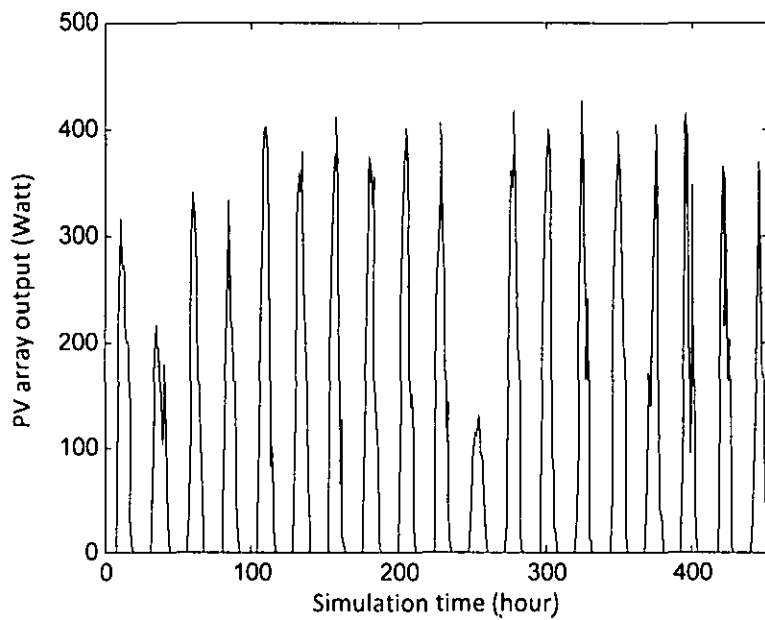


Figure 4.47: Simulation results: PV panel output power

The load input setting to the simulation model is shown in Fig. 4.48. The load is configured to be constant during the night with total value of 1400 Wh/day . Fig. 4.49 shows power input (+) and output (-) to and from the battery. The power input is

fluctuated dependent on solar radiation value while the power output is constant during the night. Fig. 4.50 shows more detail of power input and output.

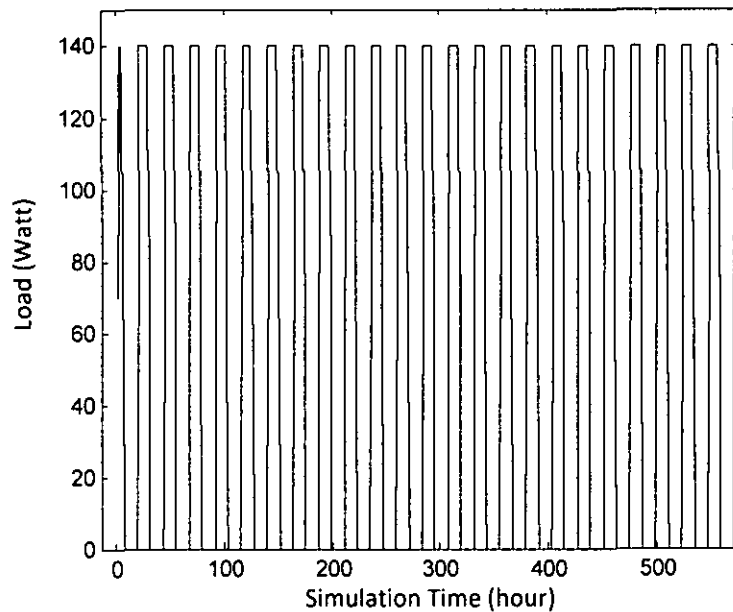


Figure 4.48: Load setting in the simulation

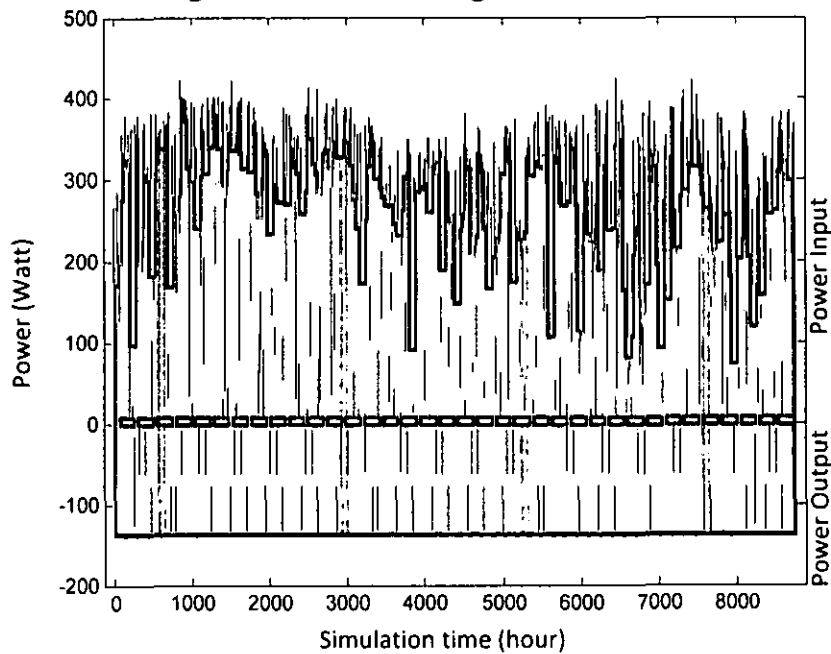


Figure 4.49: Simulation results: Power input and Output (Full simulation)

It is observed from Fig. 4.50, the system cannot fully supply energy to the load during the night for several days. Points A and B are the days when the system cannot fully supply the load. Points C and D are an example when the load is totally supplied by the PV system. The total load that is supposed to be supplied by the system is 511000 Wh. From the simulation results, it can be calculated that total load that is supplied by the system is 500130.44 Wh. Therefore, the Loss of Power Supply is =

511000 Wh - 500130.44 Wh = 10869.55 Wh. The calculated LPSP value of the system from the simulation results is 0.02 while the LPSP design is 0.001. The difference in performance results by mean of LPSP between design value (using daily-based data) and using simulation (hourly data) is because of the different model of the component, different time-step and considered parameters. However, the minimum SOC can be configured to lower value, and then the load would be supplied totally by the system.

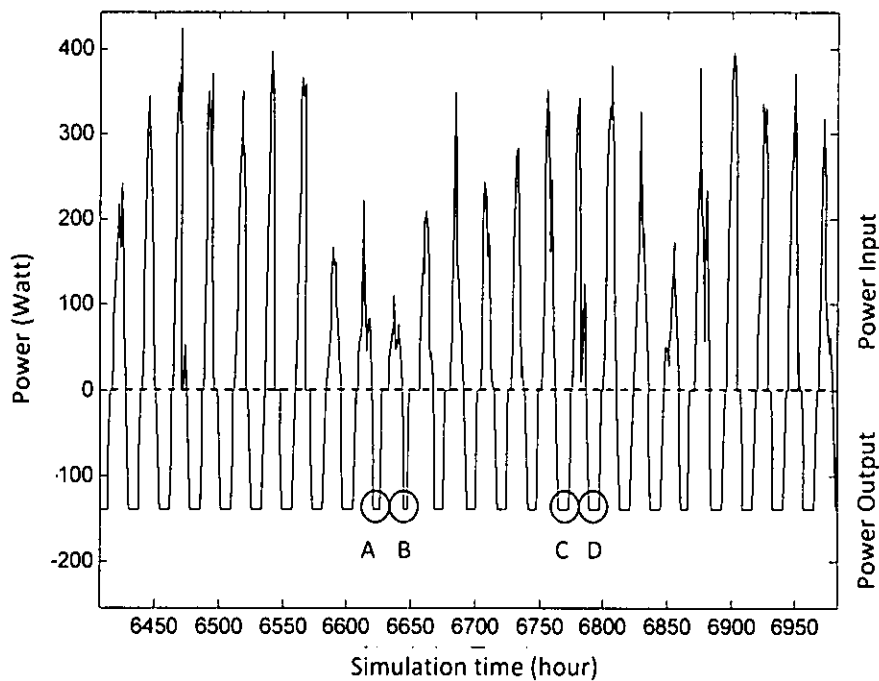


Figure 4.50: Simulation results: Power input and Output

Fig. 4.51 and 4.52 show simulation results for battery voltage. During the day, the battery voltage is increased due to the charging process. High voltage indicates high charging power. During the night, the battery voltage is decreasing linearly due to the constant loading.

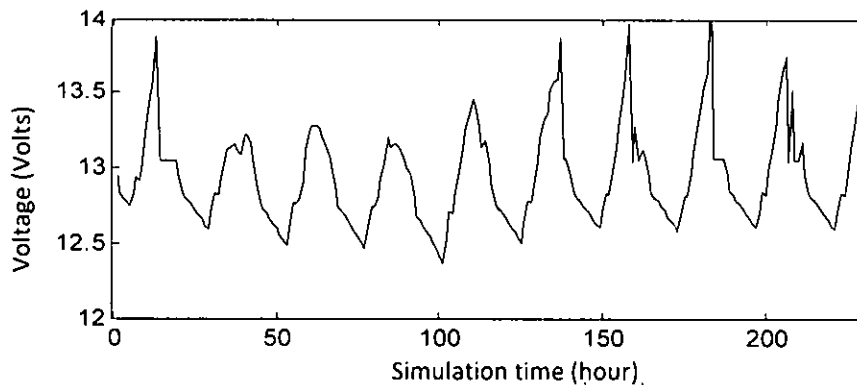


Figure 4.51: Simulation results: battery voltage monitoring

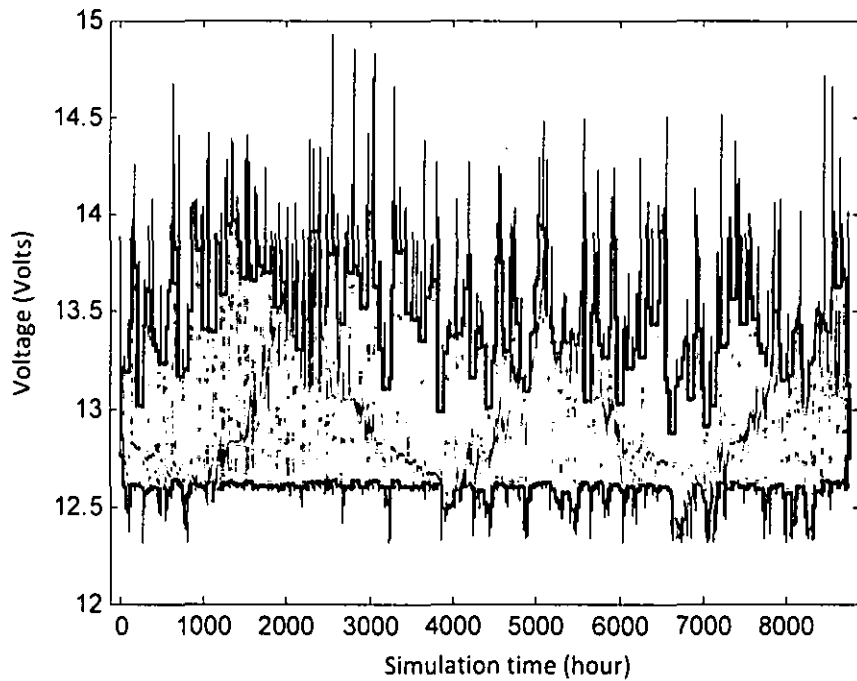


Figure 4.52: Simulation results: battery voltage monitoring (Full Simulation)

TRNSYS simulation output also presents Fractional State of Charge (FSOC) prediction. Fig. 4.53 and 4.54 shows the simulation results of FSOC. The upper limit of FSOC is one (100%) it is when the battery is fully charged. The lower limit of battery FSOC is 0.3 (30%), the controller will cut off supply to the load if the battery FSOC is lower than this value.

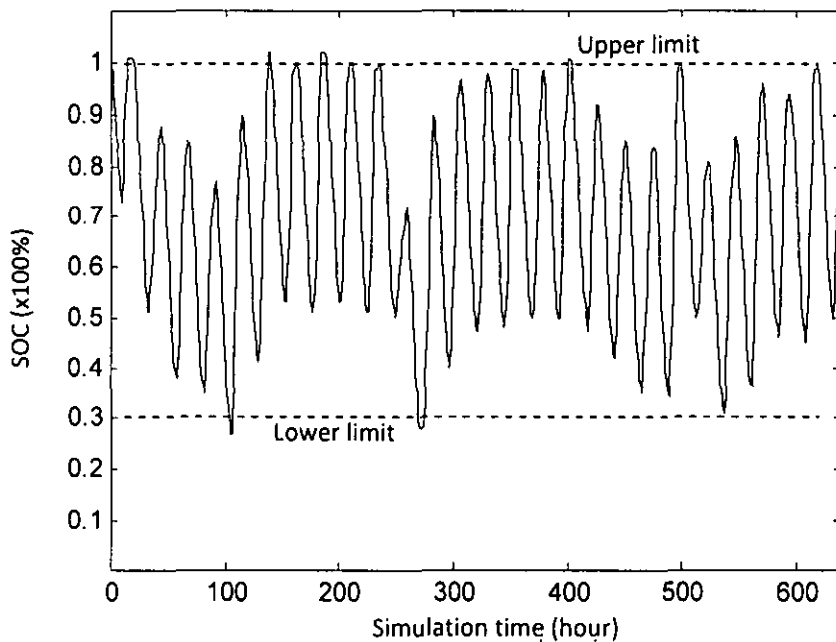


Figure 4.53: Simulation results: Battery SOC

Fig. 4.54 presents the full year simulation results of FSOC. It can be observed that the battery FSOC range during the year is between the limit, the average FSOC of the battery is 0.7. The higher operation range of FSOC will results the longer lifetime of the battery.

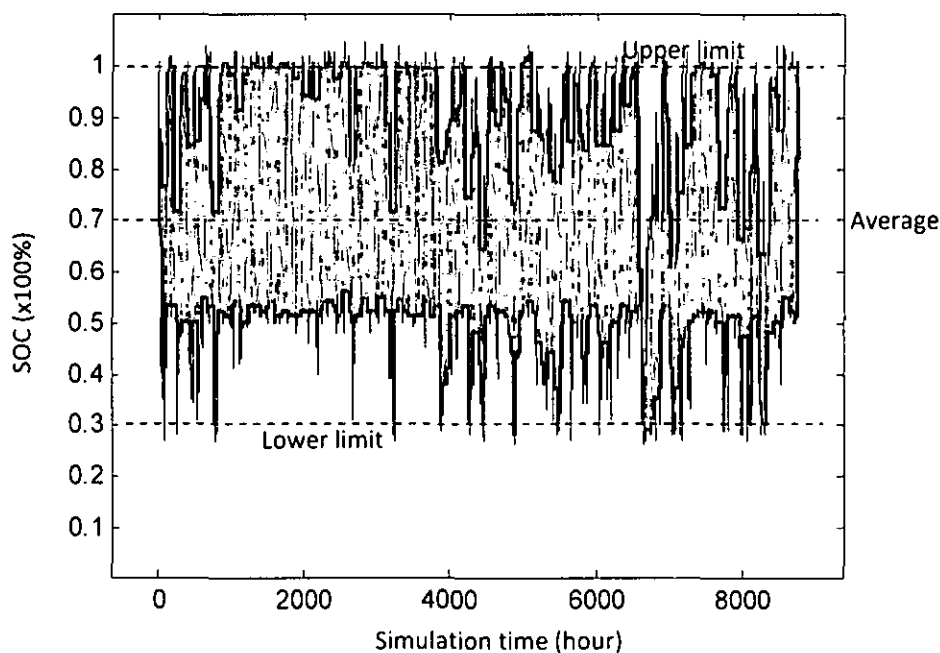


Figure 4.54: Simulation results: Battery SOC (Full simulation)

4.7 Summary

The data, calculation, experimental and simulation results have been presented in this chapter. Standalone PV system sizing has been carried out using the deterministic and stochastic method (LPSP) and compared. Simulation model has been built in TRNSYS 16 software. The model has been validated using experimental data. PV array output has been validated with $R^2=0.96$, $RMSE=27.8W$ and correlation equation between measured and simulated $y=1.2x-0.11$. Battery voltage has been validated with $R^2=0.904$, $RMSE=0.24V$ and correlation equation between measured and simulated $y=0.5431+5.974$. This result is better from previous researches that is shown by 50% smaller RMSE than L.K. Nkhonjera [87]. The simulation model has been used to simulate the selected configuration. The simulation results of selected configuration show the system works with LPSP value of 0.02. PV panel and/or battery capacity should be increased to increase the system performance.

CHAPTER 5

CONCLUSIONS AND RECOMMENDATIONS

5.1 Conclusions

The research work carried on optimizing PV panel and battery capacities in a standalone PV system for residential lighting applications has been successfully completed. Based on the research described in this study, the following conclusion can be drawn:

1. A new approach has been developed to predict solar radiation data using measured relative humidity and ambient temperature. This method is used to predict and fill missing data in the hourly time series solar radiation data that is required for LPSP calculation.
2. A methodology of LPSP calculation based on daily data has been developed for standalone PV system sizing. The method incorporates the tilted angle effect on PSH value, a feature that was not taken into consideration in previous research work. Sizing optimization has been carried out based on LPSP value and system cost by mean of CC and LCC.
3. An experimentally validated transient simulation model of a standalone PV system has been developed in this study using TRNSYS 16. The key features introduced into the model in the current work include new controller and battery parameter settings and the selection of Shepherd-Hyman battery model. With these features, the simulation result accuracy has improved as indicated by Root Mean Square Error (RMSE) between simulated and measured battery voltage has decreased by 50% compared to previous work.

5.2 Directions for Future Work

The findings in the current research work have shown the improvement in solar radiation estimation method, sizing optimization method and transient simulation model of standalone PV systems for lighting. However, there are opportunities that exist for further improvement in the following area:

1. Development of user-friendly software for PV system sizing based on proposed procedure in this study.
2. Incorporation of the day load in the PV system's sizing procedure.
3. Accuracy improvement of hourly solar radiation estimation by developing parameters correlation based on a larger data set.

5.3 Publications

1. **D.F. Al Riza**, S.I. Gilani, M.S. Aris, "A preliminary investigation into the use of solar PV systems for residential application in Bandar Seri Iskandar, Malaysia", International Conference on Plant Equipment and Reliability (ICPER) 2010, 15-17 June 2010, Kuala Lumpur, Malaysia
2. **D.F. Al Riza**, S.I. Gilani, M.S. Aris, "Measurement and Simulation of Standalone Solar PV System for Residential Lighting in Malaysia", International Symposium on Environment Friendly Energies in Electrical Applications (EFEEA) 2010, 2-4 November 2010, Ghardaïa, Algeria
3. **D.F. Al Riza**, S.I. Gilani, M.S. Aris, "Hourly solar radiation estimation from limited meteorological data to complete missing solar radiation data", International Conference on Environment Science and Engineering (ICESE) 2011, 1-3 April 2011, Bali, Indonesia (Indexed in IEEExplore)
4. **D.F. Al Riza**, S.I. Gilani and M.S. Aris, "Preliminary investigation into the use of solar PV systems for residential application in Bandar Seri Iskandar, Malaysia", Journal of Applied Sciences, Vol. 11 (11): pp. 2012-2017, 2011

5. **D.F. Al Riza**, S.I. Gilani and M.S. Aris, "Hourly solar radiation estimation using Ambient Temperature and Relative Humidity data", International Journal of Environmental Science and Development, Vol. 2, No. 3, June 2011: pp. 188-193
6. **D.F. Al Riza**, S.I. Gilani and M.S. Aris, "Measurement and Simulation of Standalone Solar PV System for Residential Lighting in Malaysia", Journal of Hydrocarbons Mines and Environmental Research, Volume 2, Issue 1a, June 2011, Available online 06 July 2011, p.234-239 (*In Press*, special issue of EFEEA 2010)
7. **D.F. Al Riza**, S.I. Gilani and M.S. Aris, "Optimal Sizing of Standalone Photovoltaic Systems for Residential Lighting Applications in Malaysia", Energy for Sustainable Development (Under Review - submitted on June 2011)

REFERENCES

- [1] Zekai Sen, "Solar Energy Fundamentals and Modeling Techniques", Springer – Verlag, 2008
- [2] Fredrik Robelius, "Giant Oil Fields – The Highway to Oil: Giant Oil Fields and Their Importance for Future Oil", Phd Dissertation, Upsala University, 2007
- [3] The Association for the Study of Peak Oil and Gas (ASPO) Newsletter #89 – May 2008
- [4] Energy Outlook for Asia and the Pacific, Asian Development Bank, 2009
- [5] Ar Chan Seong Aun, "ENERGY EFFICIENCY - Designing Low Energy Buildings Using Energy 10", Pertubuhan Arkitek Malaysia, CPD Seminar 7th August 2004
- [6] International Energy Statistics (IEA), U.S. Energy Information Administration, 2010 (tonto.eia.doe.gov accessed February 2011)
- [7] Dato' Noriyah Bt. Ahmad, "The Malaysia's Energy Sector: In Pursuit of a Better Future", Article for the star column, 22 March 2010
- [8] Statement on Notable Energy Achievements (Malaysia), 35TH APEC Energy Working Group Meeting, Iquitos, Peru 5-6 March 2008
- [9] Energy Commission of Malaysia, 2008 (http://www.st.gov.my/index.php?option=com_content&view=article&id=5436:electricity-statistics&catid=837&Itemid=1749&lang=en accessed February 2011)
- [10] L. Ramatha, "Energy in buildings in Malaysia", Proc. of AEEMTRC's 12th Seminar Workshop, Energy in Buildings, ed. A.G. Verdote, pp 335-346, AEEMTRC, Jakarta, 1994.
- [11] K. Sopian, M.Y.Othman, B. Yatim and W.R.W. Daud, "Future Directions in Malaysian Environment Friendly Renewable Energy Technologies Research and Development", ISESCO, Science and Technology Vision, Vol. 1: 30-36 May 2005

- [12] A. H. Haris, W. Chen and G. M. S. Lin, "National Survey Report of PV Power Applications in Malaysia 2009", The International Energy Agency, 2010
- [13] T. Markvart, and Luis Castener, "Practical Handbook of Photovoltaics Fundamentals and Applications", Oxford, UK, Elsevier, 2003
- [14] J. A. Duffie, W. A. Beckman, "Solar Engineering of Thermal Processes", third edition, John Wiley & Sons, Inc., New York, 2006
- [15] L.T. Wong and W.K. Chow, "Solar radiation model", *Applied Energy* 69: 191–224, 2001
- [16] T. Muneer, "Solar radiation and daylight model", 2nd edition, Elsevier Butterworth-Heinemann, 2004
- [17] Fatih Onur Hocaoglu, "Novel analytical hourly solar radiation models for photovoltaic based system sizing algorithms", *Energy Conversion and Management* 51, 2010
- [18] www.powerfromthesun.net/chapter3/Chapter3Word.htm accessed on October 2010
- [19] TRNSYS 16 Manual Book, 2007
- [20] E. Beaudette and A. T. O'Geen, "Quantifying the Aspect Effect: An Application of Solar Radiation Modeling for Soil Survey", *Soil Science Society of America Journal: Volume 73: Number 4, July–August 2009*
- [21] F.J. Batlles, M.A. Rubioa, J. Tovarb, F.J. Olmoc and L. Alados-Arboledas, "Empirical modeling of hourly direct irradiance by means of hourly global irradiance", *Energy* 25: 675-688, 2000
- [22] C.A. Gueymard, "Direct solar transmittance and irradiance predictions with broadband models. Part I: detailed theoretical performance assessment", *Solar Energy* 74: 355-379, 2003
- [23] Angström A, "Solar and terrestrial radiation", *Q J R Met Soc* 50:121–5, 1924
- [24] M. Yorukoglu and A.N. Celik, "A critical review on the estimation of daily global solar radiation from sunshine duration", *Energy Conversion and Management* 47: 2441-2450, 2006

- [25] Bristow, K. L. and G. S. Campbell, “On the relationship between incoming solar radiation and daily maximum and minimum temperature”, *Agric. For. Meteor.* 31:159–166, 1984
- [26] Hargreaves, G. H. and Z. A. Samani, “Reference crop evapotranspiration from temperature. *Appl. Eng. Agric.* 1:96–99, 1985 as cited by [18]
- [27] Hunt LA, Kuchar L, Swanton CJ. Estimation of solar radiation for use in crop modelling. *Agric. Forest Meteorol.* 91(3–4):293–300, 1998
- [28] Kurt Spokas and Frank Forcella, “Estimating hourly incoming solar radiation from limited meteorological data”, *Weed Science*, 54:182–189, 2006
- [29] Mehreen S. Gul, Tariq Muneer and Harry D. Kambezidis, “Models for obtaining solar radiation from other meteorological data”, *Solar Energy* 64, No. 1-3: 99-108, 1998
- [30] Yang K. and Koike T., “Estimating surface solar radiation from upper-air humidity”, *Solar Energy*, 72(2):177–86, 2002
- [31] J. G. Annandale, N. Z. Jovanovic, N. Benadé, R. G. Allen, “Software for missing data error analysis of Penman-Monteith reference evapotranspiration”, *Irrig. Science* 21:57-67, 2002
- [32] Kamal Skeiker, “Correlation of global solar radiation with common geographical and meteorological parameters for Damascus province, Syria.”, *Energy conversion and management* 47: 331-345, 2006
- [33] Guofeng Wu, Yaolin Liu and Tiejun Wang. “Methods and strategy for modeling daily global solar radiation with measured meteorological data – A case study in Nanchang station, China”, *Energy Conversion and Management* 48, 2447-2452, 2007
- [34] G. S. Campbell and J. M. Norman, “Introduction to Environmental Biophysics. 2nd ed. New York: Springer-Verlag. Pp. 167–183, 1998
- [35] S.M. Robaa, “Validation of the existing models for estimating global solar radiation over Egypt”, *Energy Conversion and Management* 50: 184-193, 2009
- [36] C.A. Balaras, G. Kallos, A. Strathic and S. Kritikou, “On the relationship of beam transmittance on clearness index for Athens, Greece”, *Int. J. Solar Energy* Vol. 7: 171-179, 1989

- [37] B. Ridley, John Boland and Philippe Lauret, “Modelling of diffuse solar fraction with multiple predictors”, *Renewable Energy* 35, 478–483, 2010
- [38] G. Notton, C. Cristofari, M. Muselli and P. Poggi, “Calculation on an hourly basis of solar diffuse irradiation from global data for horizontal surfaces in Ajaccio”, *Energy conversion and management* 45: 2849-2866, 2004
- [39] DT. Reindl, W. A. Beckman and J. A. Duffie “Diffuse fraction correlations”, *Solar Energy* 45:1-7, 1990
- [40] A. Skartveit and J.A. Olseth, “A model for the diffuse fraction of hourly global radiation”, *Solar Energy* 38 No. 4: 271-274, 1987
- [41] J. L Torres, M. De Blas, A. García and A. de Francisco, “Comparative study of various models in estimating hourly diffuse solar irradiance”, *Renewable energy* 35: 1325-1332, 2010
- [42] R. Perez, P. Ineichen, E. Maxwell, R. Seals and A. Zelenka, “Dynamic global-to-direct irradiance conversion models.”, *ASHRAE Trans Res* 98:354–69, 1992
- [43] R. Posadillo and R. Lopez Luque, “Evaluation of the performance of three diffuse hourly irradiation models on tilted surfaces according to the utilizability concept”, *Energy Conversion and Management* 50: 2324-2330, 2009
- [44] J.D. Mondol, “Solar radiation modelling for the simulation of photovoltaic systems”, *Renewable Energy* 33: 1109-1120, 2008
- [45] G. Notton, C. Cristofari and P. Poggi, “Performance evaluation of various hourly slope irradiation models using Mediterranean experimental data of Ajaccio”, *Energy Conversion and Management* 47:147–73, 2006
- [46] G. Notton, P. Poggi and C. Cristofari “Predicting hourly solar irradiation on inclined surfaces based on the horizontal measurements- Performances of the association of well-known mathematical models”, *Energy Conversion and Management* 47:147–73, 2006
- [47] Efim G.E. and Avraham I.K., “The assessment of different models to predict the global solar radiation on a surface tilted to the south”, *Solar Energy* 83: 377-388, 2009

- [48] A.M. Noorian, I. Moradi and G.A. Kamali, "Evaluation of 12 models to estimate hourly diffuse irradiation on inclined surfaces", *Renewable energy* 33: 1406-1412, 2008
- [49] A. Skartveit and J.A. Olseth, "Modelling slope irradiance at high latitudes", *Solar Energy* 36: 333-44, 1986
- [50] J.E. Hay, "Calculation of monthly mean solar radiation for horizontal and inclined surfaces", *Solar Energy* 23:301-30, 1979
- [51] D.T. Reindl, W. A. Beckman and J. A. Duffie, "Evaluation of hourly tilted surface radiation models" *Solar Energy* 45:9-17, 1990 as cited by [38]
- [52] R. Perez, P. Ineichen, R. Seals, J. Michalsky and R. Stewart "Modelling daylight availability and irradiance components from direct and global irradiance", *Solar Energy* 44:271-89, 1990
- [53] B.Y.H. Liu and R.C. Jordan, "Daily insolation on surfaces tilted towards the equator", *Trans ASHRAE* 67:526-41, 1962
- [54] J.E. Hay and J.A. Davies, "Calculation of the solar radiation incident on an inclined surface", *Proceedings First Canadian Solar Radiation workshop*, 59-72, 1980
- [55] P.G. Loutzenhiser, H. Manz, C. Felmann, P.A. Strachan, T. Frank and G.M. Maxwell, "Empirical validation of models to compute solar irradiance on inclined surfaces for building energy simulation", *Solar Energy* 81: 254-267, 2007
- [56] www.solar4power.com/solar-power-global-maps.html accessed on May 2010
- [57] www.oksolar.com/abctech/images/world_solar_radiation_large.gif accessed on December 2010
- [58] Alberto Escudero-Pascual, "Sizing of stand-alone PV system based on the "worst month" method", *Creative Commons Attribution Share Alike 3.0*, 2006
- [59] Arvind Chel, G.N. Tiwari and Avinash Chandra, "Sizing and cost estimation methodology for stand-alone residential PV power system", *Int. J. Agile Systems and Management*, Vol. 4, 2009
- [60] A. Benatiallah, R. Mostefaoui and M. Boubekri "A comparison of simplified and statistical methods of sizing photovoltaic installation for a remote dwelling

- in the saharan region”, *Journal of the Human-Environmental System* Vol. 8 No. 1: 1-6, 2005
- [61] M.M.H. Bhuiyand and M.A. Asgar, “Sizing of stand-alone photovoltaic system at Dhaka”, *Renewable Energy* 28: 929-938, 2003
- [62] I. Abouzhar and R. Ramakumar, “Loss of power supply probability of stand-alone photovoltaic systems: A closed form solution approach”, *IEEE Transactions on Energy Conversion*, Vol. 6, No. 1, March 1991
- [63] E. Ofry and A. Braunstein, “The loss of power supply probability as a technique for designing stand-alone solar electrical (photovoltaic) systems”, *IEEE Transactions on Power Apparatus and Systems*, Vol. PAS-102, No. 5, May 1983
- [64] L.L. Bucciarelli, “Estimating loss-of-power probabilities of stand-alone photovoltaic conversion systems”, *Solar Energy*, Vol. 32, p. 205, 1984
- [65] L.L. Bucciarelli, “The effect of day-to-day correlation in solar radiation on the probability of-loss of power in a stand-alone photovoltaic energysystems.” *Solar Energy*, Vol. 36, p. 11, 1986
- [66] X. Luo, C. Singh and Q. Zhao “Loss-of-Load Probability calculation using learning vector quantization”, *Proceeding of PowerCon 2000*, Perth, WA , Australia, 2000
- [67] A.H. Almakaleh, “A combined analytical and correlation method for sizing stand-alone photovoltaic solar power systems”, *Phd dissertation*, Dept. of Civil, Environmental and Architectural Engineering, University of Colorado at Boulder, USA, 1993
- [68] K.G. Rueb, “Loss of Energy Probability Sizing for PV Systems- Markov Mehtodology”, *MSc thesis*, System Design Engineering, University of Waterloo, Canada, 1992
- [69] Z.M. Salameh and B.S. Borowy, “Methodology for optimally sizing of the combination of a battery bank and PV array in a Wind/ PV hybrid system”, *IEEE transactions on Energy Conversion*, 11(2): 367-375, 1996
- [70] W.X. Shen, “Optimally sizing of solar array and battery in a standalone photovoltaic system in Malaysia”, *Renewable Energy* 34, 2009

- [71] R. Posadillo and R.L. Luque, "Approaches for developing a sizing method for stand-alone PV systems with variable demand", *Renewable Energy* 33: 1037-1048, 2008
- [72] R. Posadillo and R.L. Luque, "A sizing method for stand-alone PV systems installations with variable demand", *Renewable Energy* 33: 1049-1055, 2008
- [73] T. Markvart, A. Fragaki and J.N Ross, "PV system sizing using observed time series of solar radiation", *Solar Energy* 80:46-50, 2006
- [74] A. Fragaki and T. Markvart, "Stand-alone PV system design: Results using a new sizing approach", *Renewable Energy* 33:162-167, 2008
- [75] A.N. Celik, "Effect of different load profiles on the loss-odd-load probability of stand-alone photovoltaic systems.", *Renewable Energy* 32, 2007
- [76] Fatih O. Hocaoglu, Omer N. Gerek and Mehmet Kurban, "A novel hybrid (wind-photovoltaic) system sizing procedure" *Solar Energy* 83: 2019-2028, 2009
- [77] A. Balouktsis Omer N. Gerek and Mehmet Kurban, "Sizing stand-alone photovoltaic systems", *International Journal of Photoenergy*, Vol 2006:1-8, 2006
- [78] A.N. Celik, T. Muneer and P. Clarke, "Optimal sizing and life cycle assessment of residential photovoltaic energy systems with battery storage", *Progress in photovoltaics: Research and applications* 16: 69-85, 2008
- [79] J.K. Kaldellis, D. Zafirakis and E. Kondili, "Optimum autonomous stand-alone photovoltaic system design on the basis of energy pay-back analysis", *Energy* 34: 11187-11198, 2009
- [80] P. Arun, Rangan Banerjee and Santanu Bandyopadhyay, "Optimum sizing of photovoltaic battery systems incorporating uncertainty through design space approach", *Solar Energy* 83: 1013-1025, 2009
- [81] Jeremy Lagorse, Damien Paire and Abdellatif Miraoui, "Sizing optimization of a stand-alone street lighting system powered by a hybrid system using fuel cell, PV and battery", *Renewable Energy* 34: 683-691, 2009
- [82] A. Mellit, "ANN-based GA for generating the sizing curve of stand-alone photovoltaic systems", *Advances in Engineering Software* 41: 687-693, 2010

- [83] A. Mellit, Soteris A. Kalogirou and Mahmoud Drif, "Application of neural networks and genetic algorithm for sizing of photovoltaic systems", *Renewable Energy* 35: 2881-2893, 2010
- [84] H.L. Tsai, "Insolation oriented model of photovoltaic module using Matlab/Simulink", *Solar Energy* 84: 1318-1326, 2010
- [85] R. Perez, Rebecca Reed and Thomas Hoff, "Validation of a simplified PV simulation engine", *Solar Energy* 77: 357-362, 2004
- [86] Feng Shao, "Measurement and Simulation of Stand Alone Photovoltaic Systems", MSc Thesis, European Solar Engineering School, Högskolan Dalarna, Sweden, 2007
- [87] L.K. Nkhonjera, "Simulation and performance evaluation of battery based stand-alone photovoltaic systems of Malawi", MSc Thesis in Environmental Sustainable Development, National Central University, 2009
- [88] D. Turcotte, M. Rpss and F. Sheriff, "Photovoltaic Hybrid System Sizing and Simulation Tools: Status and Needs", Workshop on Photovoltaic Hybrid Systems, Canada, 2001
- [89] Chvis Bales, Wolfgang Streicher, Thomas Letz and Bengt Perevs, "Solar Heating Systems for Houses: A Design Handbook for Solar Combisystems", James & James, 2003, pp 209-219.
- [90] Timothy U. Townsend, "A Method for Estimating the Long-Term Performance of Direct-Coupled Photovoltaic Systems", M. S. Thesis – Solar Energy Laboratory, University of Wisconsin, Madison: 1989
- [91] Jürgen Helmut Eckstein, "Detailed Modeling of Photovoltaic Components". M. S. Thesis – Solar Energy Laboratory, University of Wisconsin, Madison: 1990
- [92] W. De Soto, S.A. Klein and W.A. Beckman, "Improvement and validation of a model for photovoltaic array performance", *Solar Energy* 80: 78-88, 2006
- [93] D.L. King, J.A. Kratochvil, W.E. Boyson, and W.I. Bower, "Field Experience with a New Performance Characterization Procedure for Photovoltaic Arrays", presented at the 2nd World Conference and Exhibition on Photovoltaic Solar energy Conversion, Vienna, Austria, July 6–10, 1998

- [94] D.L. King, "Photovoltaic array performance model", Sandia Report No.SAND2004-3535, 2004
- [95] A.N. Celik and N. Acikgoz, "Modeling and experimental verification of the operating current of mono-crystalline photovoltaic modules using four- and five-parameter models", *Applied Energy* 84: 1-15, 2007
- [96] www.ecodirect.com/Charge-Controller-Comparison-s/251.htm accessed December 2010
- [97] P. Diaz and M.A. Egido, "Experimental analysis of battery charge regulation in photovoltaic systems", *Progress Photovoltaic: Res. Appl.* 11:481–493, 2003
- [98] C.M. Shepherd, "Design of Primary and Secondary Cells II: An Equation Describing Battery Discharge," *Journal of Electrochemical Society*, 112, 657 (1965).
- [99] Hyman, E.A., "Phenomenological Cell Modelling: A Tool for Planning and Analyzing Battery Testing at the BEST Facility," Report RD77-1, Public Service Electric and Gas Company & PSE & G Research Corporation, Newark, (1977).
- [100] Ayu Wazira Azhari, K. Sopian, Azami Zaharim and Mohamad Al Ghoul, "A New Approach For Predicting Solar Radiation In Tropical Environment Using Satellite Images – Case Study Of Malaysia", *WSEAS Transactions on Environment and Development*, 2008
- [101] R. Saidur, H.H. Masjuki, M. Hasanuzzaman and G.S. Kai, "Investigation of Energy Performance and usage Behavior of Domestic Refrigerator Freezer Using Clustering and Segmentation.", *Journal of Applied Sciences* 8 (21), 2008
- [102] Azni Zain Ahmed, "Integrating Sustainable Energy in Buildings: A Case Study in Malaysia.", FAU Conference, Copenhagen, Denmark, 2008
- [103] CK Tang, "Energy Efficiency in Residential Sector", Report Malaysia-Danish Environmental Cooperation Program, 2005
- [104] www.powerstridebattery.com/sidebar/deep-cycle-batteries.html accessed on January 2010

- [105] C.J. Rydh, B.A. Sanden, "Energy analysis of batteries in photovoltaic systems. Part I: Performance and energy requirements", *Energy Conversion and Management* 46: 1957–1979, 2005
- [106] Liu, B. Y. and R. C. Jordan, "The interrelationship and characteristic distribution of direct, diffuse, and total solar radiation", *Sol. Energy* 4: 1–19, 1960
- [107] D. Sadot, O. Zaarur, S. Zaarur, "A technique for active measurement of atmospheric transmittance using an imaging system: implementation at 10.6 um wavelength", *Infrared Physics & Technology* 36, 1995, pp. 1105-1114
- [108] Sheldon M. Ross, "Introduction to probability and statistics for engineer and scientists". 4th Edition, Academic Press, Elsevier, Canada, 2009
- [109] www.mpoweruk.com/performance.htm, accessed November 2010
- [110] www.yuasaeurope.com/images/uploads/uk/images/charts/SWL/self-discharge-characterist.jpg, accessed November 2010
- [111] www.yuasaeurope.com/images/uploads/uk/images/charts/SWL/-discharge-characteristic-cu.jpg, accessed November 2010
- [112] A. Chel, G.N. Tiwari and A. Chandra, Simplified method of sizing and life cycle cost assessment of building integrated photovoltaic system, *Energy Build* 41: 1172–1180, 2009.
- [113] Tim Mearig, Nathan Coffee, Michael Morgan, "Life Cycle Cost Analysis Handbook" 1st Edition, State of Alaska - Department of Education & Early Development, Education Support Services/Facilities, 1999
- [114] H. Paul Barringer, "A Life Cycle Cost Summary", International Conference of Maintenance Societies (ICOMS) - 2003, Perth, Australia, 2003
- [115] www.tnb.com.my/residential/pricing-and-tariff/tariff-rates.html accessed 20 January 2011
- [116] K.Y. Lau, M.F.M. Yousof, S.N.M. Arshad, M. Anwari, A.H.M. Yatim, "Performance analysis of hybrid photovoltaic/diesel energy system under Malaysian conditions", *Energy* 35: 3245-3255, 2010
- [117] www.mbipv.net.my accessed November 2010
- [118] www.solarbuzz.com accessed November 2010

- [119] www.tradechakra.com/economy/malaysia/goods-and-services-tax-in-malaysia-214.php accessed November 2010
- [120] www.taxrates.cc/html/malaysia-tax-rates.html accessed November 2010
- [121] PV panel Data Sheet, PM100, Photon Solar India, 2008
- [122] www.campbellsci.ca/Catalogue/SPLite.html accessed november 2010
- [123] Low Voltage Humidity Sensors, HIH 5030 datasheet, Honeywell, 2009
- [124] Precision Centigrade temperature sensor, LM35 datasheet, National Instruments, 2000
- [125] Pierre Herckes, Wendling R, Sauret N, Mirabel P, Wortham H., “Cloudwater studies at a high elevation site in the Vosges Mountains (France)”, *Environmental pollution*, 117: 169–177, 2002
- [126] Hyeung-Sik Choi, Sangkook Yuna and Kwang-il Whang, “Development of a temperature-controlled car-seat system utilizing thermoelectric device”, *Applied Thermal Engineering*, 27: 2841–2849, 2007
- [127] Current Transducer HTFS 200..800-P/SP2 datasheet, LEM
- [128] www.microsln.com/msln/images/SIE_ARTICULOS/USB/-con_USB.JPG accessed November 2010
- [129] www.campbellsci.com accessed November 2010
- [130] www.youngusa.com accessed November 2010
- [131] Julie M. Tarara and Gwen-Alyn Hoheisel, “Low-cost Shielding to Minimize Radiation Errors of Temperature Sensors in the Field”, *Hortscience* Vol. 42(6): 1372-1379, 2007

APPENDIX A
RESIDENTIAL HOUSE LOAD PROFILE DETAILS

Table A.1: Residential House Load Profile

Time	TV (Watt)	Fan (Watt)	Refrigerator (Watt)	Other (Watt)	Lamp1 (Watt)	Lamp2 (Watt)	Lamp3 (Watt)	Lamp4 (Watt)	Lamp Total (Watt)	Total (Watt)
1:00	0	0	75	0	54	0	0	0	54	129
2:00	0	0	75	0	54	0	0	0	54	129
3:00	0	0	70	0	54	0	0	0	54	124
4:00	0	0	70	0	54	0	0	0	54	124
5:00	0	0	70	0	54	0	0	0	54	124
6:00	0	0	60	0	54	0	0	0	54	114
7:00	0	0	60	0	54	0	36	40	130	190
8:00	0	0	60	100	0	0	0	0	0	160
9:00	0	0	100	100	0	0	0	0	0	200
10:00	0	80	100	50	0	0	0	0	0	230
11:00	0	160	100	50	0	0	0	0	0	310
12:00	0	160	100	50	0	0	0	0	0	310
13:00	0	160	110	50	0	0	0	0	0	320
14:00	0	160	110	50	0	0	0	0	0	320
15:00	0	160	100	50	0	0	0	0	0	310
16:00	0	80	100	50	0	0	0	0	0	230
17:00	100	0	100	100	0	0	0	0	0	300
18:00	100	0	100	100	0	0	0	0	0	300
19:00	100	0	85	100	0	54	36	40	184	469
20:00	100	0	85	100	54	54	0	80	188	473
21:00	100	0	80	50	54	54	0	80	188	418
22:00	100	0	80	0	54	54	0	80	188	368
23:00	0	0	75	0	54	54	0	0	108	183
0:00	0	0	75	0	54	0	0	0	54	129
Total	600	960	2040	1000	648	324	72	320	1364	5964

APPENDIX B

DAILY DATA BASED LPSP CALCULATION ALGORITHM

- IF $E_{PV(n)} + E_{B(n-1)} > E_{Bmax}$ then
 $E_{excess(n)} = E_{B(n-1)} + E_{PV(n)} - E_{Bmax}$
 $E_{Bhalf(n)} = E_{Bmax}$
 IF $E_{Bhalf(n)} - E_{load(n)} > E_{Bmin}$ then
 $E_{B(n)} = E_{Bhalf(n)} - E_{load}$
 $LPS(n) = 0$
 IF $E_{Bhalf(n)} - E_{load(n)} = E_{Bmin}$ then
 $E_{B(n)} = E_{Bmin}$
 $LPS(n) = 0$
 IF $E_{Bhalf(n)} - E_{load(n)} < E_{Bmin}$ then
 $E_{B(n)} = E_{Bmin}$
 $LPS(n) = E_{Bmin} - E_{Bhalf(n)} - E_{load(n)}$
- IF $E_{PV(n)} + E_{B(n-1)} = E_{Bmax}$ then
 $E_{excess(n)} = 0$
 $E_{Bhalf(n)} = E_{Bmax}$
 IF $E_{Bhalf(n)} - E_{load(n)} > E_{Bmin}$ then
 $E_{B(n)} = E_{Bhalf(n)} - E_{load(n)}$
 $LPS(n) = 0$
 IF $E_{Bhalf(n)} - E_{load(n)} > E_{Bmin}$ then
 $E_{B(n)} = E_{Bmin}$
 $LPS(n) = 0$
 IF $E_{Bhalf(n)} - E_{load(n)} > E_{Bmin}$ then
 $E_{B(n)} = E_{Bmin}$
 $LPS(n) = E_{Bmin} - E_{Bhalf(n)} - E_{load(n)}$
- IF $E_{PV(n)} + E_{B(n-1)} < E_{Bmax}$ then
 $E_{excess(n)} = 0$
 $E_{Bhalf(n)} = E_{B(n-1)} + E_{PV(n)}$
 IF $E_{Bhalf(n)} - E_{load(n)} > E_{Bmin}$ then
 $E_{B(n)} = E_{Bhalf(n)} - E_{load(n)}$
 $LPS(n) = 0$
 IF $E_{Bhalf(n)} - E_{load(n)} > E_{Bmin}$ then
 $E_{B(n)} = E_{Bmin}$
 $LPS(n) = 0$
 IF $E_{Bhalf(n)} - E_{load(n)} > E_{Bmin}$ then
 $E_{B(n)} = E_{Bmin}$
 $LPS(n) = E_{Bmin} - E_{Bhalf(n)} - E_{load(n)}$

APPENDIX C
ELECTRICITY TARIFF FOR DOMESTIC COSTUMER

Table C.1: Electricity tariff for domestic consumer (TNB) [104]

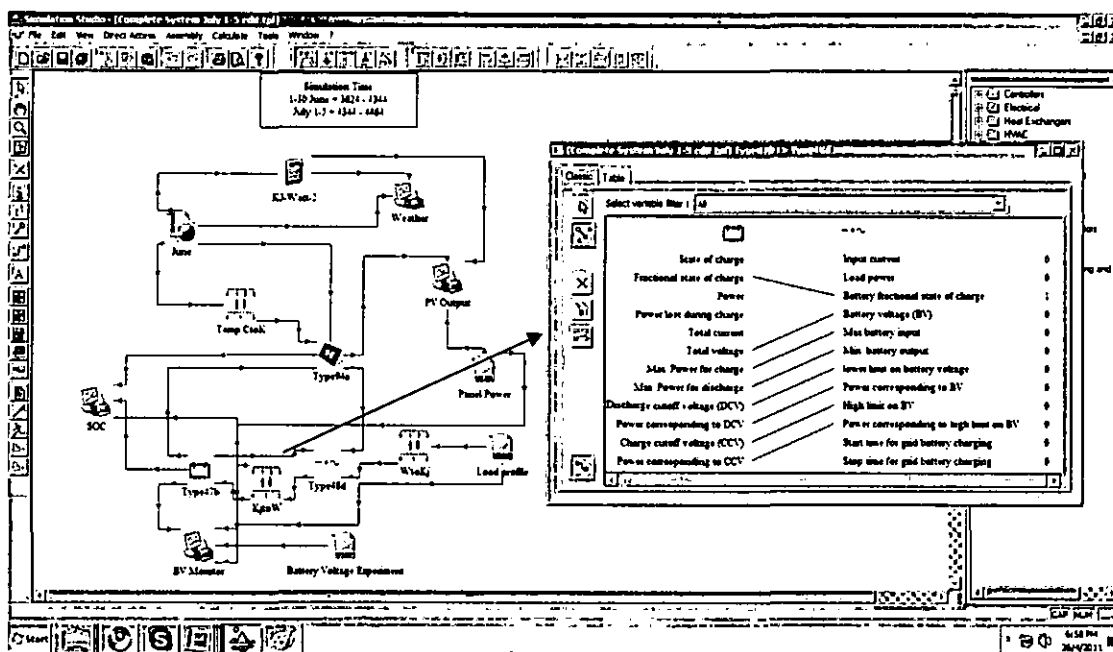
Tariff A - Domestic Tariff	UNIT	RATES
<i>For Monthly Consumption Between 0-400 kWh/month</i>		
For the first 200 kWh (1 - 200 kWh) per month	sen/kWh	21.8
For the next 200 kWh (201 -400 kWh) per month	sen/kWh	33.4
<i>For Monthly Consumption More Than 400 kWh/month</i>		
For the first 500kWh (1-500kWh) per month	sen/kWh	28.6
For the next 100 kWh (501-600kWh) per month	sen/kWh	37.8
For the next 100 kWh (601-700kWh) per month	sen/kWh	38.7
For the next 100 kWh (701-800kWh) per month	sen/kWh	39.7
For the next 100 kWh (801-900kWh) per month	sen/kWh	41.7
For the next kWh (901 kWh onwards) per month	sen/kWh	44.6

APPENDIX D
PV SYSTEM SPECIFICATION

Description	Characteristic/Value
PV Module	
Type	Multi-Crystalline Silicon
Nominal Peak Power (Pp)	100 Watt
Rated Voltage (Vr)	17.2 Volt
Rated Current (Ir)	5.81 Ampere
Open Circuit Voltage (Voc)	21.6 Volt
Short Circuit Current (Isc)	6.46 Ampere
Temperature Coefficient	-0.074 V/°C; +2.80 mA/°C
Number of modul in parallel	4
Company/Country of origin	Photon Solar - India
Charge Controller	
Brand	ProStar Solar Controler PS-30
Type	PWM-type
System Voltage	12 Volt
Max Current	30 Ampere
Battery Bank	
Brand	Universal
Type	Deep Cycle Battery, Sealed Lead Acid
Capacity	100 Ah
Max Charging Current	30 Ampere
Max Discharge Current	800 Ampere (5 seconds)
Number of Cell in parallel	4
Cell/Operation Voltage	12 Volt

APPENDIX E SIMULATION SETTING

E.1 SCREEN SHOOT OF COMPONENTS CONNECTION SETTING



E.2 COMPONENTS CONNECTION SETTING DETAILS

Table E.2.1: Weather data (type 109) output

No	Specifications	to	Corresponding inputs
1	Total radiation on tilted surfaces	PV panel	Total incident radiation
2	Ambient temperature	PV panel through unit converter	Ambient temperature
3	Total radiation on tilted surfaces	Plotter	Input
4	Total radiation on horizontal	Plotter	Input

Table E.2.2: PV Panel (type 94a) output

No	Specifications	to	Corresponding inputs
1	Array current	Charge controller	Input current
2	Array current	Plotter	Input
3	Array power	Plotter	Input
4	Array temperature	Plotter	Input
5	Array voltage	Plotter	Input
6	Power at maximum power point	Plotter	Input

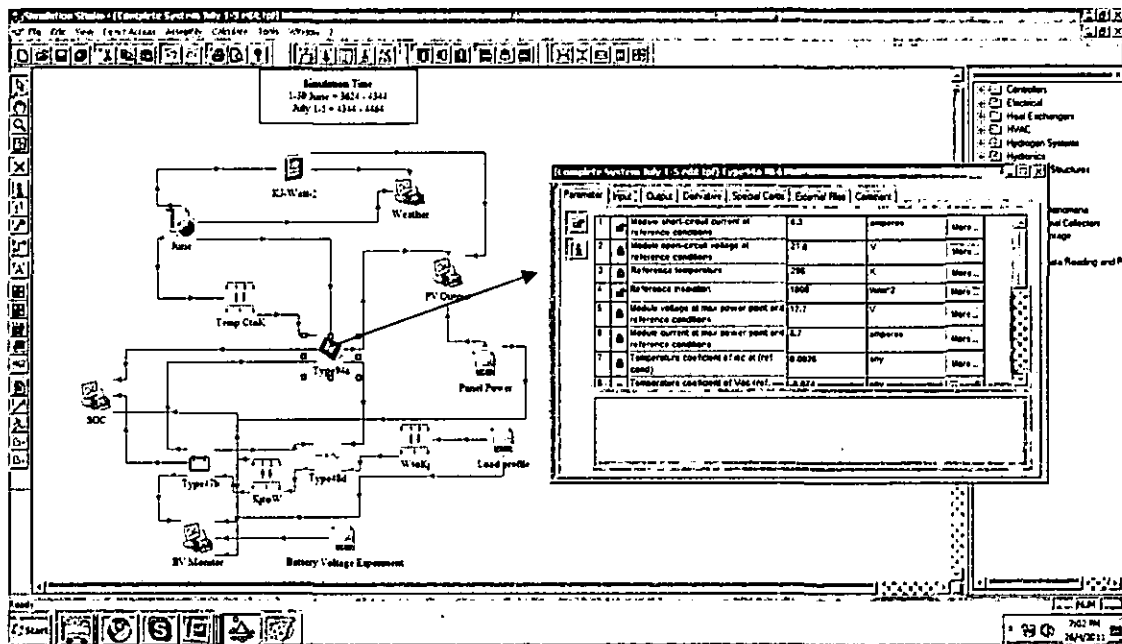
Table E.2.3: Battery (type 47c) output

No	Specifications	to	Corresponding inputs
1	Fractional state of charge	Charge controller	Battery FSOC
2	Total voltage	Charge controller	Battery voltage
3	Max. Power for charge	Charge controller	Max. battery input
4	Max. Power for discharge	Charge controller	Min. battery input
5	Discharge cut off voltage	Charge controller	Lower limit on battery voltage
6	Power corresponding to DCV	Charge controller	Power corresponding to BV
7	Charge cut off voltage	Charge controller	High limit on battery voltage
8	Power corresponding to CCV	Charge controller	Power corresponding to high limit on BV
9	Total voltage	PV panel	Load voltage
10	State of charge	Plotter	Input
11	Fractional state of charge	Plotter	Input
12	Total voltage	Plotter	Input

Table E.2.4: Controller (type 48b) output

No	Specifications	to	Corresponding inputs
1	Power to or from battery	Battery through unit converter	Power to or from battery
2	Power in from generation	Plotter	Input
3	Power to load	Plotter	Input

E.3 SCREEN SHOOT OF COMPONENTS PARAMETERS SETTING



E.4 COMPONENTS PARAMETERS SETTING DETAILS

The user need to set the value of the parameters based on the datasheet or use the default value in the TRNSYS component. Table 3.14 – 3.17 shows detailed parameter setting of main components in TRNSYS simulation which are using for validation.

Table E.4.1: Weather data (type 109) parameter setting

<i>No</i>	<i>Parameter/mode</i>	<i>value</i>	<i>Quantifying</i>
1	Sky model for diffuse radiation	3	Reindl model
2	Tracking mode	1	Fixed
3	Ground reflectance	0.2	Default
4	Slope of surface	5	Experimental setup
5	Azimuth of surface	0	Facing south/equator

Table E.4.2: PV Panel (type 94a) parameter setting

<i>No</i>	<i>Parameter</i>	<i>value</i>	<i>Quantifying</i>
1	Module short circuit current at ref.	6.3	PV panel datasheet
2	Module open circuit voltage at ref.	21.6	PV panel datasheet
3	Reference temperature	298	(K) Default
4	Reference insolation	1000	Default
5	Module voltage at MPP and ref.	17.7	PV panel datasheet
6	Module current at MPP and ref.	5.7	PV panel datasheet
7	Temperature coefficient of Isc at ref.	0.0028	PV panel datasheet
8	Temperature coefficient of Voc at ref.	-0.074	PV panel datasheet
9	Number of cell in series	1	Experiment
10	Number of cell in parallel	4/5	Experiment/selected conf.
11	Module temperature at NOCT	313	Default
12	Ambient temperature at NOCT	293	Default
13	Insolation at NOCT	800	Assumption
14	Module area	0.89	Default
15	Tau alpha for normal incidence	0.95	Default
16	Semiconductor bandgap	1.12	Default
17	Slope of IV curve at ISC	0	Default
18	Module series resistance	0.353	PV panel datasheet

Table E.4.3: Controller (type 48d) parameter setting

<i>No</i>	<i>Parameter</i>	<i>value</i>	<i>Quantifying</i>
1	Mode	3	Default
2	Regulator efficiency	0.95	Assumption
3	Inverter efficiency (DC to AC)	1	DC load only
4	High limit on FSOC	1	Default
5	Low limit on FSOC	0.3	Set by intention
6	Charge to discharge limit on FSOC	0.1	Set by intention ^{*)}
7	Power output limit	3600	Default
8	Inverter efficiency (AC to DC)	0	No grid charging
9	Current for grid charging of battery	0	No grid charging
10	Upper limit on FSOC for grid charging	0	No grid charging

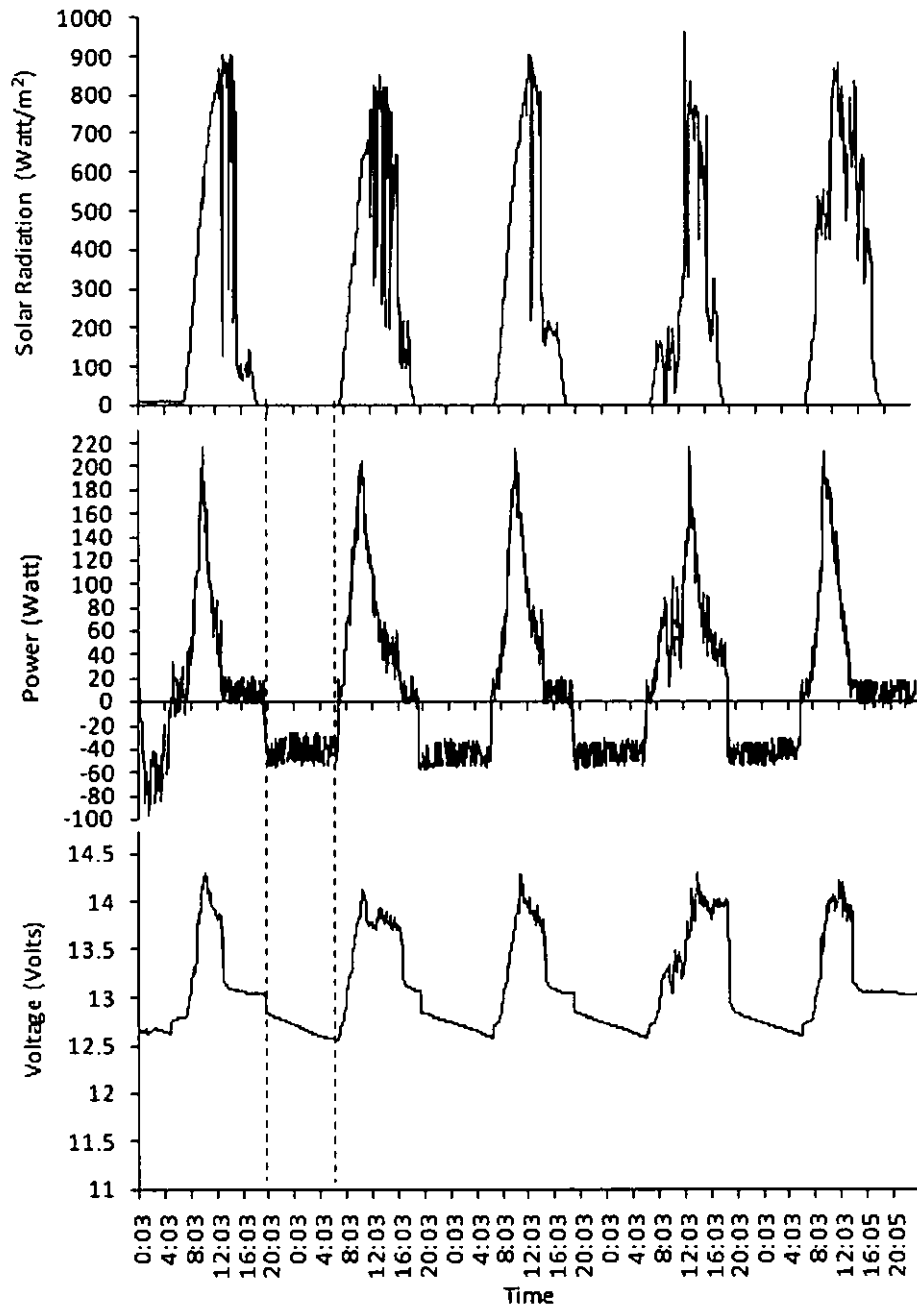
*) Disable total charge mode

Table E.4.4: Battery (type 47b) parameter setting

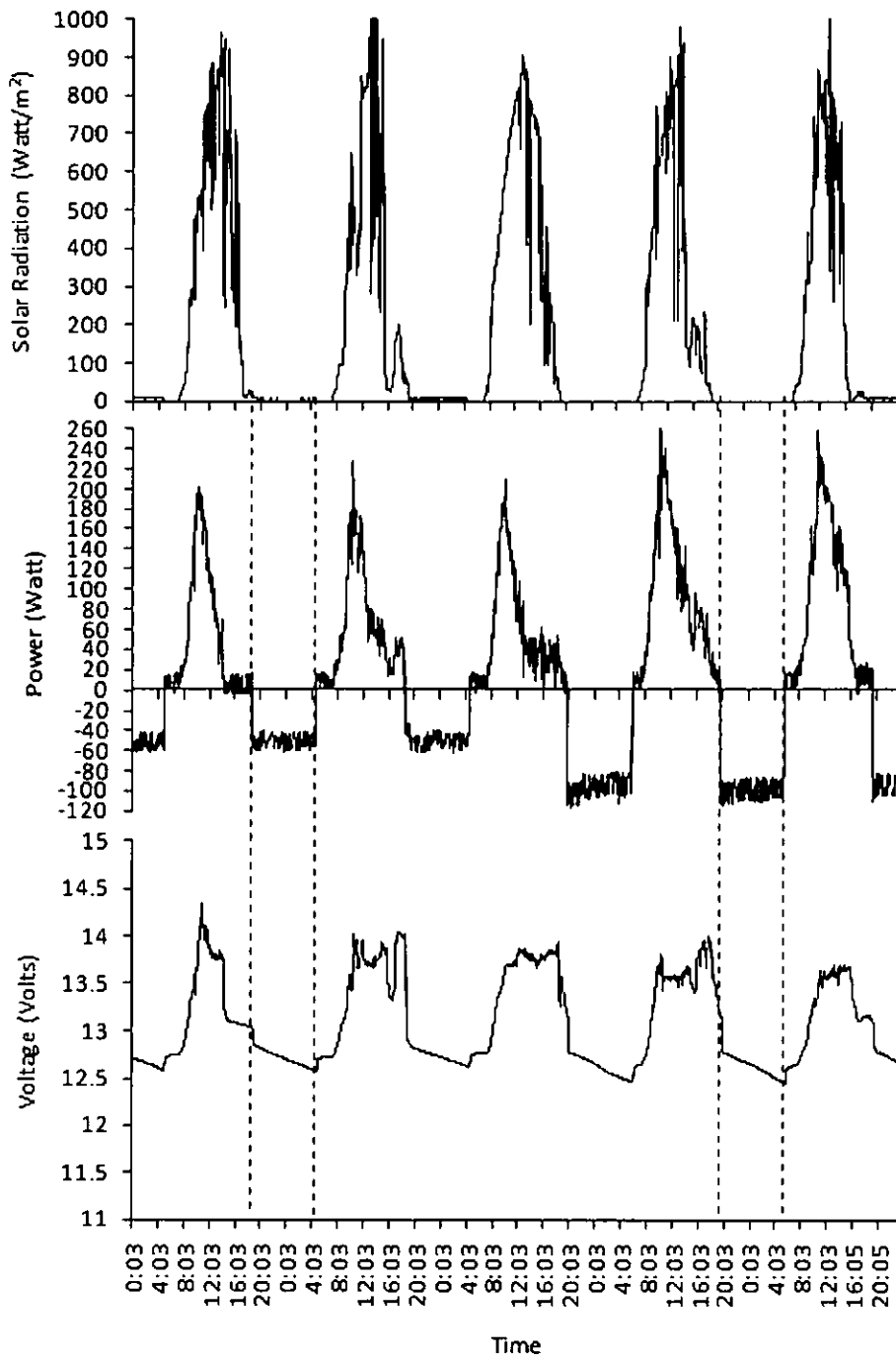
<i>No</i>	<i>Parameter</i>	<i>value</i>	<i>Quantifying</i>
1	Mode	2	Default
2	Cell Energy Capacity	16.7	Default
3	Cell in parallel	4	Set by intention to get 400Ah
4	Cell in series	6	Default
5	Charging efficiency	0.95	Assumption
6	Max. current per cell charging	6.66	Set by intention (enable max current)
7	Max. current per cell discharge	-6.66	Set by intention
8	Max. charge voltage per cell	2.5	Default
10	Calculate discharge cut off voltage	-1	Default

APPENDIX F
EXPERIMENTAL RESULTS

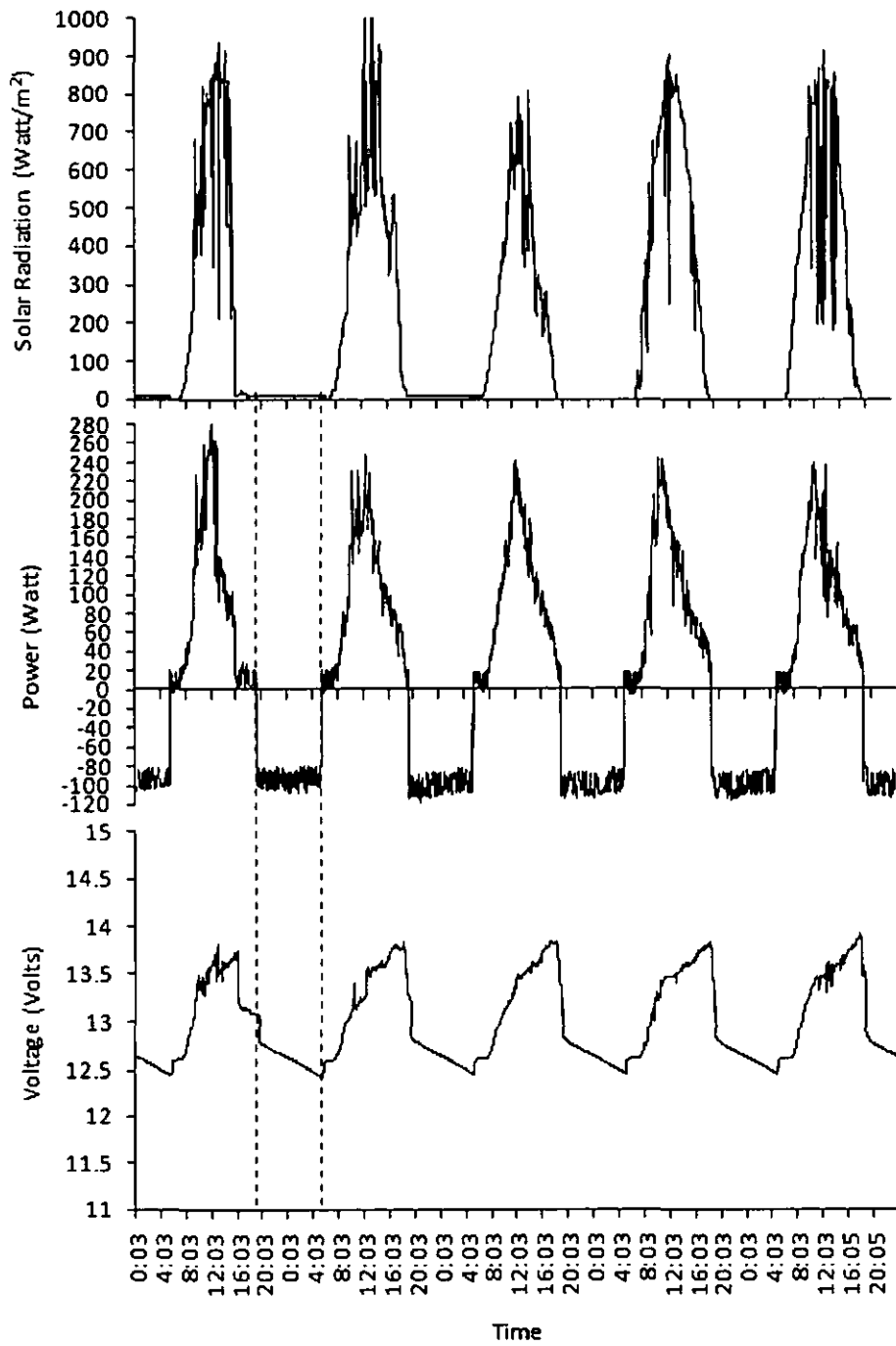
F.1 PV system monitoring 1-5 June 2010 (Load \pm 500 Wh/day)



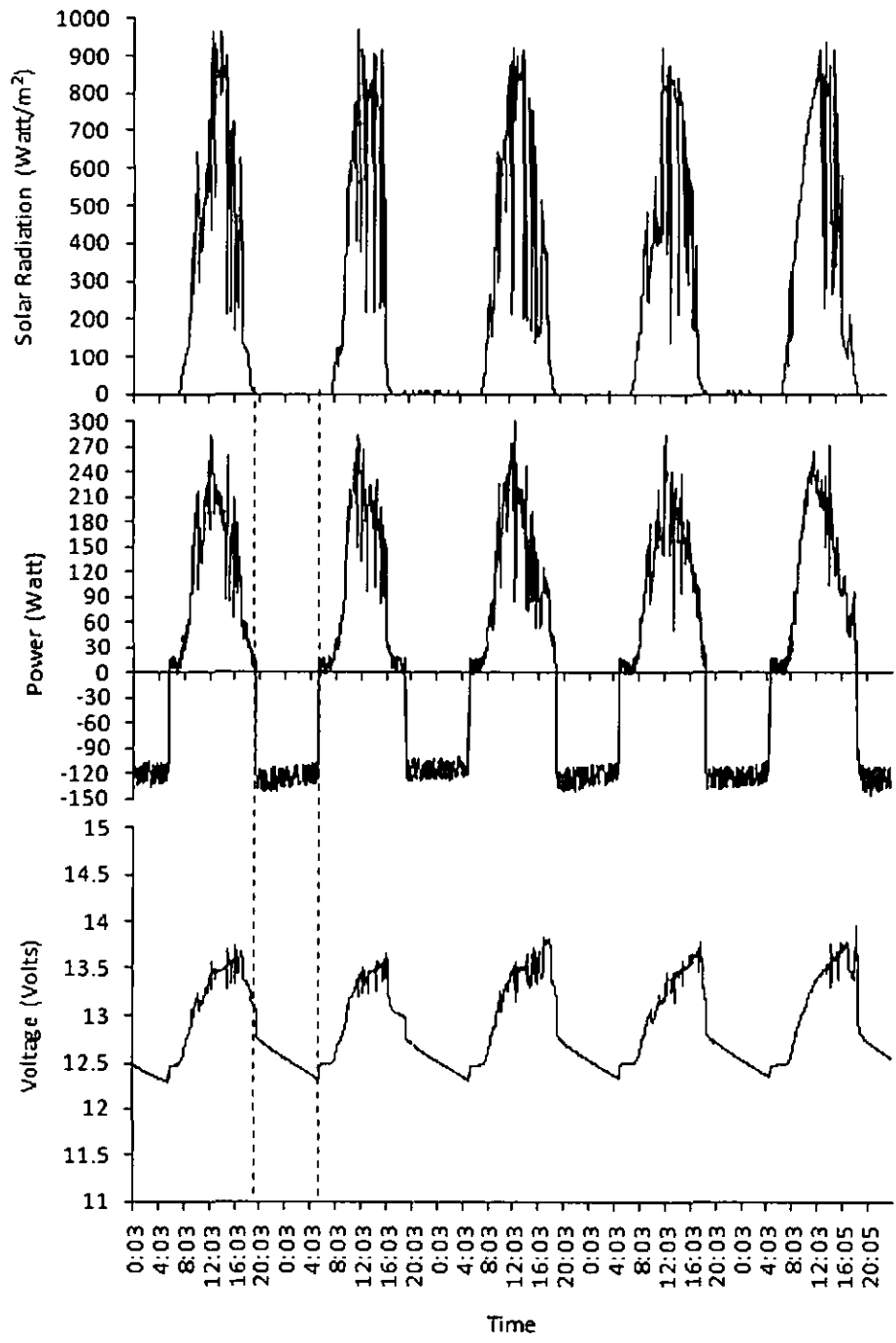
F.2 PV system monitoring 11-15 June 2010 (Load \pm 500 Wh/day to \pm 1000 Wh/day)



F.3 PV system monitoring 16-20 June 2010 (Load \pm 1000 Wh/day)



F.4 PV system monitoring 26-30 June 2010 (Load \pm 1200 Wh/day)



F.4 PV system monitoring 18-21 July 2010 (Load ± 1600 Wh/day)

